A Study of Instrumentation
for a Gas Chromatograph
Using Flame Ionization Detection
Final Report

Analog Technology Corporation

A Study of Instrumentation
for a Gas Chromatograph
Using Flame Ionization Detection
Final Report

Prepared for
National Aeronautics and Space Administration
Ames Research Center
Moffett Field, California 94035

5 December 1966

By Staff
Analog Technology Corporation
3410 E. Foothill Boulevard
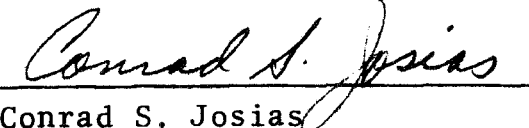Pasadena, California

Approved by:

Conrad S. Josias
President

Table of Contents

Appendices

List of Figures and Tables

1.0 INTRODUCTION

This report discusses results of a study of instrumentation techniques suitable for processing signals from a total organics experiment. The basic experiment involves pyrolysis of a sample having suspected organic constituents and subsequent detection of the volatile products by an organics-sensitive device, the Flame Ionization Organic Detector (FIOD). The purpose of this study is to investigate the feasibility and adaptability of various signal-processing configurations to the FIOD. The report is divided into two major sections. The first discusses the investigation of the various methods of performing the signal processing. This includes the investigation of various electrometer systems, different ways in which the detector background current can be stabilized, various types of integrators, and the data handling system. Since the experiment is still in the formative stage, minor emphasis was placed on the investigation of the kind of system supporting functions that would be required in a flight model. However, the over-all system operation, including a thorough study of the sequencing and data requirements of the instrument, was studied because of its importance in the selection of some of the basic signal processing circuits.

The second major section compares the different circuits studied in the report and describes criteria for the selection of certain ones for this instrument. While reliability, weight and power are always important considerations in space instrument design, particular stress is also placed on over-all simplicity for this application. The reason is that the experiment is not intended to perform a detailed analysis, but, rather to answer the very fundamental question as to whether or not there are organics present on the surface of the other planets in the solar system. The importance of performing the measurement reliably cannot be overstressed. An important goal of this study, then, is to instrument the experiment with the most light-weight, simple and reliable components and circuits possible.

The instrumentation recommendations are divided into two categories, namely: those for a scientific feasibility model for the laboratory; and those for a flight model.

Since the heart of the instrument is the flame detector, and, since the design of the signal processing electronics is so heavily dependent on the detector's parameters, the study has included the design of a flight-type detector. A functional laboratory version of the flight detector is therefore submitted with the final report, which includes a complete discussion on its performance.

2.0 PARAMETRIC STUDY

The parametric study is principally a compilation of parameters important to the experiment.

The over-all experiment is designed to accept a solid sample, pyrolize it and, by means of a hydrogen flame detector, determine whether organics are present in the pyrolysis products. The basis of the experiment is that the hydrogen flame detector is sensitive to all but a few select organics and does not detect inorganics.

Since the instrument will see only a single peak if organics are present (and no peak if none is present), a retention time measurement is not necessary in the experiment. This is perhaps the main basic distinction between this instrument and a hydrogen-flame gas chromatograph.

The following is a discussion of the various parameters important to the instrument design.

1) Maximum analysis time. The maximum analysis time is
    important for two basic reasons: 1) it affects the
    gas supplies and electrical power required; and 2)
    it determines the detector background current stability
    requirements. Since the time is expected to be less
    than five minutes, the amount of gas required, and total
    power even for several analyses, is not significant.
    The maximum analysis time of five minutes does not pose
    a problem for the baseline stabilization either; but,
    by placing the expected peak in a window (by actuating
    the signal processing electronics only during the time
    the peak is expected) the stabilization problem is
    simplified, and transients caused by sample injection
    and other system events make the integration problem
    simpler.

2. **Dynamic range.** The detector's linear dynamic range is between 10^{-6} and 10^{-13} amperes.

3. **Sensitivity.** The sensitivity, as determined in the feasibility model flight detector, is about 10^{-12} gm/s.

4. **Flow and pressure dependence.** Since the detector is both flow and pressure dependent, means were investigated to minimize the contributions of each to the instrument's error.

5. **Baseline characteristics.**

   a) Background current. The expected maximum background current is about 10^{-10} amperes.

   b) Noise level. The shot noise is approximately 10^{-14} A/$\sqrt{Hz}$ for $I_D = 10^{-10}$ A. DC drifts as much as 10^{-10} A from the nominal 10^{-11} A are possible.

6. **System accuracy.** The target accuracy for the instrument is 10%.

7. **Peak width.** The peak width can be anything between 2 and 20 seconds. It was assumed that once the experiment was designed the peak would not vary between 2 and 20 seconds but, rather, would be a particular width between 2 and 20 seconds known to within about five seconds.

3.0 ELECTROMETERS

An ideal detector and electrometer system for gas chromatography would possess all of the following properties:

1) Zero baseline error (current and voltage);

2) Linear output, proportional to current, for recording chromatograms and verifying system operation;

3) Output proportional to charge, to enable direct reading of the areas under peaks;

4) Up to seven decades of dynamic range;

5) Maximum sensitivity of at least 10^{-13} A.

In practice, the dynamic range and sensitivity required are so large that no existing instrument meets all of these requirements in a totally satisfactory way. The design of such an electrometer thus depends rather sensitively on the exact use contemplated. The following discussion of various kinds of electrometer systems will identify the compromises made in each system. Some of the electrometers to be described have already been constructed, tested and flown. The limitations of these systems will be indicated. The details of design and performance are discussed in references which are either cited or included as appendices.

Advances in components and in design concepts have made feasible the development of new kinds of electrometer systems. The performance limitations and general organization of such newer systems will be discussed in detail.

The discussion in the immediately following paragraphs
will be limited to problems of the electrometer amplifier
design. A specific recommendation of an experimental system,
based on the relation of the following discussion to the
needs of the proposed experiment, will be made in a later
section.

3.1 Direct-Coupled Electrometers

The conventional direct-coupled electrometer measures
the voltage developed across a resistor by the current to be
measured. To minimize the effects of amplifier gain drifts
and the total leakage resistance and capacitance at the input,
such an electrometer is ordinarily operated in the inverting
feedback configuration shown in Figure 3.1-1.
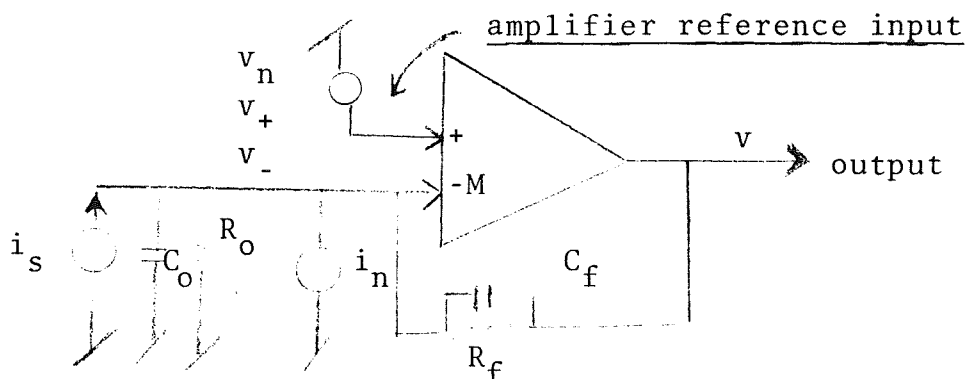
Figure 3.1-1 - Direct-Coupled Electrometer

In this diagram,

i_s =   signal current to be measured.

i_n =   noise or offset current, including detector and
             amplifier leakage.

v_n = noise or offset voltage.

R_o = parallel combination of source and amplifier input impedances.

C_o = source capacitance.

R_f = total capacitance in parallel with R_f.

If the amplifier gain function can be approximated as

$$v-v_+ = M(v_+ - v_-) \qquad (3.1-1)$$

the closed-loop transfer function becomes

$$v = \frac{-MR_f(i_s + i_n) + (M+1) v_n [R_f/R_o + 1 + p(C_o + C_f)R_f]}{R_f/R_o + (M+1)(1 + pC_fR_f) + pC_oR_f}$$

$$(3.1-2)$$

where p is the Laplace transform operator.

If the amplifier gain is much larger than R_f/R_o and then if the noise can be neglected, the output is given by the infinite-gain approximation:

$$v = \frac{-R_f \, i_s}{1 + pC_fR_f} \, , \quad M \gg R_f/R_o \qquad (3.1-3)$$

The minimum value of C_f is typically 0.1 pF, so that the time constant, R_fC_f, can be long. (For $R_f = 10^{12}$ Ω, $R_fC_f \geq 0.1$ sec.)

The high-frequency voltage noise can be quite large, since at higher frequencies only the capacitative elements are important, so that the rms output is

$$v = \left(\frac{C_o + C_f}{C_f} \right) v_n \qquad (M \gg 1, \ \omega \gg 1/R_f C_f) \qquad (3.1\text{-}4)$$

which is normally much larger than v_n (the ratio C_o/C_f is typically 100 to 1000).

Filtering is ordinarily provided to remove the noise at frequencies higher than the maximum frequency, $\omega = 1/R_f C_f$, that the electrometer passes.

This analysis shows that the following considerations are important in the design of an electrometer:

1) The value of detector or amplifier leakage current.

2) The voltage noise of the amplifier (or detector).

3) The value of the source capacitance, including the capacitance of the detector, its leads, and the input capacitance of the amplifier.

4) The ohmic source impedance R_o should be at least comparable to the feedback resistance R_f.

The selection of the detector and the device used for the first stage of the amplifier is determined largely, but not entirely, by these considerations. Particularly in a space instrument, the selection of the devices must also be consistent

3.1-3

with the requirements of low power consumption, high reliability, and freedom from unpredictable drifts requiring complex adjustment or calibration schemes. Designs satisfying the constraints imposed by the space environment will perform superbly in the laboratory.

Ordinarily, a direct-coupled amplifier of the type shown in Figure 3.1-1 can be expected to perform well over up to three decades of dynamic range. To extend the range, it is necessary to change the gain of the system. In a direct-coupled system, such a gain change can be accomplished by switching feedback resistors. Low-leakage reed switches have been found to be suitable.[3.1-1] The presence of the switches increases the feedback capacitance; and hence the response time. Such range-switching schemes are discussed in Section 5.1.

In the usual application, the detector and amplifier input leakage currents greatly exceed the smallest variation to be measured. To obtain an on-scale reading, the baseline current must be measured and subtracted at the input. Techniques for performing this function are discussed in Section 6.

To average the current over a period of time, or to measure the total charge delivered to the input, it is useful to connect an electrometer as an integrator, by increasing the feedback capacitance, C_f. The feedback resistance, R_f, may be omitted, but is still present in the form of the capacitor leakage. The form of the transfer function is still the same, but it is convenient to rewrite Equation 3.1-2 by

(3.1-1) J. H. Marshall, JPL Space Programs Summary 37-14, Vol. VI, pp 38-40.

dividing the numerator and denominator by R_f/R_o:

$$v = \frac{-M(i_s + i_n)R_o + (M + 1)v_n[1 + R_o/R_f + p(C_f + C_o)R_o]}{1 + (M + 1)[R_o/R_f + pC_fR_o] + pC_oR_o}$$

$$(3.1-5)$$

In the limit of large amplifier gain and small values of R_o/R_f and C_o/C_f, the output voltage becomes

$$v = -\frac{(i_s + i_n)}{pC_f} + v_n\left[1 + \frac{1}{pC_fR_o}\right] \qquad (3.1-6)$$

with an effective integration time constant $\tau = MR_oC_f$. High-frequency current noise is filtered out, while high-frequency voltage noise is transmitted without amplification. Low-frequency noise is amplified by the reciprocal of the frequency.

In particular, current offset errors cause a linearly increasing output (zero drift). Equation (3.1-6 shows that a voltage offset also produces an effective current offset v_n/R_o if the source impedance R_o is finite.

Because of the existence of low-frequency flicker noise (also called 1/f, or current noise), with a power density increasing with the reciprocal of the frequency, the use of an input integrator does not necessarily result in better noise performance. Electrometer tubes, large-value resistors, and insulated-gate field effect transistors exhibit large flicker noise effects. Carrier systems operating at a frequency at which flicker noise is negligible ordinarily provide superior noise

performance with the same input devices and feedback elements.

3.1.1 Vacuum Tube Input

Most existing laboratory systems have relied on the well-known electrometer tube to obtain a high impedance and low leakage current at the input of the electrometer. A typical modern electrometer tube (CK-587) has the following parameters at the nominal operating point:

Offset (control grid) current (nominal)	3×10^{-15} A
Offset voltage	-2 V
Offset stability, long term <u>estimate</u>	100 mV
Transconductance	14 μA/V
Input impedance	$\gtrsim 10^{15}$ Ω
Power consumption (includes filament)	7 mW

All of these parameters are subject to rapid and even catastrophic changes as a result of tube aging, cathode poisoning, microphonics, external shock, and vibration, in a manner characteristic of all vacuum tubes.

A NASA-funded effort to improve the characteristics of these tubes is in progress(3.1.1-1). At present, an electrometer tube fully qualified for the space environment does not appear to be available.

(3.1.1-1) H. Z. Reed, <u>Status Report on Physics Branch Low Current Detector Program</u>, Report No. X-623-65-391, Goddard Space Flight Center, Greenbelt, Maryland, October, 1965.

Two particular electrical deficiencies of existing electrometer tubes make them unattractive for new instrument design. First, their absolute voltage offset is inconveniently large and unstable. Two similar devices may be used in a differential configuration, but good tracking of two different tubes with different cathodes in different envelopes cannot be expected. Furthermore, electrometer tubes possess extremely low gain (transconductance). The low value of the transconductance, g_m, is reflected in a high value of the equivalent noise resistance,

$$R_n \sim \frac{2.5}{g_m} \quad \text{(triode)} \qquad (3.1.1-1)$$

The corresponding noise voltage per unit bandwidth is, for the device mentioned

$$v_n = 50 \text{ nV}/\sqrt{\text{Hz}} \quad (1 \text{ nV} = 10^{-9} \text{ V}) \qquad (3.1.1-2)$$

Hence, although the actual thermal noise performance of electrometer tubes is, in fact, close to the theoretically expected value, the absolute value of the voltage noise referred to the input is quite large. Furthermore, the gain in a typical circuit is usually not high enough to eliminate contribution from noise in the following amplifier stage.

These considerations, as well as some tedious experiences with electrometer tubes in the Mariner II program, lead us to conclude that electrometer tubes are not desirable as low-current detectors in space applications. The discussion in the next section shows that the performance of insulated-gate field-effect transistors, while capable of much improvement,

is now competitive with that of electrometer tubes. We do
not expect the trend in favor of solid-state devices to be
reversed, so that there seems to be no reason to consider
further the use of an electrometer tube in a project with
several years of lead time except perhaps as a temporary
laboratory expedient.

3.1.2 Field Effect Transistor Input

The unipolar field effect transistor (FET) is a
voltage-operated device whose characteristics and mode of
operation bear many similarities to those of a vacuum tube.
The resistance of a semiconductor channel, either N type or P
type, is modulated by applying a voltage to the so-called
gate terminal, analogous to the control grid of a vacuum tube.

The electric field of the gate produces a deple-
tion layer which decreases the total resistance by narrowing
the channel. The gate may be simply a back-biased diode (junc-
tion field effect) or an insulated electrode (insulated-gate
field effect, or IGFET). Presently attainable gate leakage
currents are typically 10^{-12} A in a junction FET, and 10^{-13}
in an IGFET. There are data[3.1.2-1] which indicate that a parti-
cular type of IGFET (2N3796) can be operated at a point at
which the gate leakage is only about 10^{-15} A. This effect
depends on the cancellation of two leakage current components,
like the similar cancellation which occurs in an electrometer
tube at the so-called cross-over point. The insulated-gate
type is clearly more suitable for electrometer applications,
but has not been developed to the same degree as the junction
type.

(3.1.2-1) E. J. Kennedy "Gate Leakage Current in MOS Field Effect
Transistors," Proceedings of IEEE, p 109A, August, 1966.

The design of any dc amplifier is greatly facili-
tated by the use of two similar devices in a differential
configuration. The devices should preferably be mounted not
only in the same can but on the same substrate. Still, if
care is taken to provide a common heat sink for two matched
but separately packaged devices, performance approaching that
attained by a single-package can be attained. Junction FET
pairs with absolute offsets of a few millivolts and voltage
offset temperature drifts of 10 μV/°C are commercially avail-
able. At the present time only one differential IGFET is
available, a P-channel device (2N3609) manufactured by General
Microelectronics (Philco). This device, which has been avail-
able for about two years, has the following parameters at the
recommended operating point:

Offset current	$< 10^{-13}$ A
Offset voltage	50 mV
Offset stability (long term estimate)	50 mV
Offset voltage (temp. coefficient)	0.1 mV/°C
Transconductance	250 μA/V
Input impedance	$\gtrsim 10^{15}$ Ω
Power consumption	3 mW

The offset voltage of a given device exhibits hysteresis
effects under temperature cycling, and severe flicker noise,
of magnitude 100 μV $(f_o/f)^{\frac{1}{2}}/\sqrt{Hz}$, where f_o = 1 Hz. This value

is unacceptably high for some applications. Flicker noise
usually results from inadequate treatment of surface layers,
and in insulated-gate FET's is probably caused by impurities
in the silicon dioxide insulating layer at the gate, or by
inadequate techniques in producing it.

Electrometers using this device as an input stage
have been constructed and tested by ATC staff members. An
instrument using the device has been flown in a sounding rocket[3.1.2-2]
The double-differential configuration shown in Figure 3.1.2-1
was used in each instance. In this configuration the differen-
tial electrometer stage is followed by a differential pair of
bipolar transistors and an emitter follower stage, which may
be complementary as shown. The advantages of this configuration
are simple biasing, high common-mode rejection, and excellent
zero stability compared to the ordinary single-ended arrange-
ment. The disadvantage is increased reference noise produced by
the second transistor.[3.1.2-3] Because of the relatively poor voltage
gain and matching of the FET stage, the second stage should be
a matched pair of high-gain transistors, which are commonly
available. The noise output of the circuit shown in Figure
3.1.2-1 has been measured using a 10^{12} ohm feedback resistor.
The total broadband noise observed at the output was 2 mV rms,
corresponding to 2×10^{-15} A referred to the input. The noise
sources include 30 nV/$\sqrt{Hz}$ of midband noise, 1/f noise below
100 Hz, second stage noise, and feedback resistor noise. At
the recommended operating point, the theoretical voltage noise
is that of a resistor of magnitude

$$R_n \approx \frac{0.8}{g_m} \approx 3.2 \text{ K} \qquad\qquad (3.1.2-1)$$

(3.1.2-2)   R. A. Emerling, J. H. Mullins, J. Van Putten, J. O. Maloy,
            and H. G. Bartholomew, "Rocket Gamma Scanning of Nuclear
            Bursts," IEEE Transactions on Nuclear Science, Vol. NS-13,
            No. 1, p 569, February, 1966.

(3.1.2-3)   R. D. Middlebrook, Differential Amplifiers, John Wiley &
            Sons, New York, 1963

or about 10 nV/$\sqrt{\text{Hz}}$, allowing for the contribution of both input transistors. An ideal feedback resistor contributes a thermal noise current

$$\frac{i_n}{(\Delta f)^{\frac{1}{2}}} = \left(\frac{4kT}{R_f}\right)^{\frac{1}{2}} \approx 0.4 \times 10^{-15} \text{ A/}\sqrt{\text{Hz}}, \quad R_f = 10^{11} \; \Omega.$$

$$(3.1.2-2)$$

Unfortunately, resistors in the high megohm range are far from ideal in their noise performance.

ATC experience thus indicates that the measured performance of IGFET devices, in particular the 2N3609 in a complete electrometer, is now comparable to or even superior to the theoretical performance of the best electrometer tube alone, although the measured performance is still about a factor of 3, or 10 db, worse than the theoretically expected value. Newer devices should show improvements.

The ATC staff feels that the 2N3609 device is satisfactory for some laboratory uses and short-term space applications (sounding rocket or balloon flights). Informal reports of difficulties with this and similar IGFET devices may be based on inadequate data taken on inadequately designed circuits. For example, it seems reasonably clear that reports of the fragility of the devices are in fact reports of the failures of improperly protected circuits, since much of the ATC experience is based on the performance of a high-voltage probe used daily in the laboratory. Before such a device is used in a deep-space application, a careful program to improve and qualify the device should be undertaken. Initiation of such a program has been recommended within NASA[3.1.1-1]

(3.1.1-1)   Loc Cit   3.1-11

Junction field effect transistors possess larger input offset currents than insulated gate types, but at present exhibit markedly superior noise performance. Advanced types currently commercially available, which can presumably be packaged in differential configurations, have the following parameters:

Offset current $\quad\quad\quad\quad\quad\quad\quad\quad\quad$ < 10^{-12} A

Offset voltage $\quad\quad\quad\quad\quad\quad\quad\quad$ 10 mV (estimate)
(differential configuration)

Offset voltage (temp. coeff.) $\quad\quad\quad$ 10 µV/°C (estimate)
(differential configuration)

Transconductance $\quad\quad\quad\quad\quad\quad\quad$ 300 µA/V

Power consumption in typical $\quad\quad\quad$ 2 mW
$\quad$ application

The noise voltage produced by such a device should be relatively close to the theoretical value of 5 nV/√Hz. Flicker noise in such devices is for lower than that in existing IGFET devices.

For the specific device (2N4119A) on which the above numbers are based, the manufacturer quotes the following typical noise voltages per root Hertz vs. frequency:

Frequency	Equivalent Noise Resistance	Noise Voltage nV/√Hz
1 Hz	8 M	200
100 Hz	80 K	20
1 KHz	10 K	11
100 KHz	0.6/gm ≈ 2K	5

The value at 1 Hz is an extrapolation based on a 1/f variation
of the noise power density, which the manufacturer states is
approximately the correct low down to frequencies of order
1 Hz. The voltage noise at 1 Hz is thus almost three orders
of magnitude smaller than that of the 2N3609 IGFET. Then com-
parisons are based on typical experiences and are not necessar-
ily representative of the best that can be done with either
device.

3.2 Carrier Electrometers

The effects of amplifier offset and drift may be elimin-
ated if the source current is modulated to produce an ac signal
which is amplified and subsequently synchronously detected and
compared with the input. Flicker noise from the input ampli-
fier may also be eliminated. ATC personnel have designed suc-
cessful flight systems of this type. Two techniques have been
used: modulation of the input capacitance of the amplifier,
and modulation of the detector power supply. These techniques
will be discussed in turn.

3.2.1 Dynamic Capacitor Electrometer

ATC staff members were the first to harden a dy-
namic capacitor electrometer into a flightworthy design and
demonstrate its effectiveness in space applications.$^{(3.2.1-1)}$ A
large portion of the electrometer technology developed for those
missions can be applied to the development of a gas chromato-
graph. A new design would, of course, contain many modifica-
tions and improvements compared to the device described in
Reference 6.

(3.2.1-1)   C. S. Josias and J. L. Lawrence, Jr., "An Electrometer for
Use in Scientific Space Instruments," IEEE Transactions on
Nuclear Science, October, 1966.

For example, the carrier amplifier should use a field-effect transistor, thereby improving noise performance and reducing circuit complexity. Feedback will be linear (resistive). (A/D conversion may be logarithmic if desired.) The reverse was the case in the Mariner II Solar Plasma experiment. The stability of the Mariner electrometer amplifier was masked by the thermal and temporal drift of the vacuum-tube log-diode.

Newer dynamic capacitor modulators are available which are lighter, consume less power, and operate at higher frequencies. Two such devices have been studied by ATC: (1) a piezo-electrically driven tuning-fork unit; and (2) an electrostatically driven diaphragm-type unit.

The most difficult problem among dynamic capacitor manufacturers is usually that of obtaining reasonable unit yields on contact potential specifications. It is our opinion that repeatable industrial control of thermal and temporal variations in contact potential still lies within the realm of witchcraft, notwithstanding applicable textbook theory. Since yields in past projects have seriously affected cost and delivery schedules, we have considered relaxation of contact potential requirements in favor of compensating drifts through frequent periodic rezeroing of the electrometer. In this method, the input signal is disconnected and the output voltage is compared to ground potential and forced close to ground by a subsidiary loop that is closed only during the zeroing operation. During normal operation of the electrometer, the zero correction signal is stored in some manner at the return leg of the dynamic capacitor.

The discussion of the system errors in Reference 6 allows us to compare the expected performance of the dynamic

capacitor modulator with that of the direct-coupled electro-
meter described above. The system described had the following
parameters:

Offset current	$<< 10^{-13}$ A
Offset voltage (long term)	5 - 10 mV
Offset voltage (temp. coeff.)	70 μV/°C
Effective input transconductance (includes capacitor conversion efficiency, transformer ratio, and preamplifier gain)	$\sim$ 20 μA, rms V_{DC} (estimate)
Input impedance	$> 10^{15}$ Ω
Power consumption	$\cong$ 20 mw

The use of field-effect transistors, without a
transformer, should result in a ten-fold increase in input
stage transconductance and a corresponding decrease in voltage
noise.

Examination of this table makes it clear that the
primary advantage of the dynamic capacitance electrometer lies
in its negligible low offset current. The offset voltage var-
iation is an order of magnitude lower than that observed with
existing IGFET devices, but this low value represents a low-
yield selection and is not easily achieved. The automatic re-
zeroing loop suggested above is applicable to the IGFET electro-
meter as well.

For gas chromatographic applications, in which the detector quiescent current may lie in the range 10^{-11} to 10^{-10} A, the low offset current of the dynamic capacitor modulator seems to offer no particular advantage, since the detector current must be subtracted in any case.

3.2.2 Electrometer for Use with Modulated Detector

Some types of current detectors lend themselves to AC modulation of the current stream either by variation of the collector voltage or by the associated grid structures. A plasma wake electrometer of this type was flown on the Agena vehicle used for rendezvous in the Gemini program (Reference 3.2.2-1). In this system a stream of ions entering a Faraday Cup was interrupted 3840 times per second with retarding potential on a control grid. The collected signal was a square-wave current that was processed with a 3840-Hz AC electrometer and 5-decade logarithmic A/D conversion system designed by ATC. The electronic system errors in this experiment contributed about 1% to the total measurement uncertainty.

A modulated detector system is still sensitive to baseline errors in the detector current during the portion of the cycle that the detector operates. One important consideration affecting the desirability of detector modulation is that the signal be modulated exclusively as compared to modulation of all inherent detector characteristics including errors such as baseline and offset. One excellent example of this consideration in the field of Gas Chromatography is the electron capture detector. This detector, though not applicable to this experiment, provides most stable operation in a pulsed mode (Reference 3.2.2-2).

3.2.2-1   ATC Staff, "Final Report on the Gemini Plasma Wake Instrument Development Program," prepared for Electro-Optical Systems, Inc., 1 January 1966.

3.2.2-2   J.E. Lovelock, "Electron Absorption Detectors and the Technique for Use in Quantitative and Qualitative Analysis by Gas Chromatography," Vol. 35, No. 4, p 474, April, 1963.

With respect to the signal processing chain, off-sets are introduced by the synchronous demodulating device. The AC amplifier must be stable and sufficiently fast to follow the input variations without introducing appreciable variations in either amplitude or phase. The plasma wake instrument used a chain of stable broadband feedback amplifiers followed by a full-wave demodulator and active filter. The absence of over-all feedback to the detector was acceptable in this instance since the error from amplifier gain and demodulator offset variation was negligible compared to detector variations.

Such a system would also be acceptable for gas chromatography. The complexity of the electrometer section is comparable to that of the dynamic capacitor electrometer.

3.3 AC-DC Electrometers

The carrier electrometers discussed in the previous sections are still subject to voltage offset errors. For example, the dynamic-capacitor electrometer is subject to thermally-induced voltage offset error in the order of 5 to 10 mV.

When the feedback loop is closed, the offset error of the input device appears as a voltage difference between the input summing mode and the voltage reference (ground). If this voltage is chopped with a switch whose offset is lower than that of the input amplifier, the resulting AC voltage may be amplified and fed back to the reference point to reduce the offset to that of the switching device. This technique is particularly important in the design of integrators with extremely low drift. A block diagram of such a system is shown in Figure 3.3-1.

Typical parameters of the three commonly used chopping devices are listed in Table 3.3-1.

Device	Voltage Offset	Current Offset (leakage)	Closed Resistance
Mechanical Chopper	10-20 µV	not applicable	0 Ω
Bipolar transistor dual-emitter chopper	50 µV	10^{-9} A	50 Ω
FET chopper	0	10^{-11} - 10^{-12} A	10 K

Table 3.3-1

Chopper Parameters
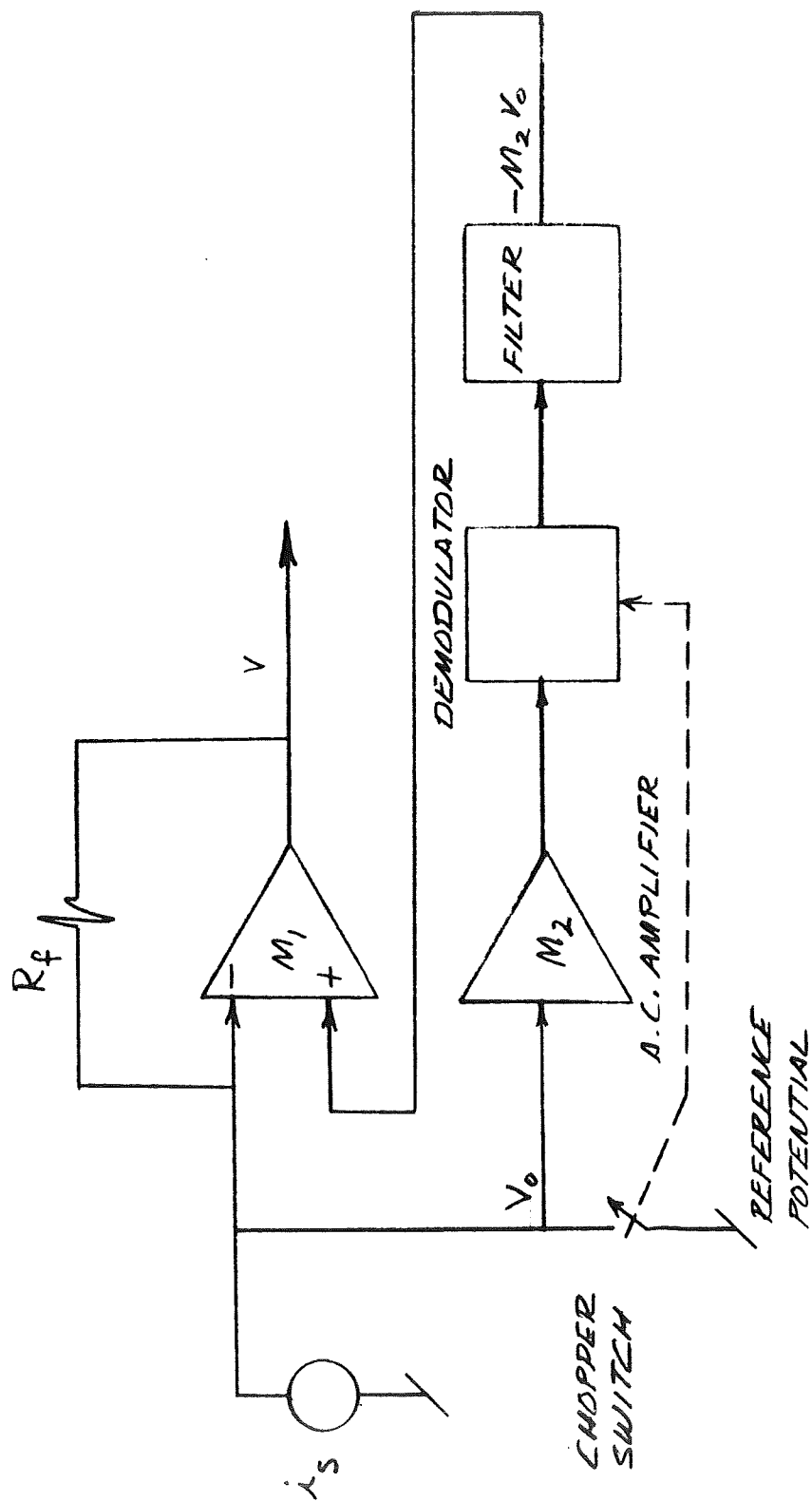
AC - DC ELECTROMETER

FIGURE 3.3-1

The DC performance of these devices described in the table is not the only criterion of use, since mechanical choppers have limited lifetime and require high drive power. The chopper drive signal can be capacitively or inductively coupled into the AC amplifier input to produce a spurious offset signal. Such difficulties are aggravated by use of choppers requiring high drive power. The data in the table shows that except for electrometer applications requiring current offsets of less than 10^{-11} or 10^{-12} A at room temperature, an IGFET chopper offers superior performance, since it is essentially a modulated resistance with no inherent voltage offset.

4.0 INTEGRATION

This section is devoted to discussion of techniques for measurement of areas of chromatographic peaks. Considerable thought has been given to this topic since integration provides the truly quantitative measurement independent of form factor.

4.1 Direct Analog Integration

This section discusses direct analog integration of the detector signal current. This approach utilizes an operational amplifier with Miller-type capacitive feedback to integrate the detector current for a time interval sufficiently long to measure any detector output.

4.1.1 Integrator Configuration

Since voltage changes at the input of the integrator will upset the baseline stabilization, integration is best performed operationally as shown in Figure 4.1.1-1. This type of circuit maintains a "virtual ground" at the input by use of negative feedback.

Within limitations (to be discussed later), the integrator output can be shown to be

$$e_o \cong - \frac{1}{C} \int_0^T i_d \, dt, \qquad (4.1.1-1)$$

where e_o is the integrator output voltage,
   C is the integrating capacitance,
   T is the time (since the last reset) of integration,
   i_d is the detector current in excess of the static (or baseline) value, I_d, and
   t is time.

4.1.1.1 Feedback Capacitors

Since the input of the operational amplifier will remain very close to ground, the feedback capacitors

RESET

FROM
DETECTOR

$i_d + I_d$

$\approx I_d$

BASELINE
STABILIZATION

$-A$

e_o
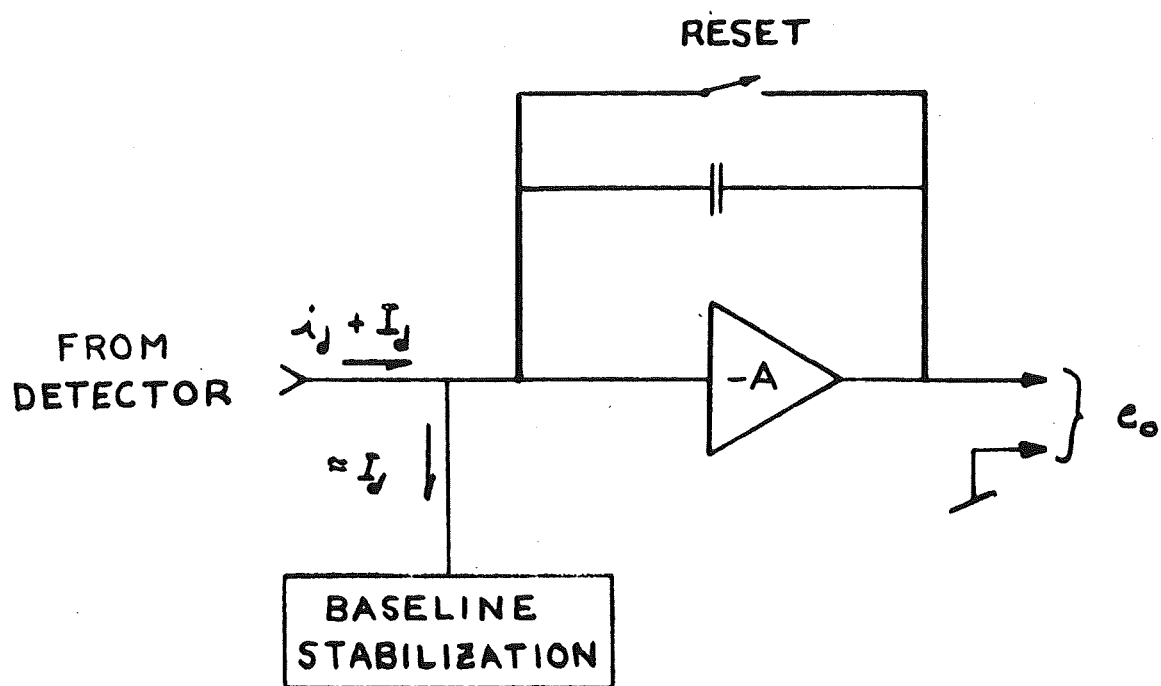
BASIC INTEGRATOR

FIGURE 4.1.1-1

required can be computed from the net charge accumulated in Equation 4.1.1-1

$$C = \frac{Q}{V} , \qquad\qquad (4.1.1.1-1)$$

where Q is the net accumulated charge and V is the corresponding output voltage desired.

The smallest capacitor is determined by the minimum charge which must be detected and the corresponding voltage. This sets the system threshold. Assuming output measurement will be in the form of logarithmic analog-to-digital conversion, a typical threshold would be 100 mV. Using this value and a charge of 10^{-12} coulomb, we calculate 10 pF for the minimum capacitance. For $10^{3/2}$ (≈ 31.6) volts full-scale and 10^{-5} coulomb, the maximum required capacitance is 0.316 µF. Since 2.5 decades are covered on each logarithmic scale, three scales will be required to cover the specified input charge range. Since the quantizing resolution is approximately constant for a logarithmic converter throughout the range, integrators using such conversion will not require over-lapping scales. The capacitances and corresponding charge ranges are shown in Table 4.1-2.

If a 10-bit linear analog-to-digital converter were used, the combined amplifier/converter threshold could be about 10 millivolts and amplifier full scale 10 volts. The integrator feedback capacitors would then be calculated using these lower voltages; however, the circuit considerations are not basically changed. The integrator used with a linear analog-to-digital converter must include enough scale overlap

Table 4.1-2

Integrator Scaling Parameters (Using Log A/D Conversion)

Scale Designation	Capacitance (pF)	Charge Range (Coulombs)
00	10	10^{-12} to 3.13×10^{-10}
01	3,160	3.16×10^{-10} to 10^{-7}
10	10^6	10^{-7} to 3.16×10^{-5}

to preserve the scale-to-scale accuracy. The largest error occurs just after scale switching. If switching occurs at almost full scale (10 volts) and the voltage readout resolution is 10 millivolts, the maximum error is computed as follows:

$$\% \text{ error } = \left(10^{-2}\right) \left(\frac{k}{10}\right) \left(100\%\right) = 0.1 \text{ k}\%, \quad (4.1.1.1-2)$$

where k is the ratio of the feedback capacitance on the higher scale to the capacitance on the lower scale. For ± 5% error, k is 50. The required feedback capacitances and corresponding charge ranges are shown in Table 4.1-3.

4.1.1.2 Error Calculations

A block diagram of the approach is shown in Figure 4.1-4. For purposes of error and response calculations, we can use the equivalent circuit shown in Figure 4.1-5. C_f is the feedback capacitance including any stray capacitances, and R_f is the resistance shunting C_f. R_i is the equivalent resistance shunting the amplifier input, and includes the amplifier input resistance, the detector shunt resistance, and the baseline stabilization resistance. Similarly, C_i includes all the capacitance shunting the amplifier input. A_v is the amplifier voltage gain. V_o and I_o are the amplifier offsets.

4.1.1.2.1 Capacitor Leakage Resistance Error

The transfer impedance, Z_T, is given by

$$Z_T \equiv \frac{e_o}{i_i} = -Z_f \left[\frac{1}{1 + \left(\dfrac{Z_i + Z_f}{A_v Z_i}\right)} \right] . \quad (4.1.1.2.1-1)$$

Table 4.1-3

Integrator Scaling Parameters (Using Linear A/D Conversion)

Scale Designation	Capacitance (F)	Charge Range (Coulomb)
00	10^{-10}	10^{-12} to 10^{-9}
01	5×10^{-9}	5×10^{-11} to 5×10^{-8}
10	2.5×10^{-7}	2.5×10^{-9} to 2.5×10^{-6}
11	1.25×10^{-5}	1.25×10^{-7} to 1.25×10^{-4}
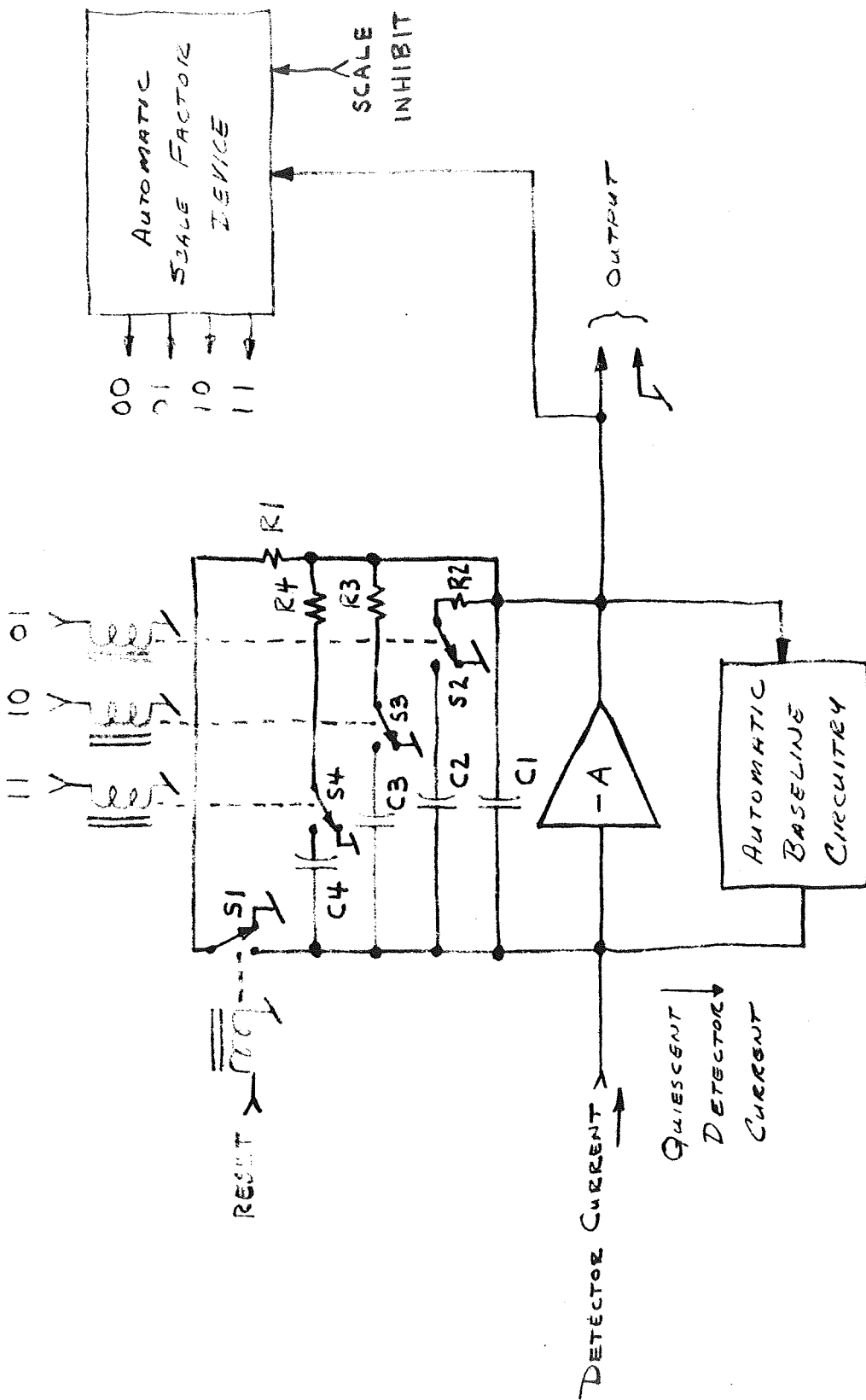
INTEGRATOR SCHEMATIC

FIGURE 4.1-4

$$z_f = \frac{R_f}{1 + s R_f C_f}$$

$$z_i = \frac{R_i}{1 + s R_i C_i}$$
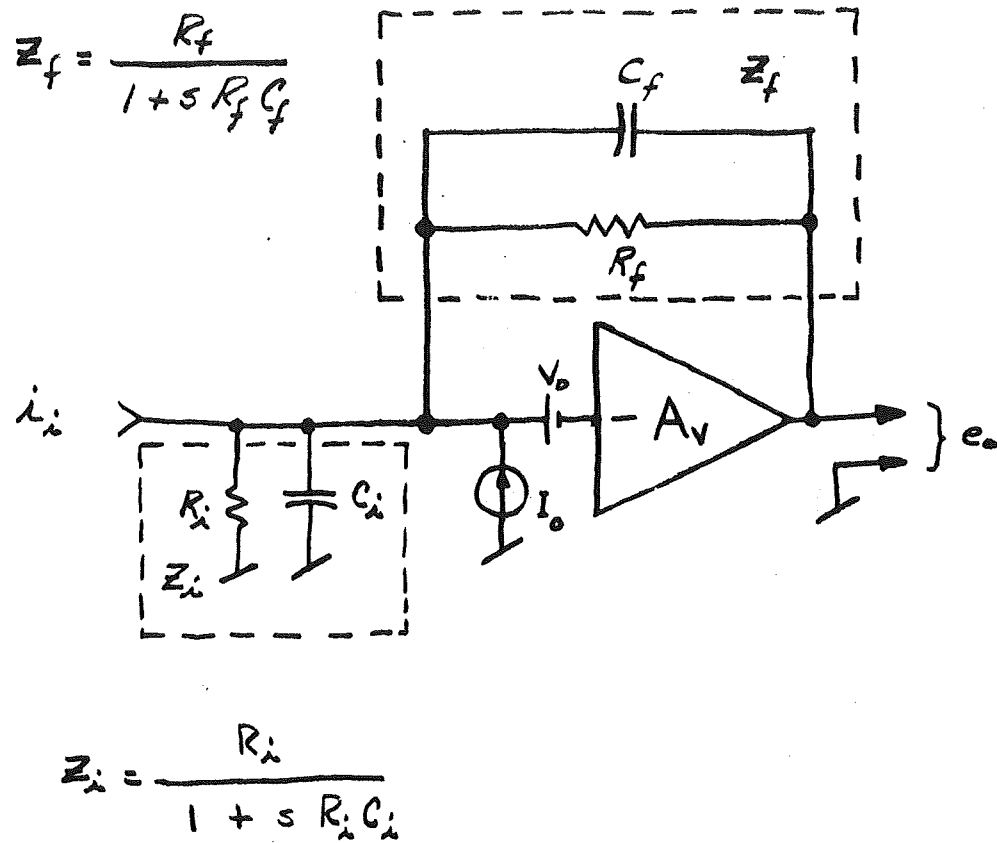
INTEGRATOR EQUIVALENT CIRCUIT

FIGURE 4.1-5

Thus if Z_T is to approximate closely Z_f, $\dfrac{A_v Z_i}{Z_i + Z_f}$ (which is the voltage gain around the integrator loop) must be made large at all frequencies of interest. For the range of frequencies where the integrator loop gain is high, Equation 4.1.1.2.1-1 becomes

$$Z_T \cong Z_f = \frac{R_f}{1 + C_f R_f} . \qquad (4.1.1.2.1-2)$$

For frequencies significantly higher than $1/(2\pi C_f R_f)$,

$$Z_T \cong \frac{R_f}{C_f R_f} = \frac{1}{C_f} . \qquad (4.1.1.2.1-3)$$

Equation 4.1.1.2.1-3 is recognized as the proper transfer impedance for an integrator.

The basic accuracy limitation is due to the resistance shunting the feedback capacitor. The feedback time constant, $R_f C_f$, must be large compared to the analysis time if accuracy is to be maintained. For small errors due to the feedback time constant, it can be shown that the fractional error, k, is

$$k \cong \frac{T}{R_f C_f} , \qquad (4.1.1.2.1-4)$$

where T is the time from the integration until readout. If the readout occurs 10 seconds after a charge impulse and 1% error is allowed (k = 0.01), $R_f C_f \geqq 1000$ seconds and $R_f = 10^{14}$ ohms for the 10 pF capacitor. By careful attention to circuit design,

component selection, and integrator layout, the required R_f
can be realized. The time constant is more easily realized
with the higher-valued capacitances since the required R_f is
smaller.

The shunting paths through
the relay contacts (S_1, S_2, S_3, S_4 in Figure 4.1-4) are elimin-
ated by shorting to ground the output side of any relay not in
use. For example, when the integrator is on the most sensi-
tive scale (00), all relay wipers are grounded. Therefore the
output voltage cannot appear across the relay leakage resistance.
To increase the output-to-input leakage resistance further, the
amplifier input must be completely guarded by grounded shields.
By careful attention to these details, error (on the 10 pF
scale) due to output-to-input leakage resistance can be held
to about 1% for a 10-second measurement interval.

4.1.1.2.2 Integrator Input Offset Errors

Input offsets are represented
by V_o and I_o in Figure 4.1-5. The current offset, I_o, must
include the difference between the detector quiescent current
and the baseline bucking current.

The tolerable current offset
can be determined by calculating its charge (time integral of
the current) over the integration interval. For this charge to
equal the integrator threshold, the tolerable current offset is

$$I_o = \frac{Q_T}{T} , \qquad\qquad (4.1.1.2.2\text{-}1)$$

where Q_T is the desired charge threshold of the integrator and
T is the time that the integrator is gated on. For example,

if Q_T were 10^{-12} coulomb and T were 10 seconds, the net offset current (after baseline compensation) must be less than 10^{-13} amperes.

The allowable voltage offset can be approximated by calculating the voltage required across R_i to develop the permissible I_o.

$$V_o = I_o R_i = (10^{-13})(10^{11}) = 10^{-2} \text{ V or 10 mV.}$$

$$(4.1.1.2.2-2)$$

The baseline compensation circuitry will be required to null the offsets to less than the values shown above for a 10-second integration interval and 10^{-12} coulomb threshold. By reducing the integrating time or increasing the threshold charge, the offset specifications can be relaxed.

4.1.1.2.3 Finite Loop-Gain Errors

There are two major errors caused by the finite loop gain. The most serious is the scale factor decrease and its instability at low loop-gain levels. The second error is caused by charge loss to the shunt input capacitance (C_i in Figure 4.1-5) of the integrator and through the shunt input resistance (R_i in Figure 4.1-5).

Figure 4.1-6 (a) is a schematic of the integrator and Figure 4.1-6 (b) is an equivalent circuit from which the gain-induced errors can be calculated.
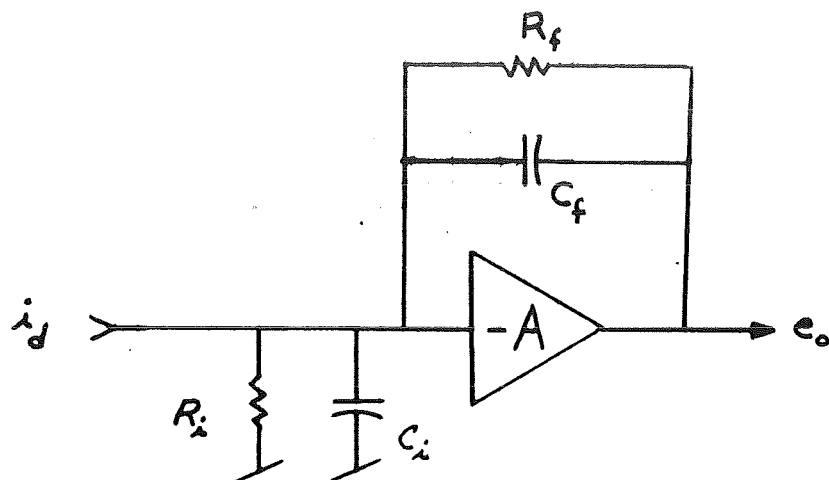
(a) INTEGRATOR SCHEMATIC (SIMPLIFIED)
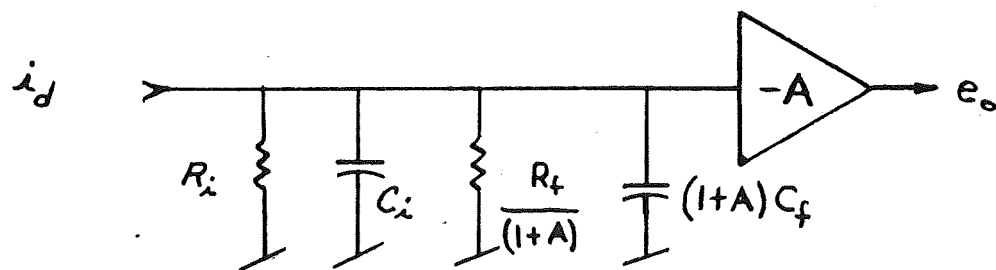
(b) EQUIVALENT CIRCUIT

INTEGRATOR SCHEMATIC TRANSFORMATION

FIGURE 4.1-6

4.0-12

From Figure 4.1-6 (b) it is clear that the integrator shunt input capacitance, C_i, causes a relative error, k, given by

$$k = \frac{C_i}{C_i + (1 + A) C_f} \approx \frac{C_i}{(1 + A) C_f} . \qquad (4.1.1.2.3-1)$$

The gain requirement deduced from Equation 4.1.1.2.3-1 is

$$A \geq \frac{C_i}{k C_f} - 1 . \qquad (4.1.1.2.3-2)$$

For example, if $C_i = 10^{-10}$,

$$C_f = 10^{-11}, \text{ and}$$

$$k = 0.01 \text{ (1\% error)},$$

then

$$A = 999. \qquad (4.1.1.2.3-3)$$

The time decay of the output voltage is determined by the time constant of the equivalent circuit. C_i can be neglected since it must be much smaller than $(1 + A) C_f$. The remaining elements yield a time constant of

$$T = C_f \frac{(1 + A) R_i R_f}{(1 + A) R_i + R_f} \qquad (4.1.1.2.3-4)$$

This is the same as the time constant of a capacitor C_f which is shunted by resistors $(1 + A) R_i$ and R_f. The value of R_f for an error of 1% has been computed in Section 4.1.1.2. If R_i is allowed to cause the same error, the required gain is

$$A \geq \frac{R_f}{R_i} - 1. \qquad (4.1.1.2.3-5)$$

The minimum allowed value of R_f is 10^{14} Ω. If $R_i = 10^{11}$ Ω,

$$A \geq 999. \qquad (4.1.1.2.3-6)$$

A summary of the integrator errors is tabulated in Figure 4.1-7. These errors can be reduced by changing amplifier gain and details of scaling, baseline stabilization technique, and A/D conversion. More specific detector characterization is required before the optimum configuration can be determined. The amplifier frequency response must extend to about 1.6×10^{-4} Hz (1000-second time constant) on the low end. The high-frequency response will be determined by the shape of the current pulse. The upper cutoff frequency will probably by about 10 Hz.

4.1.1.3 Amplifier Rate Limit

The final amplifier characteristic to be considered is its rate limit. It is by no means simple to specify this characteristic since it involves specific detector characteristics, baseline stabilization details, and electrometer input characteristics.

Error Source	Equivalent Offset (Coulomb)	Scale-Factor Error (%)
* A/D Conversion (log, 8 bits)	10^{-13}	$\overline{<}$ 1%
Feedback Capacitor Tolerance	---	$\overline{<}$ 1%
Feedback Capacitor Leakage Resistance	---	$\overline{<}$ 1%
Amplifier Offset Current	$\overline{<}$ 10^{-12}	---
Amplifier Offset Voltage	$\overline{<}$ 10^{-12}	---
Amplifier Finite Loop Gain		
1) Scale Factor	---	$\leq$ 1%
2) Input Capacitance	---	$\leq$ 1%
3) Input Resistance	---	$\leq$ 1%

Maximum total worst-case error $\leq$ 2.1 x 10^{-12} + 6% of signal.

* Linear 10-bit conversion (4 scales)
  yields 10^{-13} coulomb ± 5%

Figure 4.1-7

Summary of Integrator Errors

If the amplifier rate limit is too low, the integrator loop opens and a voltage builds up on the summing point capacitance. This can have two detrimental effects:

1) Detector current might change due to the change in voltage across the detector.

2) Integrator performance may degradate due to bias change.

For modest detector voltage changes (say 10 V), the detector current will not change appreciably since the detector operates in the current-saturated mode. However, much larger voltage changes are apt to cause serious errors. The actual detector current sensitivity to detector voltage will have to be determined by breadboard tests.

High electrometer input voltages may cause performance degradation or failure in certain types of electrometers. For example, the electrometer may block when overloaded, may require a long recovery time, or it may dissipate the charge signal by drawing excessive input current.

It should be noted that simple nonlinearity itself or temporary blocking is not harmful as long as the signal charge is stored on the input capacitance.

In order to be perfectly safe, however, a rate limit can be specified such that linearity is maintained throughout the analysis. The integrator (Figure 4.1-8) output voltage is

$$v_o = \frac{q}{C} \qquad (4.1.1.3-1)$$

$$I_p = 10^{-6}A$$
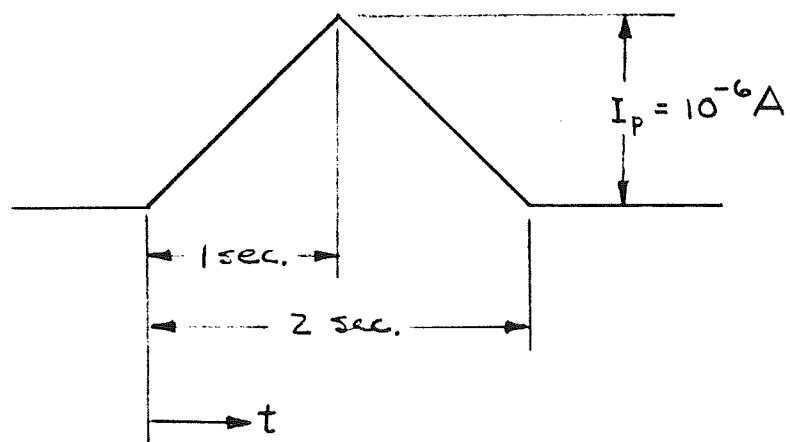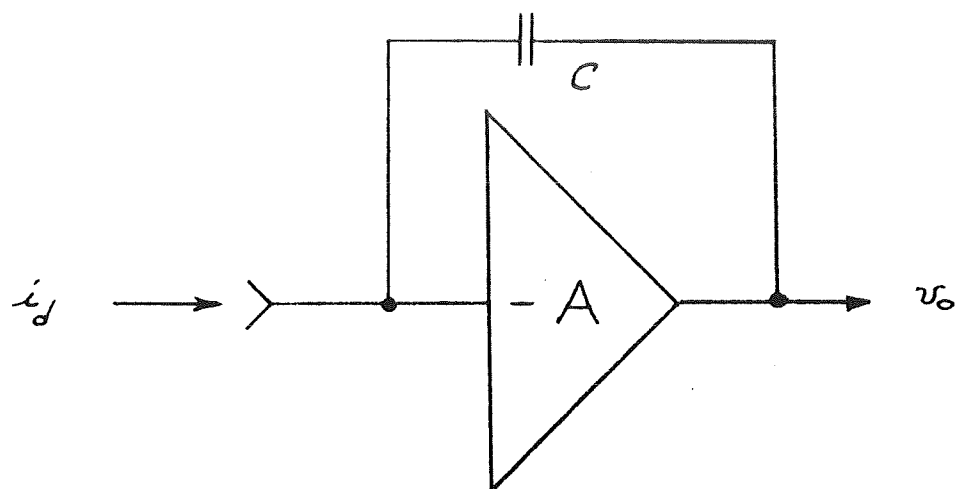
LEADING EDGE SLOPE = $10^{-6}A/sec$

CURRENT = $10^{-6}t$ AMPERES, for $0 < t < 1\,sec.$

FIGURE 4.1-8 INTEGRATOR & CURRENT PULSE

and the output voltage slope is

$$\frac{dv_o}{dt} = \frac{1}{C}\frac{dq}{dt} = \frac{i_d}{C} . \qquad (4.1.1.3-2)$$

For the leading edge of the pulse shown in Figure 4.1-8

$$i_d = kt \qquad (4.1.1.3-3)$$

where k is the slope of the pulse. From this it can be shown that

$$i_d = \sqrt{2qk} \qquad (4.1.1.3-4)$$

where q is the charge accumulated. This can be refined to show that

$$i_d = \sqrt{2v_oCk} . \qquad (4.1.1.3-5)$$

By substituting (4.1.1.3-5) into (4.1.1.3-2) we obtain

$$\frac{dv_o}{dt} = \sqrt{\frac{2kv_o}{C}} . \qquad (4.1.1.3-6)$$

Equation 4.1.1.3-6 shows that the maximum dv_o/dt occurs when v_o and k are maximum and C is minimum. The greatest value of

v_o is at full scale, and k is maximum for the largest input. C is lowest on the most sensitive scale. Thus the maximum slewing rate occurs on the most sensitive (10 pF) scale and is

$$\frac{dv_o}{dt}\bigg|_{max} = \sqrt{\frac{2 \times 10^{-6} \times 31.3}{10^{-11}}} = 2500 \text{ V/sec.}$$

$$(4.1.1.3-7)$$

A summary of the electrometer specifications are tabulated in Table 4.1-9.

4.1.5 Integrator Operating Cycle

The integrator sequencing is as follows (refer to Figure 4.1-5:

1) Close all feedback switches to reset integrator.

2) Open all switches and baseline stabilize using the 10 pF feedback capacitor.

3) Set baseline current constant and start analysis.

4) Switch to next larger capacitor if output voltage exceeds full scale.

5) Continue integration for specified time interval, then

6) read output voltage and scale factor.

Programmer commands are required to control the integrator sequence.

Input resistance	$> 5 \times 10^{11}\ \Omega$
Input capacitance	< 50 pF
Input offset current	$< 10^{-11}$ A
Input offset voltage	< 1.0 V
Voltage gain (from 10^{-4} Hz to 10 Hz)	1000 V/V
Output voltage rate limit	> 2500 V/sec.
Output impedance	$< 200\ \Omega$

Table 4.1-9

Electrometer Specifications

4.2 Post Analog Integration

Post analog integration is defined here as analog integration following an analog electrometer. In this configuration the integrator must process the electrometer output to obtain the integral of the detector current.

Consider the electrometer required to handle the specified range of currents (10^{-13} to 10^{-6} A). This dynamic range (10^7) requires scale switching such as shown in Figure 4.2-1. The output of the electrometer can be shown to be

$$e_o = -Z_f \left(\frac{1}{1 + \frac{Z_f + Z_i}{A_v Z_i}} \right) i_i \qquad (4.2-1)$$

The parameters are defined in Figure 4.2-2.

For sufficiently high loop gain $\dfrac{A_v Z_i}{Z_i + Z_f} \gg 1$,

$$e_o = -Z_f i_i; \qquad (4.2-2)$$

and for radian frequencies far below

$$\omega = \frac{1}{R_f C_f}, \qquad (4.2-3)$$

$$e_o = -R_f i_i. \qquad (4.2-4)$$

The automatic scale-factor device is required to select a scale such that the output voltage remains at a level that can be processed by the integrator without excessive error.

Now that the current is converted into a voltage, this voltage must be reconverted into a current in order to integrate the voltage. The circuitry required to integrate the
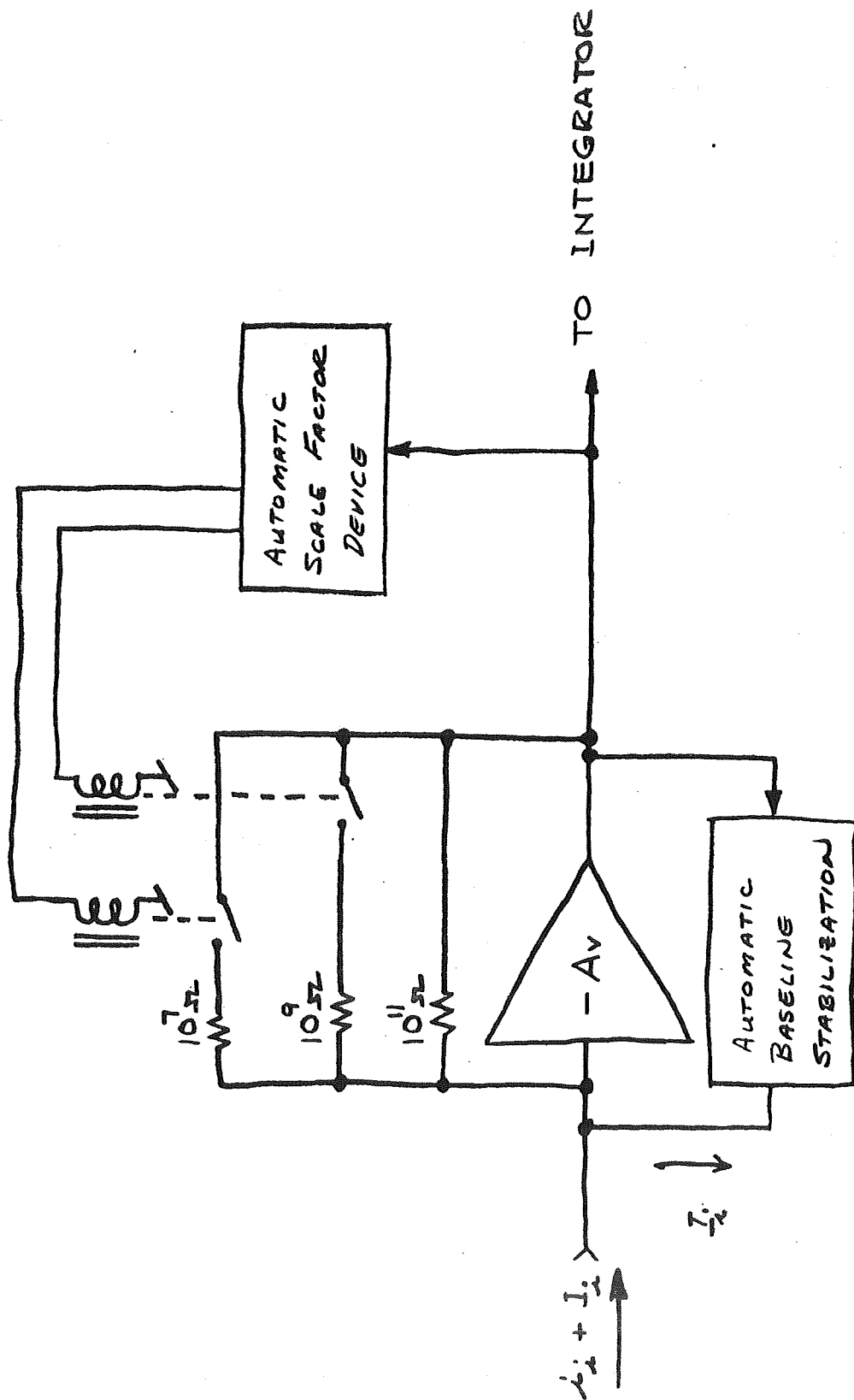
FIGURE 4.2-1   AUTOMATIC SCALE-SWITCHING ELECTROMETER WITH BASELINE STABILIZATION

$$z_f = \frac{R_f}{1 + s R_f C_f}$$

$$z_i = \frac{R_i}{1 + s R_i C_i}$$
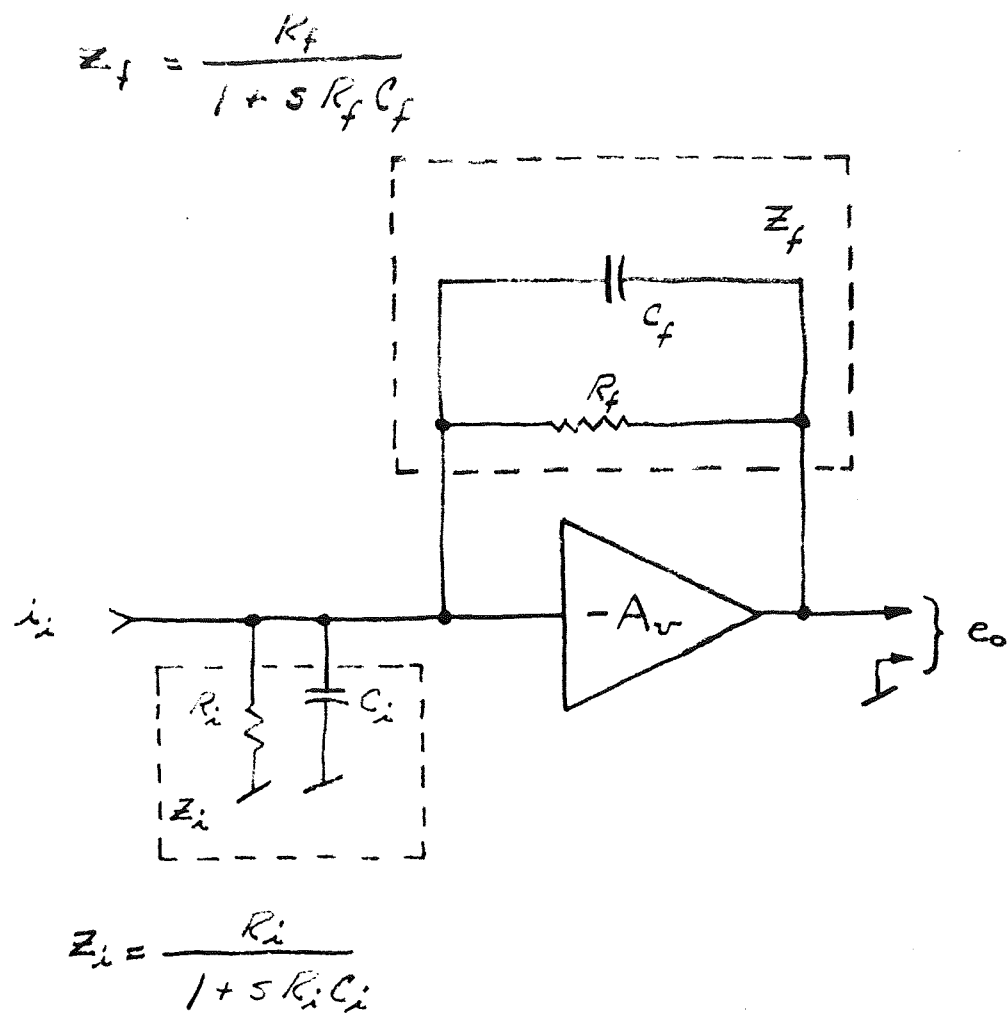
FIGURE 4.2-2 ELECTROMETER EQUIVALENT CIRCUIT

reconstructed current accurately is virtually the same cir-
cuitry required for direct integration. In view of this fact,
the electrometer circuitry can hardly be justified for deter-
mination of the net charge delivered by the detector. If one
is required to determine other parameters of the current pulse,
use of the electrometer may be indicated.

For low accuracy, restricted-range measurements, use of
the electrolytic cell integrator may be indicated.

4.2.1 Electrolytic Cell Integrator

The Bissett Berman "E" cell is an electroplating
component that integrates by plating silver from one electrode
to another as a function of current between the electrodes. One
of the electrodes contains all of the silver. At the beginning
of the sequence, current through the cell causes the silver to
plate onto the bare electrode. Thus, the amount of plating
accumulated is a function of charge through the cell. Since
the action is completely reversible, the cell can be read out
by applying a fixed reverse current of a known value. The time
for the solution to be replated is proportional to the integral
of the signal.

The voltage drop across the cell during plating is
about 50 mV. As the plating terminates, the voltage drop in-
creases to greater than 400 mV, and this abrupt change is used
to signal the end of integration.

The cells typically are rated at 120 µA/hr. The
maximum current permissible is less than 5 mA, and the minimum
measurable charge is 1 µAs, or 10^{-6} C.

The cell, however, has a dynamic range which is
limited by the maximum and minimum currents required for re-
liable operation over the temperature range. Typically, I_{max}=120 µA
and I_{min} = 5 µA at -55°C which are less than two decades apart.
The cells, thus, are not practical for use in wide dynamic range

devices such as gas chromatographs.

4.3 Digital Integrating Electrometer

The digital integrating electrometer shown in Figure
4.3-1 operates as follows: The input current, i_s, is inte-
grated on the electrometer feedback capacitor C_f. The out-
put of the electrometer may be amplified by a stable dc post-
amplifier as required. The eventual output is fed into a
level discriminator or comparator whose digital output is
used for two purposes: 1) to trigger a digital counter;
2) to deliver a pulse of negative charge to the input by
means of an appropriate pulse-forming network. If the magni-
tude of the feedback charge per pulse is Q_f, then the dis-
criminator operates at a frequency $f = i_s/Q_f$. The input
charge delivered by the source during an interval of time
T is given by

$$Q = \int_0^T idt, \qquad\qquad (4.3\text{-}1)$$

and is approximated by NQ_f, where N is the number of charge
pulses fed back as well as the number of events recorded by
the digital counter. The synchronizer shown ensures that
only discrete quanta of charge are fed back and that the
charge pulser does not operate at too high a rate.

This system has the advantage that the analog integra-
ting electrometer is used only as a null-sensing device. The
gain and stability are determined by the offset errors of the
amplifier and detector and by the gain and offset errors of
the charge pulsing network. The value of the feedback capa-
citor is not involved in the gain determination.

A breadboard system of this type, using a 2N3609 IGFET
integrating electrometer, was designed by ATC personnel for

measurement of currents from beam monitor ion chambers at the
California Institute of Technology 1.5 GeV electron synchrotron,
to replace ancient vacuum-tube integrators which work on essen-
tially the same principle. Systems operating on the same prin-
ciple are used in a number of commercially-available voltage-
to-frequency converters and integrating digital voltmeters.
These commercial devices are of course not intended for low
current measurements, but even so, have a typical maximum sensi-
tivity of about 10^{-9} A, and have been used as ion current inte-
grators at the Cambridge Electron Accelerator.

The considerations relevant to the design of such an elec-
trometer system are discussed in the following subsections.

4.3.1 Effects of Offset Errors

Unavoidable system errors are introduced by the
current and voltage offset of the electrometer and by the cur-
rent and voltage offset errors and gain variations of the charge-
forming network, as well as the corresponding errors of the post-
amplifier, if one is used.

Errors which are avoidable, at least in principle,
are introduced by the finite open-loop gains of the amplifier
and by the rounding error inherent in the discrete charge feed-
back scheme. (The gains may always be made larger, and the analog
output of the electrometer may also be read.)

The magnitudes of the unavoidable offset errors
will now be discussed.

According to equation 3.1-6 drifts are produced by
current offsets or noise at the integrator amplifier input.
Drifts are also produced by voltage offsets if the source impe-
dance R_o is finite.

The mean component of the drift can be cancelled
by an appropriate baseline stabilizing network like that des-
cribed in Ref. 4.3.2-1. The fluctuating component produced
by low-frequency noise does no harm unless it is large enough
to operate the comparator relatively frequently. If the charge
feedback system delivers only one sign of charge, noise of all
frequencies may be rectified. Acceptable commercial integra-
ting digital voltmeters contain networks which feed back both
signs of charge. The gains of the two networks must be equal
if the instrument is to possess the same calibration for positive
and negative inputs.

Use of only one sign of feedback charge is accep-
table provided that the noise counting rate can be made negli-
gible.

A device exhibiting a large flicker or excess
voltage noise, as do presently available insulated-gate field-
effect transistors, should be used in configurations with high
input impedance to minimize the fluctuation in the drift.

4.3.2 Charge Feedback Systems

Two methods for feeding back charge to the input
have been studied. The first technique employs a capacitor
which is charged to a reference voltage and is then discharged
into the input each time the discriminator operates, as shown
in Figure 4.3.2-1.

This technique is subject to thermally or temporally-
induced error in either the capacitor or the reference voltage.
With modern components, errors from these sources can be made less

---

4.3.2-1   J.H. Marshall, "A Capacitor Storage Scheme for Gas
          Chromatograph Detector Quiescent Current Compensation,"
          JPL Space Programs Summary No. 37-24, Vol. IV, 213.

Integrator

Electronic switch
operated by comparator

$Q_f = CV_o$
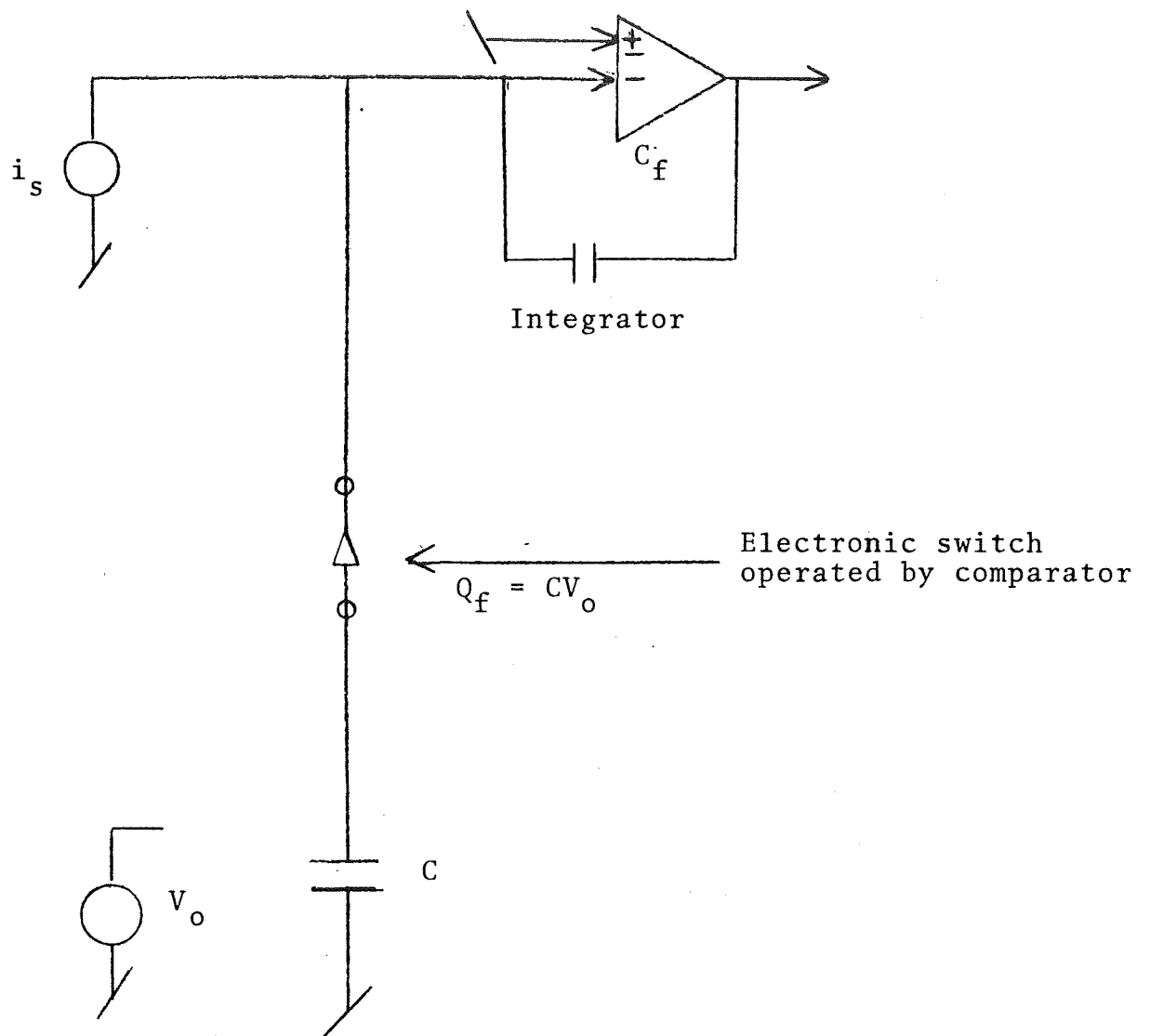
Figure 4.3.2-1

Capacitative Charge Feedback Network

than 0.1% over the full military temperature range.[4.3.2-2, 4.3.2-3]
Transistor or diode switches possess voltage offsets which
can be made less than 1 mV, or 0.01% of a 10 V reference.
However, junction devices possess large leakage currents,
typically at least 10^{-10} A at 20°C, which make them unsuitable
for low-current applications. Insulated-gate field effect
switching transistors exhibit no voltage offset at all, and
possess current offsets in the range of 10^{-11} to 10^{-12} A at
20°C. Such switches may be used in applications where a base-
line error of this magnitude is acceptable, provided the upper
limit of the temperature range is not large. At 100°C, a
10^{-12} A leakage increases to more than 10^{-9} A.

Timing of the switch operation is uncritical,
except that enough time must be allowed to charge and dis-
charge the capacitor completely through the finite on-resis-
tance of the switch.

During the time the switch is closed, high fre-
quency voltage noise at the input is amplified by the ratio
$(C_f + C)/C$.

In the simple system shown, an additional error
in the fed-back charge is introduced by the voltage offset
of the integrator, in that the capacitor does not discharge
completely. This error may be eliminated by using a double-
pole switch to connect the low side of the capacitor to the
electrometer output. If this procedure is used, the charge Q
left on the integrating capacitor depends on the ratio of

4.3.2-2 ATC Staff, "An Experimenter's Handbook for Space Instru-
         ment Design," Sections 3.1 and 3.7, 7/29/66.
4.3.2-3 T.M. Harrington and J. H. Marshall, "A Pulse-Height
         Analyzer for Charge-Particle Spectroscopy on the Lunar
         Surface." In Press.

the feedback capacitance to the integrating capacitance:

$$Q = \frac{C_f}{C + C_f} Q_f$$

The value of the integrating capacitor may become important in determining the gain of such a system, so a stable component must be used.

A second possible technique, using resistive feedback, is shown in Figure 4.3.2-2.

Errors in this system are introduced by variations in the reference voltage, the time T, and the resistance R. All may be made negligible (>0.1%) over the full military range. To achieve this accuracy, the time interval should be crystal controlled, the rise time of the switch should be appropriately short compared to T, and stable resistors must be used.

Errors are also introduced by the offsets of the switch and by rectification of voltage noise produced by the presence of a relatively low impedance at the input during the on time of the switch. A switch with a very small current offset may be made by generating the reference voltage with a stable current source loaded by a low output impedance; as shown in Figure 4.3.2-3.

This scheme was employed in the breadboard ion current integrator mentioned earlier. The output of the device exhibited relatively large low-frequency fluctuations, presumably of directly transmitted flicker noise

$$Q = \frac{V_o T}{R}$$

Electronic switch closed by
discriminator for time T
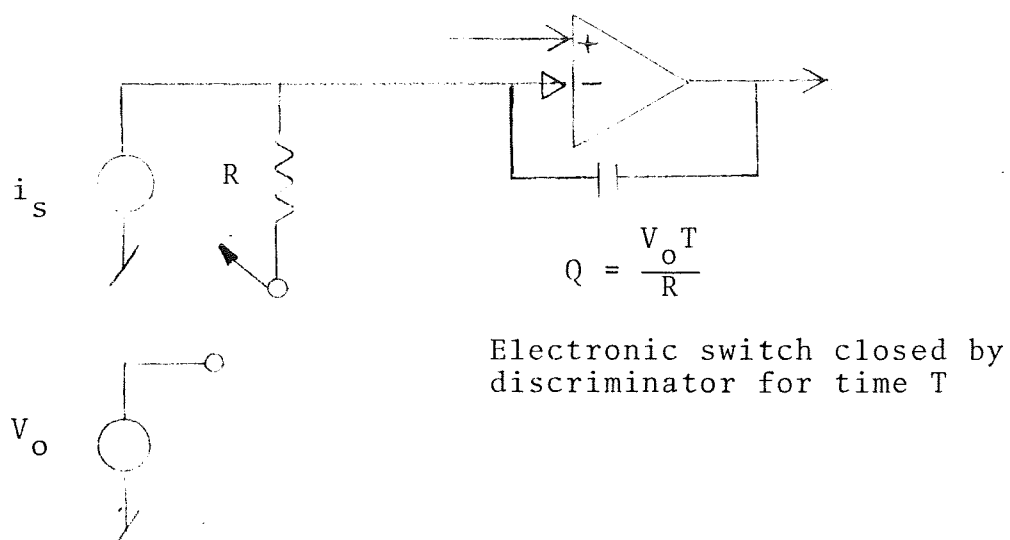
Figure 4.3.2-2

Resistive Charge Feedback Network

$$V_o = R_L i_o$$
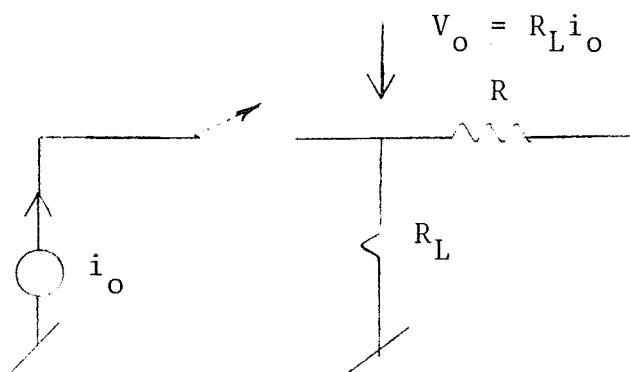
Figure 4.3.2-3

Low-Leakage Resistive Charge Pulser

and because the feedback resistor R was continually con-
nected to ground through the low impedance, R_L, making the
drift rate sensitive to noise in the IGFET input stage. The
maximum current the device could accept was comparable to that
of the proposed gas chromatograph, so that similar problems
would be expected if the IGFET device were used.

4.3.3   Rounding Error and Discriminator Threshold

When a total charge Q_t has been delivered to the
input summing mode, the discriminator operates and feeds
back a charge Q_f. If the threshold charge is chosen to be
half the feedback charge, so that $Q_t = \frac{1}{2} Q_f$, the average
output of the electrometer for a slowly varying input current
is zero, if offset errors are neglected. This choice of the
threshold then produces zero expected rounding error. The
operation is diagrammed in Figure 4.3.3-1, which shows the
behavior of the electrometer output for a constant input
current.
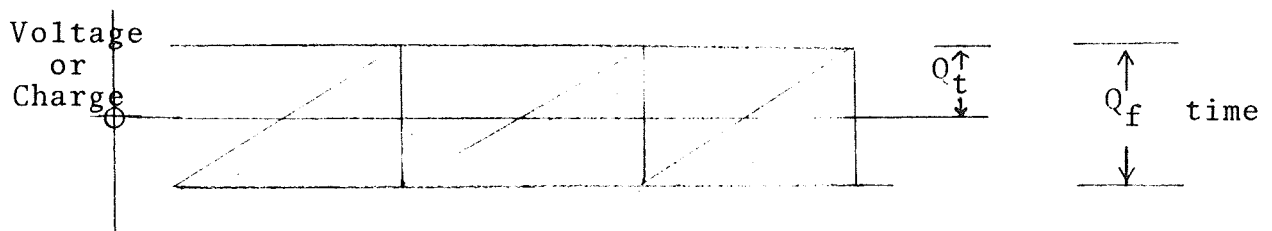
Figure 4.3.3-1   Electrometer Output

This relation implies that the threshold (bias)
voltage of the discriminator should approximately satisfy the
following relation:

$$V_{th} = M_2 \frac{Q_t}{C_f} = \frac{M_2}{2 C_f} Q_f \qquad (4.3.3-1)$$

where M_2 is the gain of the post-amplifier and C_f is the feed-
back capacitance of the integrator.
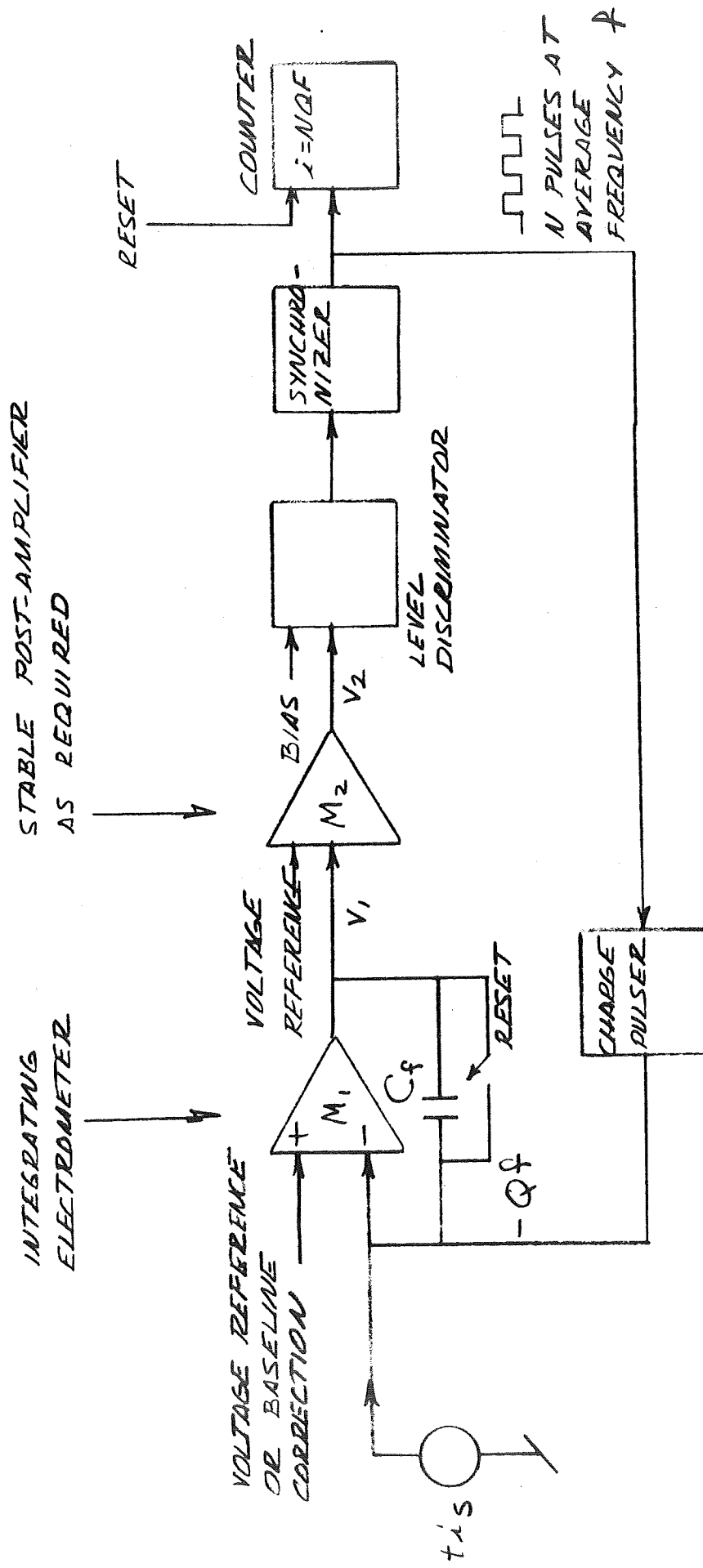
DIGITAL INTEGRATING ELECTROMETER

FIGURE 4.3-1

4.3-9

4.3.4 Dynamic Range

The dynamic range is set on the low-current end by the signal-to-noise ratio (or spurious counting rate) desired, and on the high-current end by the peak current and charge to be measured. We examine the latter limit first.

If the maximum signal consists of pulses of charge Q_m, lasting a mean time T, the electrometer cannot saturate if

$$Q_m < C_f V_m \qquad (4.3.4-1)$$

where V_m is the maximum output voltage of the integrator stage, even if the fed-back current is momentarily smaller than the feedback current. This consideration determines the minimum value of C_f:

$$C_f \geq Q_m/V_m \qquad (4.3.4-2)$$

If the maximum input consists of a steady current I_m, feedback charge Q_f must be supplied at a rate f such that

$$I_m \leq fQ_f \qquad (4.3.4-3)$$

To obtain the maximum sensitivity, consider that we initially reset the integrator perfectly and also apply a perfect drift correction. Subsequently, only the noise components can cause the integrator to drift, as a result of fluctuations in the current at the input. For the purpose of making an estimate, let us suppose that the noise can at least be bounded by a shot noise current caused by the random arrival (and departure, since the mean current into the summing node is assumed zero) of electrons at the input. The subsequent behavior of the integrator output

voltage is then a random walk. In a one-dimensional random walk, the probability that the system survives N steps and reaches a point m steps from the origin without crossing a boundary m_1 steps from the origin is (for large N) (4.3.4-1)

$$p(m,N;m_1) = \left(\frac{2}{\pi N}\right)^{\frac{1}{2}} \left\{ \exp(-m^2/2N) - \exp\left[(2m_1-m)^2/2N\right] \right\}$$

(4.3.4-4)

If the dc component of the current entering and leaving the summing mode is I, and the observation is T, the total number of "steps" is equal to the total number of electons of charge e:

$$N = \frac{IT}{e}$$

(4.3.4-5)

The number of steps corresponding to a voltage V at the discriminator input is

$$m = \frac{(C_f V/M_2)}{e}$$

(4.3.4-6)

while

$$m_1 = \frac{(C_f V_t/M_2)}{e}$$

(4.3.4-7)

Substituting these relations in the above expression, we obtain the probability that at T the output voltage has

---

4.3.4-1   S. Chandrasekhar, Stockastic Problems in Physics and Astronomy, Revs. Mod Phys. 15, 1 (1943)

reached a value between V and V + dV, where $V < V_t$, without ever reaching V_t:

$$p (V,\ IT,\ V_t = \frac{C_f}{m_2} \left(\frac{2}{\pi IT_e}\right)^{\frac{1}{2}} \left\{ \exp\left(-\frac{C_f^2 V^2}{2eITM_2^2}\right) \right.$$

$$\left. - \exp\left[-(2V_t - V)^2\, C_f^{\,2}/2eITM_2^2\right] \right\} \qquad (4.3.4\text{-}8)$$

To obtain the total probability that the system survives without operating the discriminator, we must integrate the above probability density from $V = -\infty$ to $V = V_{th}$. The result is nearly unity only if

$$C_f V_t \gg \sqrt{eIT}\ M_2 \qquad\qquad (4.3.4\text{-}9)$$

The current used in this expression must include the contribution from input flicker and voltage noise developed across the input resistance R_o, integrated over the noise bandwidth.

The directly-transmitted component of the voltage noise must be superposed on the drift. The noise introduced by the post-amplifier must be added directly to that of the integrator, indicating that the post-amplifier must also be a low-noise design.

The probability per unit time that this noise voltage passes through the discriminator threshold with positive slope can be computed if the drift is neglected. (4.3.4-2, 4.3.4-3)

4.3.4-2   S.O. Rice, Bell Systems Technical Journal, 23, (1944); 25, 46 (1945)

4.3.4-3   M. Kac, Amer. Jour. Math, LXV, 609 (1943)

$$p = \frac{1}{2\pi}\left[\frac{\sigma_2^2}{\sigma^2}\right]^{\frac{1}{2}} \exp\left(-V_t^2/2\sigma^2\right) \qquad (4.3.4-10)$$

where
$$\sigma^2 = \frac{1}{2\pi}\int_0^\infty |M_2(\omega)|^2 v_n^2(\omega)\,d\omega$$

$$\sigma_2^2 = \frac{1}{2\pi}\int_0^\infty \omega^2|M_2(\omega)|^2 V_n(\omega)\,d\omega \qquad (4.3.4-11)$$

The number of times that the discriminator operates on noise during the observation time T is $N = pT$. This number must be small compared to unity.

If the finite bandwidth of the post-amplifier is not to introduce an error, it must be larger than the charge feedback frequency f. To estimate the probability of a spurious count, we shall take

$$M_2(\omega) = M_2 \qquad \omega < 2\pi f \qquad (4.3.4-12a)$$

$$M_2(\omega) = 0 \qquad \omega > 2\pi f \qquad (4.3.4-12b)$$

and shall assume the noise spectrum to be flat. (It isn't because of flicker noise, but most of the contribution to the integral will come from higher frequencies.)

These assumptions yield the following expression for the expected number of false triggers:

$$N = \frac{1}{2\pi}\frac{fT}{\sqrt{3}} \exp\left(-V_t^2 \bigg/ 2\, v_n^2 fM_2^2\right) \qquad (4.3.4-13)$$

The breadboard ion current integration described earlier had the parameters

$$f = 100 \text{ kHz}$$

$$v_n = 30 \text{ nV} / \sqrt{\text{Hz}}$$

$$T = 1 \text{ s}$$

$$M_2 = 10^3$$

$$V_t = 0.1 \text{ V} \tag{4.3.4-14}$$

These values yield an expected counting rate of approximately 0.4 spurious counts per second after reset approximately the number observed. The agreement is fortuitous in view of the sensitivity of the Gaussian factor to the assumed mean square noise.

The corresponding probability of false triggering as a result of random drift rates was negligible. As long as the voltage noise dominates the drift, we can combine the relation given earlier to arrive at the ratio of minimum to maximum charge:

1) To make the voltage noise acceptable, we must have

$$\frac{V_t}{M_2} \geq v_n \sqrt{f} \, \log\left(\frac{fT}{2\pi N\sqrt{3}}\right)^{\frac{1}{2}} \tag{4.3.4-15}$$

where N is the maximum acceptable probability of a false count.

2) Combination of the rounding error and dynamic range conditions lead to the relation

$$\frac{V_t}{M_2} \leq \frac{Q_f V_m}{2Q_m} \tag{4.3.4-16}$$

3) Combination of these two equations leads
   to the dynamic range

$$Q_m/Qf = \left(V_m/2v_n\sqrt{f} \right)\left(\log \, fT/2\pi N\sqrt{3} \right)^{\frac{1}{2}} \qquad (4.3.4-17)$$

The frequency f is determined by the maximum
time T available to count down the charged integration:

$$f = Q_m/TQ_f \qquad (4.3.4-18)$$

Substituting this frequency into Equation 4.3.4-17,
the dynamic range Q_m/Q_f is found to be the root of the trans-
cendental equation

$$(Q_m/Q_f)^{3/2} = \left(V_m \, \sqrt{T}/2v_n \right) \left(\log \frac{Q_m/Q_f}{2\pi N\sqrt{3}} \right)^{\frac{1}{2}} \qquad (4.3.4-19)$$

If V_m = 10 v, V_n = 30 nV/$\sqrt{Hz}$, T = 10^2 s, and $2\pi N\sqrt{3}$ = 1, the
dynamic range is the solution of

$$(Q_m/Q_f) = (1.42 \times 10^6) \, (\log \, Q_m/Q_f)^{-1/3} \qquad (4.3.4-20)$$

which turns out to be

$$(Q_m/Q_f) = 6 \times 10^5 \qquad (4.3.4-21)$$

The corresponding maximum feedback frequency is 6 KHz.

This extimate of the dynamic range is valid only if
the input baseline current can be cancelled with the accuracy

4.3-15

required, namely

$$i_b \leq \frac{1}{2} \frac{Q_f}{T_m} \ . \qquad (4.3.4-22)$$

The above estimate of the dynamic range is also valid only if the principal objective is to measure single pulses of charge. Extra dynamic range is obtained by using the integrater as an analog storage device. To observe a complete chromatogram, the feedback current fQ_f must always exceed the input current.

In this case, the ratio of maximum to minimum current is

$$\frac{i_{max}}{i_{min}} = \frac{fQ_f}{Q_{f/T}} = fT \qquad (4.3.4-23)$$

unless the noise dominates. For a given observation time, the frequency may be increased until limited by systematic electronic errors or until the noise counting rate becomes significant. The voltage noise limit may be extimated as before. Equation (4.3.4-15), if multiplied by the feedback capacitance C_f, provides a condition an the threshold charge $Q_t = \frac{1}{2} Q_f$

$$Q_t \geq C_f V_n \sqrt{f} \left(\log \frac{fT}{2\pi N \sqrt{3}} \right)^{\frac{1}{2}} \qquad (4.3.4-24)$$

This condition may always be met by decreasing C_f, until the voltage swing Q_t/Q_f exceeds the saturation voltage V_m of the integrator

$$Q_t \leq C_f V_m \ . \qquad (4.3.4-25)$$

The maximum frequency is then the root of the equation

$$V_m = V_n \sqrt{f} \left(\log \frac{fT}{2 \pi N \sqrt{3}} \right)^{\frac{1}{2}}$$

(4.3.4-26)

and the dynamic range i_{max}/i_{min} the root of the equation

$$(I_{max}/I_{min}) = \left(\frac{V_m \sqrt{T}}{V_n} \right)^2 \log \frac{I_{max}/I_{min}}{2 \pi N \sqrt{3}}^{-1}$$

(4.3.4-27)

For the example given earlier, the dynamic current range is

$$(I_{max}/I_{min}) = 2.7 \times 10^{17}$$

(4.3.4-28)

which is obviously not a realistic limit. For current measurement, the dynamic range will be limited by drifts due to imperfect correlation of baseline current as well as by the random walk effect caused by shot noise input current fluctuations. The latter effect limits the minimum threshold, and hence the minimum feedback charge to a value

$$Q_f \geq \beta \sqrt{eIT} \, ,$$

(4.3.4-29)

where β is a confidence factor of order 1 to 10 in magnitude, so that the minimum detectable current determined by the random drift rate

$$I_{min} = \beta \sqrt{eIT}/T \, ,$$

(4.3.4-30)

For the example given earlier, with the additional assumption that the baseline current is 10^{-10} A, the minimum detectable

current (for β = 5) is

$$I_{min} = 2 \times 10^{-16} \text{ A.} \qquad (4.3.4-31)$$

This limit is for lower than that imposed by a constant drift resulting from imperfect baseline compensation. Compensation to 0.1% has been shown to be feasible. [4.3.2-1] For the example given, the minimum detectable current is thus 10^{-13} A (Q_f = 2, Q_t = 2, I_{min} T) with a corresponding charge resolution of 2×10^{-11} C. The maximum detectable current is determined by the maximum rate at which the charge feedback network can be operated, which is of the order of 1 MHz for 1% feedback accuracy. For the example given (T = 10^2 s), the achievable dynamic range is 8 decades. It follows, finally, that since the limiting error is the error in dc baseline compensation, that the minimum detectable current is the same as that of an electrometer, but range-switching is not required.

4.4 Post-Digital Integration

The block diagram in Figure 4.4-1 shows one method of post-digital integration. The signal from the amplifier is fed into a voltage-to-frequency converter, which produces a pulse-train with the pulse frequency proportional to the input voltage. The pulses are counted and stored for transmission to the data system. Use of a conventional VCO would require an additional bucking oscillator to produce a near-zero count at the low-signal levels. For a VCO and oscillator differential stability of 0.2%, the difference frequency could be 20 Hz at the nominal 10 KHz VCO frequency. Assuming a ten-second analysis time, this represents a nominal integration

(4.3.2-1) Loc. Cit.

RANGE SWITCHING

RANGE STATUS

DETECTOR

R_{f3}

R_{f2}

R_{f1}

−A

VCO

RANGE 1

RANGE 2

RANGE 3

FIXED FREQ. OSC.

BASELINE COMPENSATION

THRESHOLD DETECTOR
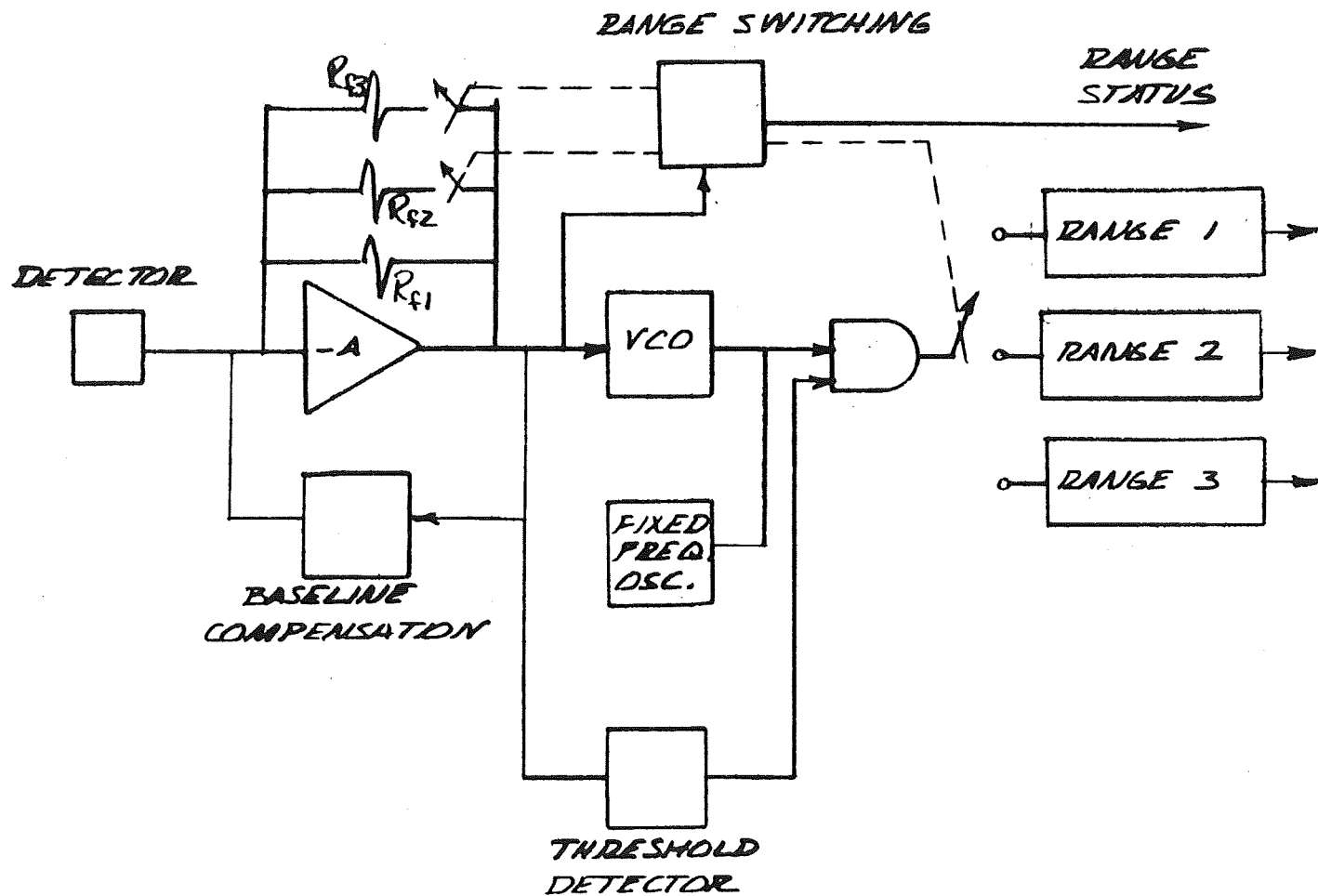
DIGITAL INTEGRATOR

FIGURE 4.4-1

error of 200 counts. This same difference would exist
at the measurement threshold of each of the three ranges.
(Because of the wide dynamic range, it is not feasible
to scale switch the VCO frequency).

Assuming a full-scale voltage of 10 V, a two-second
triangular peak and a VCO frequency swing from 10 KHz to
20 KHz, 10^4 pulses would be produced, in which case the
error due to the offset would be negligible. However, a
2-s, 50-mV peak would produce about 50 pulses and the 20-
pulse differential frequency would represent a 40% error.
The inclusion of a threshold detector would prevent a count
accumulation until the peak arrives.

The data is read into one of three accumulators depending
on the electrometer range (Figure 4.4-1). A commutator directs
the output of the converter to the appropriate counter. The
data from the first range is gated into counter number 1. When
the electrometer range switches to the second range, the data
is gated into accumulator number 2 and is similarly gated for
range number three. The third counter could be eliminated by
resetting the first range accumulator when the electrometer
switches to range three. However, the major difficulty in
throwing away the range-one data is the large error that
would result for peaks just over the third range switching
level for peaks with long tails. The total count that can be
produced at the maximum-area peak on any of the three ranges
is greater than needed for required accuracy. Therefore a
floating point accumulator or some other device for compressing
the data should be used. Since there are various straightforward
ways of designing data compression circuits, they will not be
discussed in this report.

It should be mentioned that once the gas-handling portion of the instrument is designed and tested, the peak form factor will be known and should be relatively predictable. In that event it may be feasible to approximate the area of the peak by using a threshold detector to determine the base width and a peak crest detector to provide the peak height. Four separate pieces of data would be required in addition to the range switching position. Namely, the time of occurrence of the start and ending of the peak and the time and peak height at the peak crest. This method, however, suffers from the inaccuracy that would be caused if a peak crest were lost in range switching. The logic can be mechanized to indicate that the electrometer range was changed but that a peak was not detected. In that case, the peak retention time would be given as the time the electrometer down-ranged. A more severe problem would be to determine the peak height. Additional circuitry would be required to sense the negative slope of the peak. In the absence of a detected peak crest signal, the logic would print out the height of the peak the moment it detected a negative slope. This method requires more complex data handling than would be the case with integrators that provide a single value for the integral. Its only value would be in providing crude information on the peak form factor.

5.0 RANGE SWITCHING

Certain system configurations, such as the linear analog integrator described in Section 4.1, require scale-factor changes to cover the wide dynamic range predicted for this experiment. This ranging is usually accomplished by sensing the output of the scaled device and adjusting the scale factor such that the output remains within the dynamic range of the device (see Ref. 5.0-1).

For a unipolar, monotonically increasing measurement, such as is performed by integrating the output of the hydrogen flame ionization detector, a simplified approach to scaling would be used . In this application, the integrator output is continuously and directly compared with a reference, Figure 5.0-1. When the output exceeds the reference, the integrator scale is changed to the next less sensitive scale. If, after a suitable delay, the output is still greater than the reference voltage, another scale change is effected. This process continues until the integrator output is within its dynamic range. After the analog-to-digital converter has completed its conversion, the integrator is reset to its most sensitive scale, and all capacitors are discharged. The electrometer is then prepared for the next measurement.

5.0-1 J.H. Marshall, "An Automatic Scale Factor Device for Use with Spacecraft Electrometers," JPL SPS 37-23
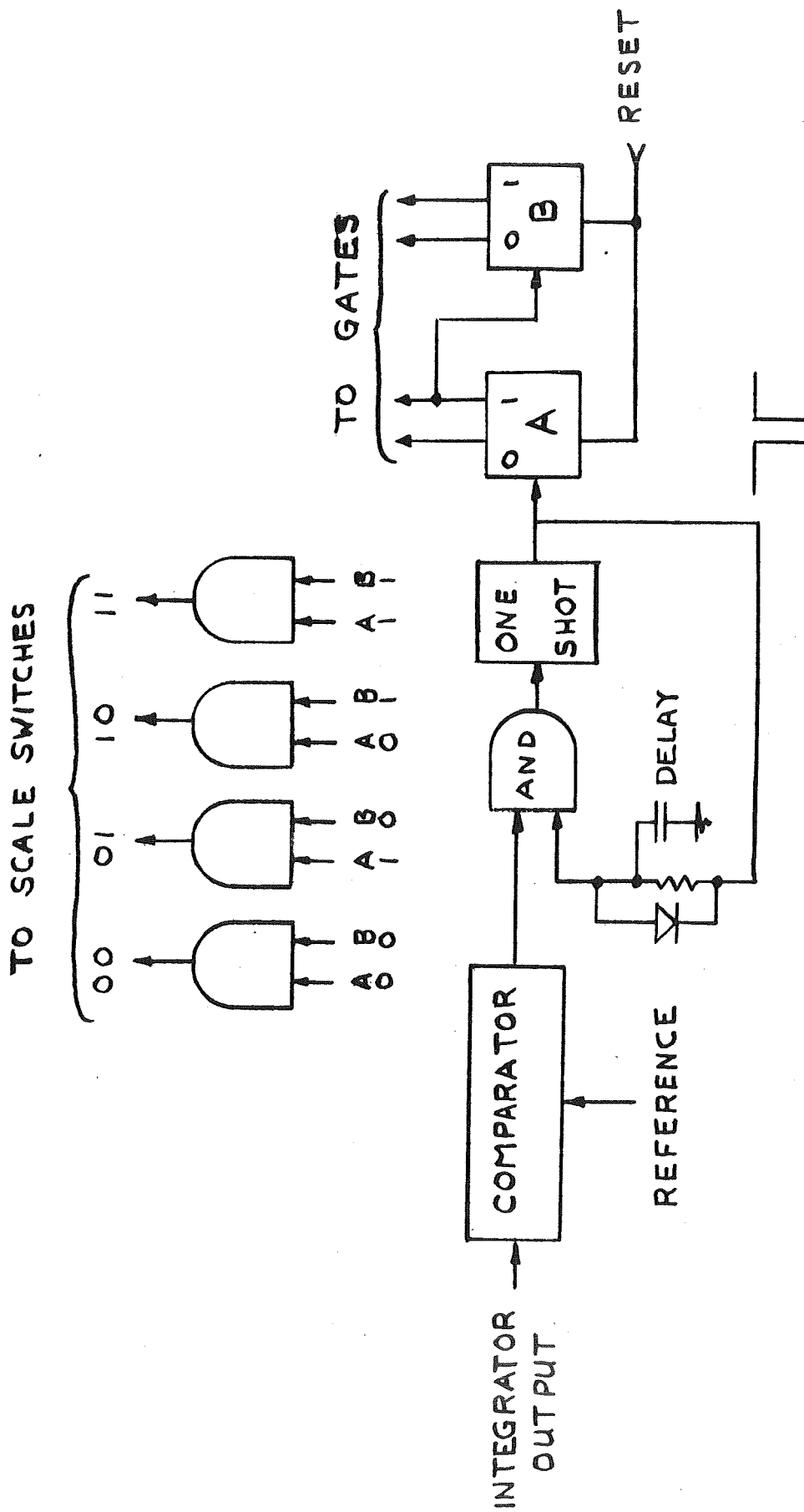
RANGE SWITCHING

FIGURE 5.0-1

6.0   DETECTOR QUIESCENT CURRENT COMPENSATION

Although the background current of the hydrogen flame detector may be as large a 10^{-10} A, to take full advantage of the detector's sensitivity, it is desirable to measure changes as small as 10^{-13} A superimposed on the quiescent or background current. This requires that the quiescent current be nulled out during the analysis. In addition, since temperature, pressure and system impurities can cause the background current to vary, a variable bucking current must be provided to null the current just prior to performing the actual analysis.

In this report, three basic methods of zero compensation are considered; namely, linear feedback with a low-pass filter, gated capacitor storage, and gated digital feedback. The first two systems have previously been reported. Although both reports are included in the Appendix, a very brief description of each will be included here.

The linear feedback technique continuously supplies a compensation current into the amplifier summing point. However, the amplifier's time constant is long compared to the total time in which the peaks appear. For this reason, the compensation system can respond to the expected slow variations in baseline current without nulling out the signal current.

The gated capacitor storage technique disconnects the compensation loop during the analysis and supplies the compensation current from a capacitor storage system. At the end of the analysis, the loop is closed and the compensation system continuously rezeros the electrometer until the start of the next analysis.

6.1 Gated Digital Stabilization

A block diagram of the digital baseline stabilization is shown in Figure 6.1-1. The current is supplied to the amplifier summing point by a ten-bit D-to-A converter. The detector current is coarsely biased by means of V_b and R_b such that the electrometer output is nominally zero at the center of the converter ramp. The converter can thus adjust the variable bucking current to within 2×10^{-13} A of $I_D - I_c$ for variations up to approximately 10^{-10} A.

Assuming a clock rate of 10 Hz, each step would be 100 ms wide. The time constant $\tau = R_1 C = 10^{-2}$ s, is 10% of the voltage step width. Therefore, the output has 10 τ of settling time before the input is stepped to a new voltage. The amount the electrometer output lags the input baseline correction voltage is negligible. The initial buck-out time could be 100 s. However, once the baseline is bucked out, the digital system would differentially track the relatively slow background current changes on subsequent corrections. Prior to the analysis, the comparator will be disabled and the counter will maintain a fixed buck-out current until the comparator is again enabled.

Although the digital system is a more complex circuit than the two other previously mentioned techniques, the state-of-the-art in integrated circuit technology is such that the circuit could be built with very low power and relatively few discrete components.

The comparator will be required to have a threshold of about 10 mV, which is stable to within ±5 mV. The clock stability is not particularly important. Modular ladder networks can be obtained that have output accuracies better than 0.05% over a temperature range of 100°C. A ten-bit ladder for the digital

GATED DIGITAL BASELINE STABILIZATION

FIGURE 6.1-1

baseline compensation would require about 0.1% accuracy in
its most significant bit.

6.2   Conclusions

Although the exact choice of compensation technique will
depend somewhat on such factors as the choice of associated
subsystems, the maximum detector current variation, the analy-
sis time, the detector noise spectrum and the expected temper-
ature range, the following general comments can be made about
the three techniques.

The linear feedback method is the simplest but has the
disadvantage of integrating the signal current during the
analysis. This will cause an error in the peak quantization
and the trailing edge of the peak will undershoot. The pro-
blem, of course, becomes more severe as the peak width increases.

The gated capacitor storage technique is more complicated
than the linear feedback technique but will not cause under-
shoot following the peak since it supplies current from a
storage system during the analysis. As mentioned in the
Appendix, a system has been constructed which maintained the
baseline current to within $\pm 10^{-12}$ A for 30 minutes.

The digital baseline technique offers a wide-range com-
pensation method with no variation in compensating current
during the analysis. However, it seems to offer no significant
advantage over the gated capacitor storage technique other than
a wider dynamic range.

7.0 ANALOG-TO-DIGITAL CONVERSION

Since analog data from scientific laboratory or space
instruments are frequently processed by way of digital or
pulse-code modulation, the analog-to-digital conversion
becomes an important accuracy factor in the signal-processing
chain. This section discusses linear and logarithmic con-
verters and their appropriate uses.

7.1 Linear Conversion

The optimum use of linear conversion is in applications
where constant incremental accuracy is desirable. Illustrative
of these applications are positional measurements; restricted-
range measurements of analog signals, such as temperature trans-
ducer outputs; and pulse-height measurements. Some of the fre-
quently used types of converters are as follows:

1) Ramp Comparator (Figure 7.1-1). In this technique, a
    precise, linear voltage ramp is compared against the
    voltage to be converted. Pulses from a precision clock
    are gated into a counter at the initiation of the ramp
    until comparison equality has been achieved so that the
    accumulated count is proportional to the voltage input.

2) Height-to-Time. This technique is similar to that of
    the ramp comparison method. In this system, a voltage
    proportional to the analog signal to be measured is
    linearly run down to zero. Precision clock pulses are
    gated into a counter between the start of run-down and
    zero crossing. Height-to-time conversion is used for
    short-term analog events where the use of series com-
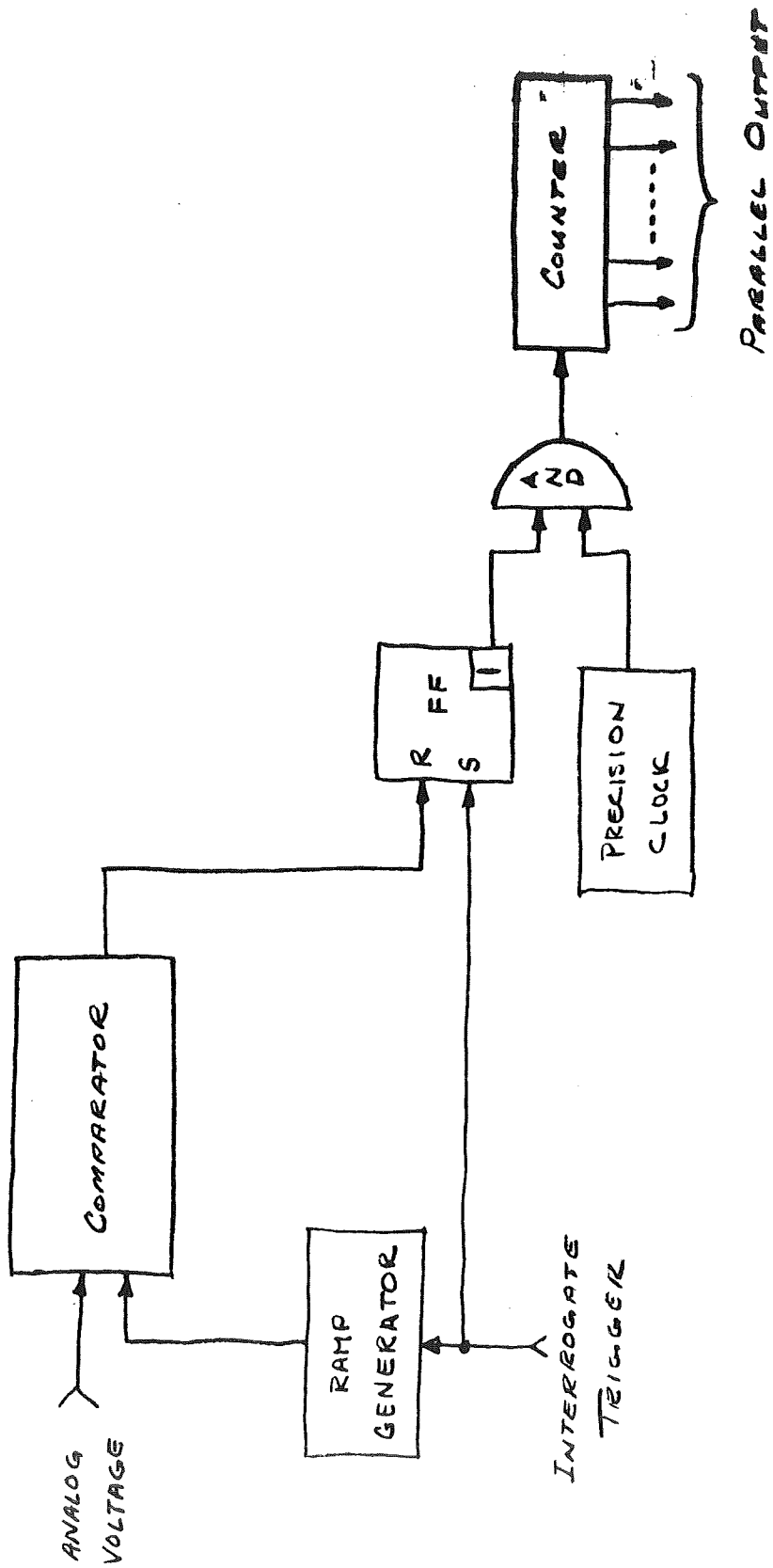   mutation and time-consuming run-up comparison voltages
    are impractical.

FIGURE 7.1-1   RAMP COMPARATOR BLOCK DIAGRAM

3) Voltage-to-Frequency Converter (Figure 7.1-2).
This technique utilizes an integrator driven from
the analog input voltage. After its output reaches
a fixed voltage, the integrator is reset and the
integration cycle repeats. The period of the inte-
gration is

$$T = \frac{V_T \, CR}{v_i} \quad \text{seconds,}$$

and the frequency is

$$f = \frac{1}{T} = \frac{v_i}{V_T \, CR} \quad \text{Hz.}$$

By counting the number of cycles for a known time
interval, the unknown voltage can be determined.
This approach has merit where there is a relatively
long time (10 to 100 msec) available for the measure-
ment and when a precision time gate is available.

4) Staircase Comparator (Figure 7.1-3). This system
introduces gated clock pulses serially into a binary
counter. The binary number in the counter is D-to-A
converted so that each successive clock pulse produces
an equal-increment step-voltage output. This analog
voltage is compared against the analog input so that
when comparison equality has been achieved, the clock
pulses are gated off and the residual binary number in
the counter is proportional to the input voltage.

5) Binary Search. This system is similar to the staircase
comparison system except that it compares through suc-
cessive approximation. Instead of gating a pulse train
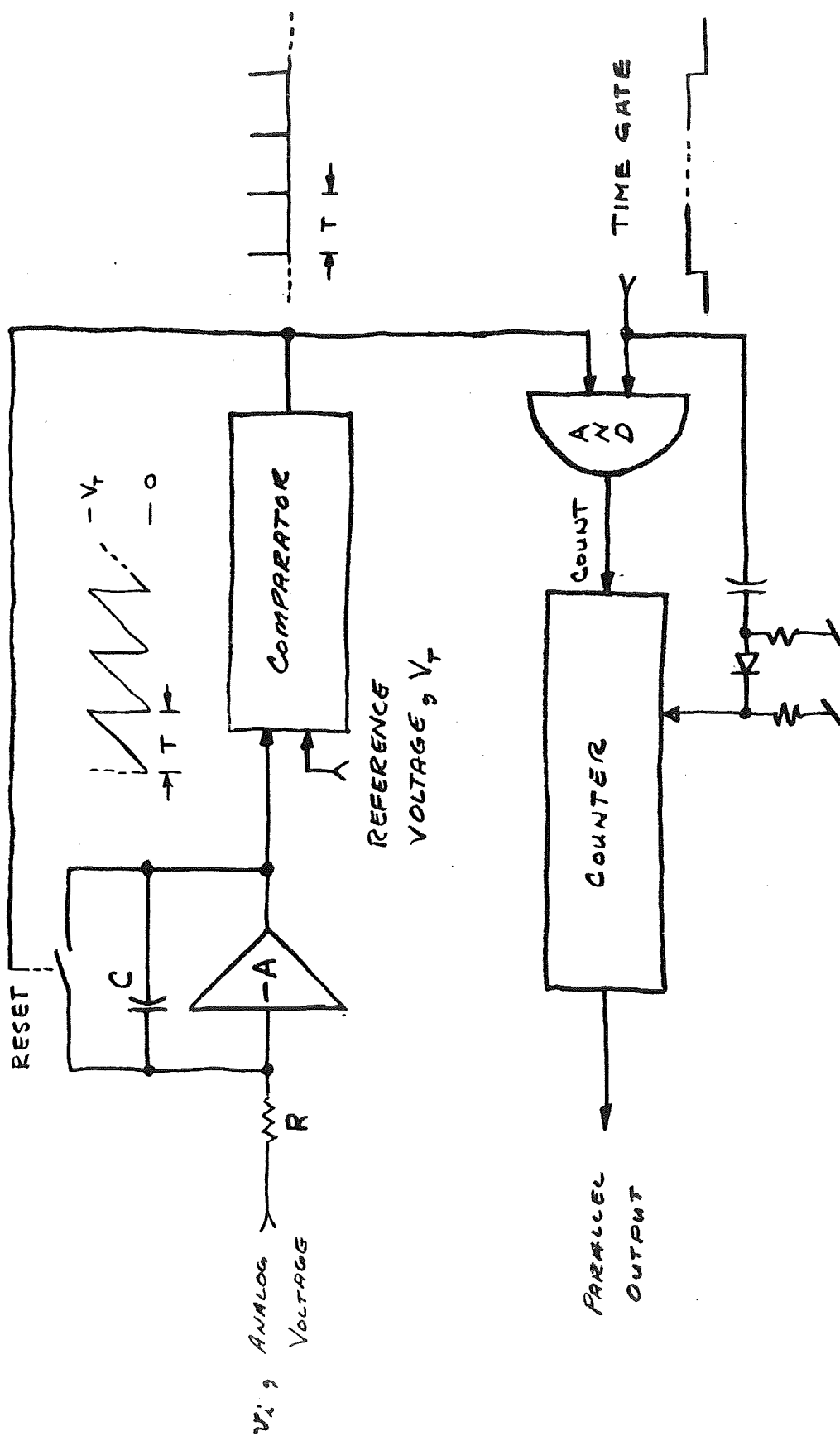serially into the counter, this converter successively

FIGURE 7.1-2   VOLTAGE-TO-FREQUENCY CONVERTER

routes the search pulses from the most significant counter stage to the least significant stage. The D-to-A output is compared against the input, and if comparison equality has not been reached, the counter stage is set to "1"; if comparison equality has been exceeded, the counter stage is reset to "0". For an n-bit conversion, only n search pulses are required to perform the complete A-to-D conversion. This system, while more sophisticated and complex than the foregoing systems, has a decided speed advantage.

There is a growing reluctance, where complicated space systems are concerned, to transmit low-level analog signals between the instrument and spacecraft data processor interface. As a result, the comparison portion of the conversion is often performed in the instrument so that the interface data are in pulse form. Three currently used systems are as follows:

1) A-to-PW. In this system the analog signal is converted to a pulse having a proportional width. Precision clock pulses are then gated into a counter at the data processor for a duration equal to the pulse width.

2) A-to-PPM. In this variation of A-to-PW conversion the instrument transmits a short pulse when the linear conversion is complete, the pulse position with respect to a conversion initiation command being proportional to the analog signal. The transmitted pulse gates off the clock pulses to the counter.

3) Pulse Train. In this system, complete A-to-D conversion is performed in the instrument except that

REFERENCE VOLTAGE

INTERROGATE
RESET

DIGITAL ATTENUATOR

COUNTER

PARALLEL OUTPUT

COMPARATOR

AND

ANALOG VOLTAGE

PRECISION CLOCK
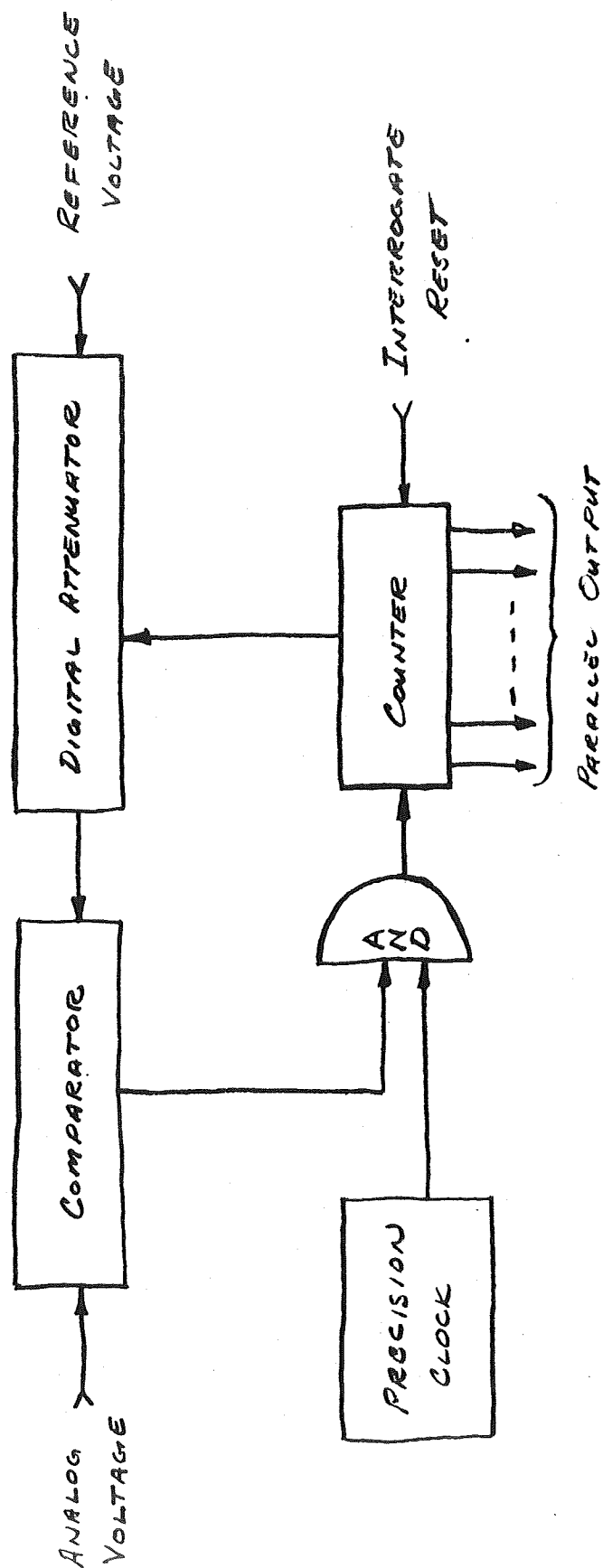
FIGURE 7.1-3 STAIRCASE COMPARATOR

the gated clock pulses are stored in a data-processor counter, which can also be used for other functions.

An important linear system parameter is the converter resolution, or quantizing uncertainty, which is given by

$$\text{Resolution} = \pm \frac{100}{2(2^n-1)} \text{ \% of full scale.}$$

In terms of other performance parameters, there is considerable similarity between A-to-D converters and the signal-processing electronics preceding the converter. For examples, important figures of merit for converter systems are

1) Scale-factor stability (SF = volts per channel or volts per digital number)

2) Offset stability

3) Differential linearity

4) Dynamic accuracy

7.2 Logarithmic Systems

Experimenters interested in wide-range quantitative measurements are often desirous of maintaining substantially constant accuracy over the entire dynamic range of their measurements. The equation that describes a quantization interval that is a constant percentage of the level being quantized is an exponential. The quantized output in this system is a logarithmic function of the input.

7.2.1 Customary Data Requirements and Applications

In specifying A-D conversion requirements for their measurements, many experimenters ask for quantization accuracy based on desired resolution at threshold levels or relatively small down-scale levels. The fact that linearly converted up-scale measurements are consequently made at excessive accuracies is generally a useless bonus and tragic waste of data bits. In actual spacecraft applications, data system design will involve several compromises between average user requirements and system constraints, which include communication bandwidth, weight, power, (etc.). These compromises often confront an experimenter with a linear conversion system having a fixed number of bits, in which case he must be reconciled to relatively coarse resolution on down-scale measurements. In the cases of experiments producing wide-range data, logarithmic A-D conversion provides an efficient and satisfactory method of obtaining required resolution and stability over the entire range.

7.2.2 Logarithmic Vs. Linear Quantization

Consider the quantization uncertainty produced by an exponential comparison voltage over three decades for the various bit conversions shown in Table 7.2.2-1.

Bits	Quantizing Levels	Quantizing Levels/Decade	3-Decade Quantizing Uncertainty,%
4	15	5	±23 (Average)
5	31	10	±11.5
6	63	21	± 5.7
7	127	42	± 3.0
8	255	85	± 1.5
9	511	170	± 0.75
10	1023	341	± 0.375

Table 7.2.2-1   Three-Decade Exponential Analog Quantization
Uncertainty.

Now consider Table 7.2.2-2, which describes the quantization accuracy of linear conversions of the same bit magnitude.

Bits	V_{fs},%	$0.1\ V_{fs}$,%	$.01\ V_{fs}$,%	$.001\ V_{fs}$,%
4	±3.3	±33	- - -	- - -
5	±1.6	±16	- - -	- - -
6	±0.8	± 8	- - -	- - -
7	±0.4	± 4	±40	- - -
8	±0.2	± 2	±20	- - -
9	±0.1	± 1	±10	- - -
10	± .05	± 0.5	± 5	±50

Table 7.2.2-2   Three-Decade Linear Quantization Uncertainty
(values are listed only where quantization
interval ≤ absolute level of scale)

Note: V_{fs} = Full-scale Voltage

The exponential quantization technique stands out as a most flexible and accurate tool from the standpoint of wide-range measurements. It also overcomes the objection to automatic gain changes in instruments that produce sudden conversion of a full-scale measurement to a down-scale measurement upon automatic reduction of sensitivity. Quantization uncertainty (or resolution) is virtually constant over the entire scale for logarithmic conversion, unlike the huge linear-system variations that are graphically illustrated in Table 7.2.2-2.

7.2.3   Basic Logarithmic System

The basic technique described here is one of logarithmic height-to-time conversion. A linear input signal is compared against an exponential time-base; this comparison produces a clock gate signal whose duration is proportional

to the logarithm of the input signal. Two configurations are
described here, both of which have similar linear counterparts.
These are

1) Exponential Run-Up. In this circuit, a positive-
exponential voltage, starting at a stable refer-
ence, is compared against the input voltage and
produces a suitable comparator output when it
exceeds the input voltage. A train of precision
clock pulses is gated into a counter between
start of run-up and comparison equality. The
flexibility in establishing instrument-data-
system interfaces should be the same as the
case of the corresponding linear converter. The
time (t) elapsed from the start of the run-up to
the point where it equals the input voltage
(V_{IN}) is given by

$$t = \tau \ln V_{IN}/V_{REF} \qquad (7.2-1)$$

where V_{REF} = Reference voltage

Positive-exponential time-base generators are
practical devices that have demonstrated their
stability both thermally and temporally.

2) Exponential Run-Down. This system, sometimes
referred to as a logarithmic height-to-time con-
verter, requires the charging of an R-C circuit
to the input voltage. The charging is then fol-
lowed by a negative-exponential run down to a
preset reference voltage. Once again the elapsed
time for the comparison is

$$t = \tau \ln V_{IN}/V_{REF}$$

7.2.4 Exponential Time-Base Generator

One approach toward the production of a stable exponential waveform employs the exponential characteristic of positive feedback amplifiers. The time-base generator shown in Figure 7.2.4-1 is a typical configuration. The amplifier is direct coupled and used a matched differential pair at the input. There are two external feedback loops; a positive loop via R_5 and a negative loop via C. For this analysis, the gain (A) is assumed infinitely large, and no dc amplifier voltage offsets are considered. In this approximation, V_1 and V_2 must be equal.

When the clamp switch (an FET switch) is closed, the negative feedback dominates and the output (V_3) rests stably at a voltage V_{REF}. When the switch is opened, the initial current flowing in the R_6 divider (formerly supplied by the switch) now starts charging the capacitor. The positive feedback raises the level of V_1 (and consequently V_2) and thereby increases the charging rate of the capacitor so that the output rises exponentially with time as soon as the clamp switch is opened. For the component values shown in Figure 7.2.4-1, the output voltage (V_3) is given by

$$V_3 = V_{REF}\ e^{2t/R_6 C} \qquad\qquad (7.2-2)$$

where   t = time after the clamp swith was opened.

For the infinite-gain approximation, all quantities in Equation 7.2-2 are determined by reference voltages, resistors and capacitors, and no critical dependence on semi-conductor parameters is present.
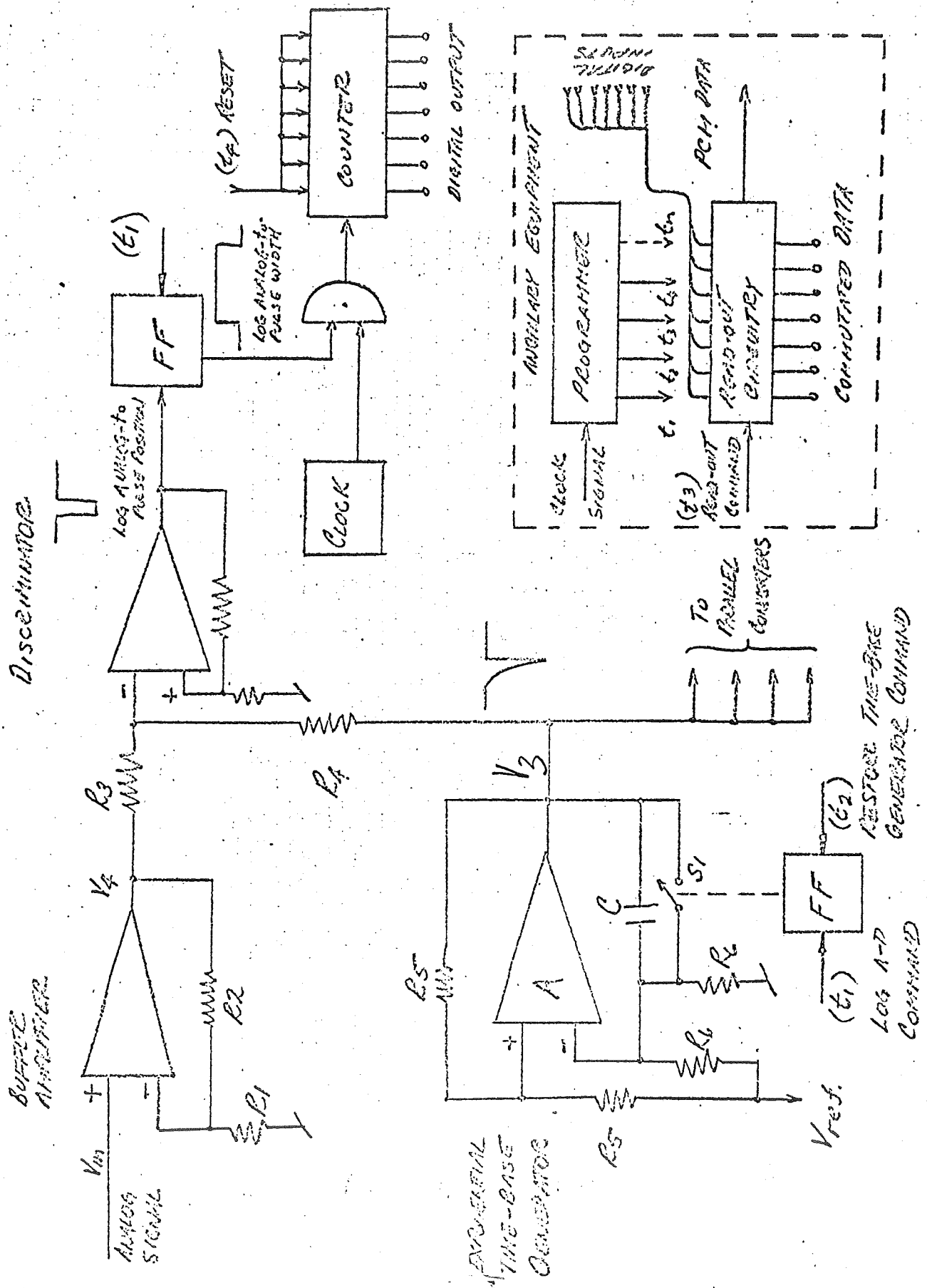
Figure 7.2.4-1 - Block Diagram of Logarithmic A-D Converter

7.2.5 Conversion Stability

Since the logarithmic converter does not yet enjoy wide usage, it seems worthwhile to mention stability factors that make logarithmic conversion a practical tool. Toward this end, the circuit of Figure 7.2.4-1 and its positive-exponential time base is used as a reference.

7.2.5.1 Time-Base Stability

Assuming infinite gain and zero delay in its generator, the exponential time-base can be described by

$$V = V_{REF} \, e^{t/\tau}.$$

The total differential is expressed as follows:

$$dV = \frac{V_{REF} \, e^{t/\tau} \, t \, d\tau}{-\tau^2} + e^{t/\tau} \, d \, V_{REF}. \quad (7.2\text{-}3)$$

The fractional error in voltage is given by

$$dV/V = -\left(t/\tau\right)\left(d\tau/\tau\right) + dV_{REF}/V_{REF}, \quad (7.2\text{-}4)$$

or

$$dV/V = -\left[\ln\left(V/V_{REF}\right)\right]\left(d\tau/\tau\right) + dV_{REF}/V_{REF}. \quad (7.2\text{-}5)$$

Considering a practical case in which a dual transistor comparator is used in the ramp generator, one could expect a combined stability of 1.5 mV in reference voltage (V_{REF}) and

time-base generator offset over a 100-°C temperature range. This would contribute $\pm 0.75\%$ absolute error over that temperature range if V_{REF} = 100 mV.

As another practical consideration, assume a time-base dynamic range of 100 mV to 32 volts (2.5 decades), which represents the range of an existing flight converter. For V/V_{REF} = 10, 100, 320, it is calculated that t/τ = 2.3, 4.6, 5.75, respectively. Estimating the time-constant instability at 0.4%/100°C, the instability in the ramp voltage due to changes in τ would be $\pm 0.46\%$, $\pm 0.92\%$ and $\pm 1.15\%$ at 1, 2 and 2.5 decades, respectively, above V_{REF}. Thermal control of critical elements such as the feedback capacitor, comparator, and the reference element will further enhance the stability of the time base.

7.2.5.2 Comparison Stability

When the discriminator is at its regeneration condition, the summing-point voltage is given by

$$\frac{V_4}{R_3} R_p + \frac{V_3}{R_4} R_p = \varepsilon \qquad (7.2-6)$$

where

$$R_p = R_3 R_4 / (R_3 + R_4)$$

$$\varepsilon = \text{input voltage for regeneration}$$

The change in input voltage, dV_4, required to compensate for a change in regeneration voltage, $d\varepsilon$, is as follows:

$$dV_4 = \frac{R_3 + R_4}{R_4} d\varepsilon. \qquad (7.2-7)$$

To establish error magnitude under representative conditions, consider $d\varepsilon$ to be approximately 1 mV over a 100-°C temperature range and the multiplier value $\frac{R_3 + R_4}{R_4}$, to be between one and two. This would place the error, dV_4, between 1 and 2 mV.

7.2.5.3 Gating Stability

Errors introduced by system timing inaccuracies are calculated as follows:

$$V = V_{REF} \, e^{t/\tau} \qquad\qquad (7.2-8)$$

$$dV = V_{REF} \, \frac{e}{\tau}^{t/\tau}$$

$$\frac{dV}{V} = \frac{dt}{\tau} \, .$$

If one arbitrarily designates the 2.5-decade quantization range as being analyzed in 1 msec, the time constant, τ, would be determined by

$$\tau = \frac{t}{\ln(V/V_{REF})} = \frac{10^{-3}}{\ln 10^{2.5}} = 175 \; \mu sec.$$

According to Equation 7.2-8, conversion errors due to rise and fall times or other delays are allocated by multiplying permissible errors due to these causes by τ. As an example, a gate timing-error allocation of ±0.5% would require gate stability of ±0.87 μsec, which is well within the capabilities of commercial transistors.

It has been the intent of this description to convey the feasibility of logarithmic analog-to-digital conversion in wide-range measurements. Respectable accuracies can be furnished at threshold levels of wide-range measurements, without the correspondingly large data volume required of a linear system.

7.2.6 Other Scale Compression Methods

There are several other scale compression methods which have been used to obtain down-scale accuracy without excessive loss of bits on up-scale measurements. The approaches generally are similar to one of the linear conversion methods, but employ a positive feedback amplifier (Figure 7.2.6-1) to generate a precision exponential. Methods which use the nonlinear characteristics of diodes or transistor require careful selection and painstaking matching to obtain reasonable accuracy.

The amplifier A shown in Figure 7.2.6-1 is a differential dc amplifier with positive feedback via R_2 and negative feedback via C. For the following analysis, A will be assumed infinitely large, and no dc amplifier voltage offsets will be considered. In this approximation V_1 and V_2 must be equal.

When the switch (a field-effect transistor) is closed, the positive feedback path is shorted out, and the output (V_3) rests stably at a voltage V_o. The output will rise exponentially with time as soon as the clamp switch is opened. For the component values shown in Figure 7.2.6-1, the output voltage (V_3) is given by

$$V_3 = V_o \exp(2t/R_1C) \qquad\qquad (7.2.6-1)$$

where t = time after the switch was opened. For the infinite gain approximation, all quantities in Equation 7.2.6-1 are determined by stable voltage, resistors and capacitors, and no critical dependence on semiconductor parameters is present.

By using combinations of positive feedback amplifiers, types of compression characteristics can be obtained.
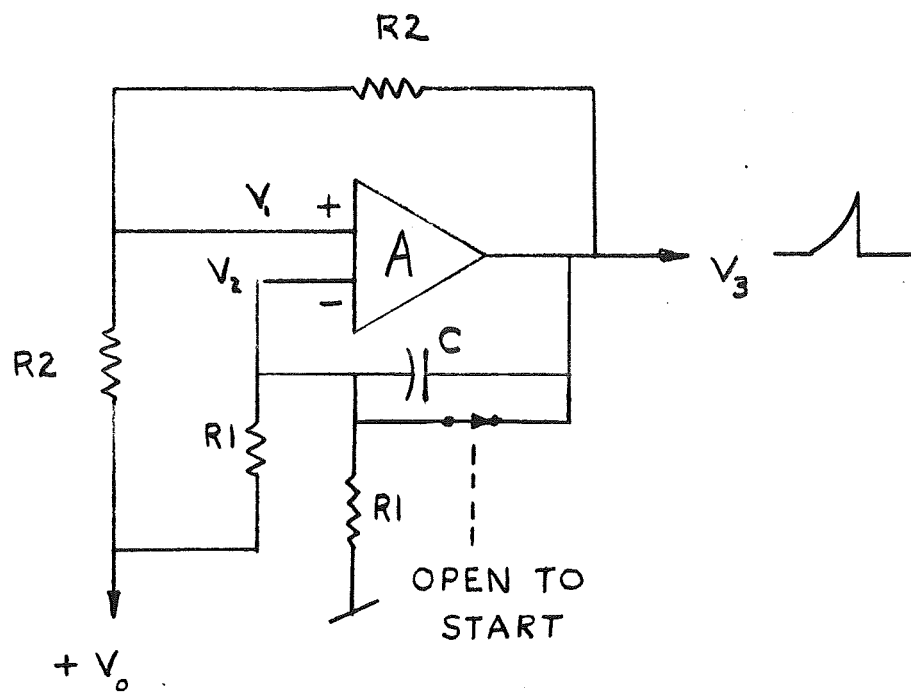
POSITIVE FEEDBACK AMPLIFIER

FIGURE 7.2.6-1

8.0   DATA HANDLING

There are three types of data acquired from the instrument. The primary data are the result of a given experiment. The secondary data are the instrument status information required to reduce the scientific data. The third type of data involves measurement of the environment in which the instrument is operated.

In addition to the handling of data, steps must be taken to ensure that the data received are accurate and that the operation of the subsystem is normal. This function is provided by calibration circuitry which stimulates the sensor.

The block diagram of the instrument data system is shown in Figure 8.0-1

An analog interface between the instrument and the capsule has been established because it provides the most noise-free and efficient interface. The transfer of analog signals between instruments and their data handling equipment can result in pick-up due to random noise or unanticipated system interactions. The former signal sources are due to electron statistics and thermodynamics, while the latter effect is the result of ground loop, electromagnetic interference and common-mode problems. Since the output from a scientific instrument generally covers a broad range, from minimum to full scale, it is important that the low level data be as accurate as that at high levels. The result of a noise signal pick-up of 10 millivolts at an output signal level of 50 millivolts is far more deleterious than the same pick-up at an output signal level of 4,000 millivolts.
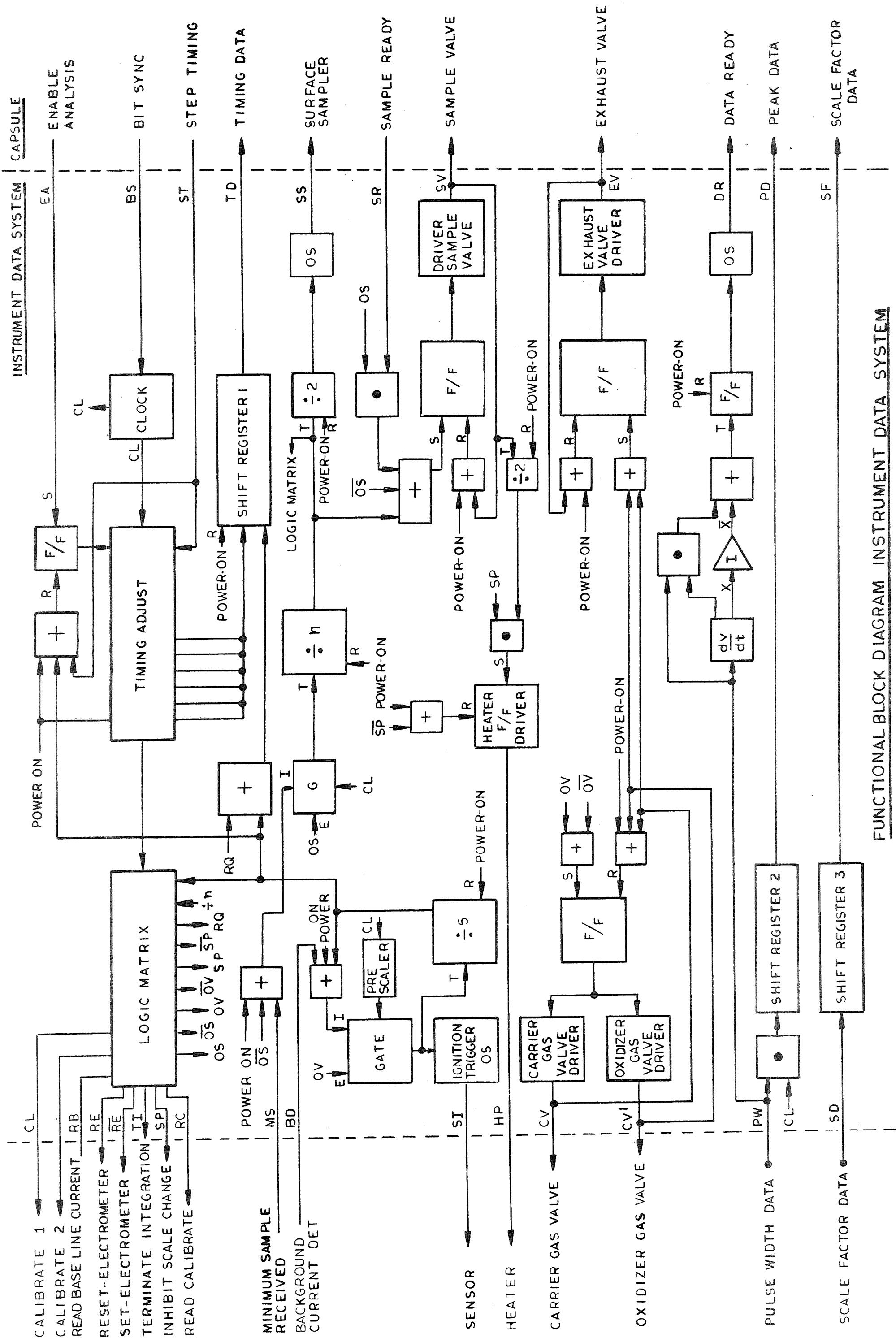
FUNCTIONAL BLOCK DIAGRAM INSTRUMENT DATA SYSTEM

FIGURE 8.0-1

Another important consideration is that the use of a digital interface allows the experimenter to calibrate his instrument completely. When an analog output is provided, the experimenter must calibrate his instrument after it has been integrated into the spacecraft or with the data-handling system. The calibration will then have to be performed under the less than optimum conditions which usually prevail after integration has been completed. These conditions are the result of the environment in which the system is operated and the equipment which must necessarily be connected to it during testing. In addition the experimenter is dependent upon the calibration stability of equipment not under his control.

For these reasons the handling of data, except for that related to temperature or power supply voltages, between this instrument and its data handling equipment is accomplished through the use of a digital interface.

8.1   Scientific Data

The scientific data are the result of the integration of ionization current until the terminate-integration signal is received from the logic matrix. For the case where direct linear integration has been performed, application of this signal stops the integration process and activates a comparator, which puts out a pulse whose width is proportional to the logarithm of the total integrated-current. This control signal opens a gate and allows clock pulses to enter the shift register. The pulses accumulated during this period represent the digital equivalent of the log of the integrated current.

The frequency of the clock input is dependent upon the accuracy required from the instrument. The resolution is dependent upon the number (n) of binary digits per sample and by the type of converter used, linear or logarithmic.

8.2 Status Data

There are four types of status data required from this instrument. They include:

a) baseline current,
b) feedback range,
c) operating mode, and
d) timing information.

Data types a) and b) are required for data reduction. The other two data types are used to enhance the value of the data received.

8.2.1 Baseline Current

The baseline-current output data are used as reference for the scientific data. These data are a measure of the current flow generated by the ionization of the carrier gas as it is consumed by the flame. This current is essentially subtracted from the input by baseline-compensation circuitry to eliminate its contribution to the integrated current. Sampling of the baseline current is controlled by the read baseline-current command from the logic matrix. This function gates a voltage proportional to the baseline current into the analog-to-pulse-width converter. The pulse width output of the converter allows clock pulses to enter the shift register. The number of pulses accumulated in the register is proportional to the pulse-width, which, in turn, is proportional to the analog voltage. If a digital baseline stabilization system is used, the status of the counter containing the digital data will be sampled and transferred to a shift register for readout in the manner indicated above.

A data-ready signal is sent to the data system immediately after termination of the pulse-width input. The data are

then transferred to the capsule data system by serial or parallel readout.

These data may be transferred from the shift register to the capsule data system by serial or parallel (bi-level) readout.

8.2.2 Feedback Scale-Factor Data

The feedback scale-factor data indicate which elements were in the feedback loop when integration of the ionization current was terminated. When the terminate-integration signal is received, the digital level of the feedback scale-factor lines are sampled and transferred to shift-register 3 for readout by the capsule data system.

Data output can be either serial or parallel, depending upon the requirements of the capsule data system.

8.2.3 Operating Mode

The operating mode data consists of one or more bits in shift-register 1. In Figure 8.2-1 one input is used to indicate that the system is either in the normal or quiescent mode. Additional information such as

a) flame on/off,
b) valves open/closed,
c) calibrate 1, on/off,
d) calibrate 2, on/off, and
e) pyrolysis oven on/off

could be added to provide additional verification of proper operation.

The use of one bit in shift-register 1 to indicate the operating mode was based on the need to know whether the system might have shut down prematurely due to ignition failure. These data are transferred to the capsule data-system with the timing data.

8.2.4 Timing Data

The timing data indicate the cycle period for one complete experiment. The status of flip-flops in the timing adjustment circuit are transferred to shift-register 1 and sampled periodically by the capsule data-system. Transfer can be accomplished either serially or in parallel.

8.3 Environmental Data

The only environmental data normally required are the temperatures of the instrument. This measurement will probably be made in the analog portion of the electronics since they are generally more susceptible to temperature variations than the digital electronics.

These data are generally acquired and processed by the capsule data system, independent of the operation of the instrument.

8.4 Calibration

A two-point system calibration is provided by calibrate commands 1 and 2 from the logic matrix in the programmer. If only one point is used to calibrate the system, non-linearities on either side of the calibration point may produce data which are abnormal. However, if two points are used, the general shape of the electronics response curve can be verified. Single point calibrations do not simultaneously distinguish between changes in offset, scale factor, and linearity.

To provide two-point calibration, the calibrate commands gate a current pulse of controlled magnitude and duration into a capacitor. This charge is transferred to the electronics input in parallel with the detector. The result is an output proportional to the charge. Calibrate-1 results in an output on the lowest scale of the electrometer. Calibrate-2 results in an output from the sensor electronics at the maximum level expected as a result of the detection of organic material.

The read-calibrate command gates these data into the analog-to-pulse-width converter. The output of the converter is handled in the same manner as scientific data.

9.0 INSTRUMENT PROGRAMMER

The instrument programmer provides the basic timing required for proper operation. This primarily involves the electronic and electromechanical sequencing of sample acquisition, flame ignition, valve actuation and oven operation. In addition, the programmer sends commands to the sensor electronics to ensure operation in synchronism with the subsystem and the landed capsule. The programmer also contains a mechanism to shut-down operation in the event that the flame does not ignite. It also provides a sample recycle mode in the event that the initial sample provided to the pyrolysis oven is inadequate.

A block diagram of the instrument data system is shown in Figure 8.0-1.

9.1 Timing Circuitry

The electronic sequencing is initiated by the application of an enable-analysis command from the spacecraft data system to the reset flip-flop. This allows the clock output to enter the timing-adjustment circuitry. Nominal timing is established by application of power to the circuit. An input to the timing-adjustment circuit changes the nominal period by a given amount and, in addition, resets the clock input to the timing adjustment circuitry. Each subsequent input results in a change in the timing circuitry until the period passes through its maximum and minimum values to return to the nominal setting. The time period used in the analysis is read-out to telemetry immediately preceeding each set of analysis data. Transfer of these data can be accomplished in parallel (bi-level) or they can be shifted-out serially to the landed-capsule data-system.

An enable-analysis command must be sent after each timing adjustment.

9.2 Logic Matrix

The logic matrix provides all of the sequencing necessary to perform an analysis. Its input from the timing-adjustment circuitry provides all the timing functions necessary to properly initiate and control the opening and closing of valves, electrometer operation and data handling. This includes the following:

	Signal	Designation
a)	Open valves	OV
b)	Open sample entrance valve	OS
c)	Close sample entrance	$\overline{OS}$
d)	Start igniter trigger	OV
e)	Reset electrometer	RE
f)	Set electrometer	$\overline{RE}$
g)	Start pyrolysis oven	SP
h)	Data ready	DR
i)	De-energize pyrolysis oven	$\overline{SP}$
j)	Close carrier gas valve	$\overline{OV}$
k)	Terminate integration	TI
l)	Inhibit scale changes	SP
m)	Read baseline current	RB
n)	Calibrate 1	C1
o)	Calibrate 2	C2
p)	Return to quiescent mode	RQ
q)	Read calibrate	RC

Signals e), f), k), l), m), n) and o) are used to control the operation of the electrometer. The functions of these

signals are discussed in the sections of this report relating to the electrometer or automatic scale factor circuitry. The remaining signals are covered in other subsections of this section.

9.3   Electromechanical Sequencing

The carrier, oxidizer and exhaust valves are controlled by the logic-matrix output. The open-valves signal output is sent to the carrier- and oxidizer-gas valves through a gate and flip-flop. Reset of the flip-flop is accomplished by the power-on reset signal and the outputs from the gas-valve drivers. The outputs of the gas-valve drivers are sent to the exhaust valve through a gate, flip-flop and driver. The delay between the opening of the gas valves and the exhaust valve allows the system to pressurize before being vented to the Martian atmosphere. This ensures a minimum possibility of contamination entering the system from outside the capsule.

The valves are closed a fixed time after the end of the data accumulation-period. This allows the system to be flushed before the valves are closed and the flame extinguished. In the event that the flame does not ignite, the valves are closed when the output from the divide-by-five counter enables an output from the logic matrix to the input gate of the flip-flop and valve drivers. Closing of these valves also results in the exhaust valve being closed.

9.4   Flame Ignition

The flame ignition trigger is activated by the open-valves signal. The trigger input consists of clock pulses which are prescaled and transferred to the input through a gate. This gate is enabled by the open carrier-gas-valve command and inhibited by the power-on reset, a divide-by-five counter and the background-current detector.

The divide-by-five counter output provides an inhibit to the gate after 32 prescaled clock-pulses have been accumulated. This ensures that, if the flame fails to ignite, the ignition trigger will not continuously pulse the igniter. The counter cannot accumulate 32 prescaled clock-pulses if the baseline-stabilization circuitry detects a quiescent background-current, which is due to the small amount of carrier-gas ionization. In addition, failure of the flame to ignite causes the system to return to the quiescent mode. The return of the system to the quiescent mode is indicated by the change-of state of one bit in shift-register 1.

9.5 Sample Acquisition

The spacecraft provides both the analysis enable-signal and the sample for analysis. A signal is also required from the spacecraft to indicate that a sample has been collected and is ready to be injected into the pyrolysis oven. Receipt of this signal enables the sample-entrance valve through the sample-valve driver-circuit. The sample-ready signal is combined with open sample-entrance valve signal and then sent through the "or" gate to a flip-flop, which triggers the sample-valve driver. This flip-flop is inhibited (reset) during power turn-on to prevent the sample-valve driver from operating. An output from the sample-valve driver is fed back to reset the flip-flop after each operation.

The complement of the open sample-entrance-valve signal is applied to the "or" gate, a preset period after the sample valve is opened, triggering the flip-flop and enabling the sample-valve driver circuitry. This closes the valve and causes the flip-flop to be reset.

The additional input to the "or" gate driving the flip-flop is operated in conjunction with the pyrolysis oven. If the sample injected into the oven is above a minimum size, an output from the oven circuitry will inhibit the clock pulses being sent to the divide-by-n counter. If the signal to inhibit the gate is not received because the sample is below the acceptable minimum, the output of the divide-by-n counter will trigger the sample valve. The value of "n" will be established when the sampling requirements are finalized. In any case, it will result in an output after the close sample-valve signal has been received.

An output from the divide-by-n counter is also sent to the logic matrix to cause it to issue a close sample-valve signal a fixed period after the divide-by-n output is received. This will ensure that the entrance to the pyrolysis oven is closed during system operation.

If an adequate sample is not received on the second try, an output is sent to the surface sampler to tell it to acquire more material. The sample-ready line drops to a "zero" level, and the instrument cycles until the sample acquisition is successful. Reapplication of the sample ready signal (at a "one" level) also activates the enable analysis signal line, causing the timing-adjust circuitry to be set and initiating a new analysis cycle.

9.6 Pyrolysis Oven Operation

The operation of the pyrolysis oven is controlled by the logic matrix. The second output from the sample valve-driver circuit sets the level at the input gate so that the start pyrolysis-oven function can activate the heater. The period between the start pyrolysis-oven signal and the second output

of the sample valve-driver is such that the heater power appli-
cation will be inhibited if the sample received is below the
minimum acceptable level. If an acceptable sample is received,
a signal is sent to the gate at the input of the divide-by-n
counter, inhibiting it.

The heater is operated until the terminate-integration
signal is received. This signal resets the heater flip-flop
driver. The continuing flow of carrier gas through the system
purges it of the gaseous material left in the oven.

10.0 THE DESIGN OF A FLAME IONIZATION DETECTOR FOR USE ON OTHER PLANETS

The FID is among the best of devices for measuring the concentration of volatile carbon compounds in a convenient inert carrier gas. Its detection limit is low, 10^{-12} gms sec^{-1}. It can be constructed with a linear dynamic range of 10^6 and has a response to different carbon compounds which is well established and consistent over a wide range of operating conditions. The complete insensitivity of the FID to the fixed gases and to water vapor is a great convenience and makes the detection of traces of organic compounds in an excess of these other gases easy.

Its drawbacks are a poor ionization efficiency (10^{-5}) so that for high sensitivity an electrometer amplifier is mandatory, and the fact that three gas supplies are necessary; carrier gas, hydrogen and air or oxygen.

At first sight it would seem that this queen of detectors would be the one choice for the reliable analysis of volatile carbon compounds in planetary exploration experiments. The adaptation of this detector to an extraterrestrial environment is unfortunately a comparatively difficult although an interesting and challenging problem. This section describes such an adaptation and the means by which the various environmental problems were met. Also described are the construction and circuit connections of an experimental FID for planetary probe use and the results of its performance under simulated alien conditions.

10.1   The Problem

On Earth a flame ionization detector can operate with
air at atmospheric pressure as the oxidizer and under condi-
tions where the exhaust products vent freely to the atmosphere.
A generous excess of air over that required for combustion of
the hydrogen is easily available and is usually 20 times the
volume flow of hydrogen. This excess flow serves to support
efficient combustion and detectivity and also to carry away
the water formed during combustion.

Earth is unique in its oxygen-containing atmosphere.
Consequently, for other planets the scavenging and combustion
supporting properties of air flow must be replaced by a supply
of pure oxygen. It would be tempting to consider mixing oxy-
gen with the planetary atmosphere so that the scavenging func-
tion at least could be supplied locally. This is not possible,
however, for two reasons: (1) It is probable that detectable
gases (eg. CH_4) exist on other planets; (2) The atmospheric
pressure of Mars, for example, is far too low for efficient
operation.

It is therefore necessary to design an enclosed detector
with its own oxygen supply and, as will be shown later, with an
internal pressure in the region of 1000 mb. These design con-
straints require a detector construction different from that
which would be suitable on Earth. The various problems aris-
ing from these constraints are now considered in sequence.

(1)   Insulation: The heat of combustion and the generous
flow of air in an FID on Earth maintain the internal
relative humidity at a low value, so that water
condensation on the insulator surfaces is rarely a
problem. Temporary failure immediately after

ignition and before the detector has warmed up,
although avoidable, is regrettably common in
many commercial detectors. For the planetary
problem this is intolerable; yet due to the high
internal humidity more likely.

This problem has been solved in the design shown
in Figure 10.1-1 by ensuring that the water exhaust
from the flame never encounters the insulator sur-
faces. Furthermore, the only internal exposure of
the insulator is at the oxygen entry port. This
gas is intentionally dry and continuously scavenges
the insulator surface.

(2) Oxygen Requirement: The FID gives the highest detec-
tivity with a diffusion flame seated on a jet. Such
a flame requires a flow of oxygen at least twice the
stoichiometric amount for stability and efficient
operation. The most economical use of oxygen occurs
when the flame burns in a narrow chimney so that
there is the highest possible linear flow rate of
oxygen consistent with keeping the flame away from
the walls of the chimney. (See Figure 10.1-1) By
good fortune this requirement is consistent with the
most efficient collection of ions and hence the
largest possible dynamic range. It also enables the
detector to function in any orientation and probably
at zero gravity.

The ionization efficiency of the detector in Fig-
ure 10.1-1 does not greatly improve at oxygen flow
rates above four times stoichiometric. Two times
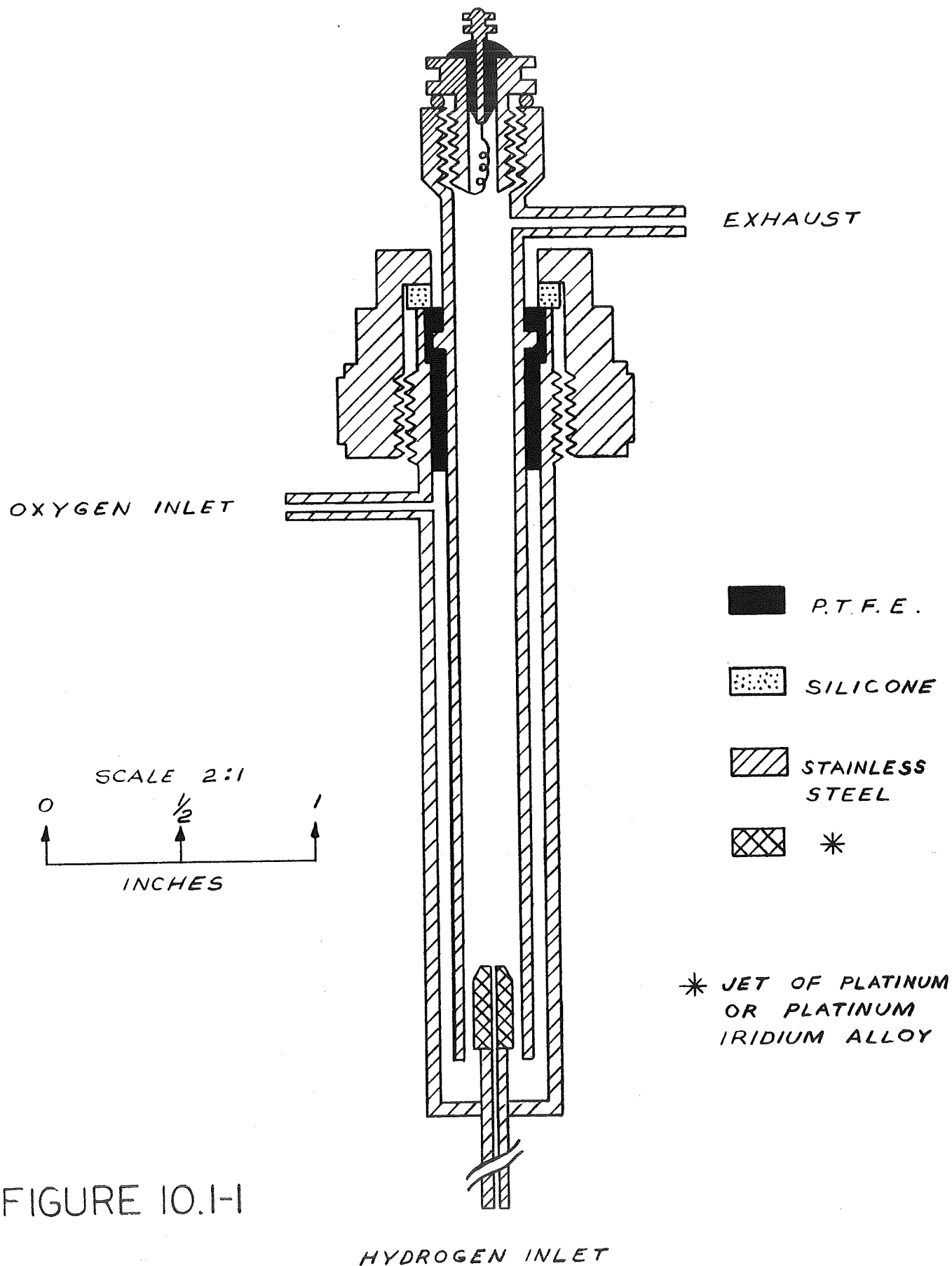the stoichiometric value produced approximately

EXHAUST

OXYGEN INLET

P.T.F.E.

SILICONE

STAINLESS
STEEL

✳

SCALE 2:1

0   ½   1

INCHES

✳ JET OF PLATINUM
OR PLATINUM
IRIDIUM ALLOY

FIGURE 10.1-1

HYDROGEN INLET

EXPERIMENTAL FLAME IONIZATION DETECTOR

10.1-3

50% of the maximum efficiency. An oxygen flow rate of three to four times the stoichiometric value is recommended.

(3) <u>Internal Pressure</u>: Figure 10.1-2 shows the variation of detector efficiency with pressure. The variation is linear down to 50 mb, the lowest value tried. The exact choice of internal pressure is an arbitrary one, but in the interests of efficiency should be in the region of 1000 mb. This internal pressure is easily maintained by means of throttles on the inlet and exhaust gas. These could conveniently be capillary tube flow restrictions. Such a procedure was used in the experimental trials of the detector with good results.

(4) <u>Heat Production</u>: Under normal conditions an FID generates 20 watts of waste heat. The design in Figure 10.1-1 was chosen by trial and error as the smallest in which this heat production would not cause, at maximum hydrogen flow (40 ml/min. NTP) and exposed in air at 20°C, a rise of insulator temperature above 150°C.

In packaging for instrument use, a careful evaluation of possible temperature limits under specified environmental conditions is essential.

(5) <u>Hydrogen Flow</u>: The detector can be operated at hydrogen flows between 10 and 40 ml/min. NTP. 20 ml/min. is recommended.

(6) <u>Electrical Connections</u>: The complete enclosure of the detector makes the introduction of lead-in connections
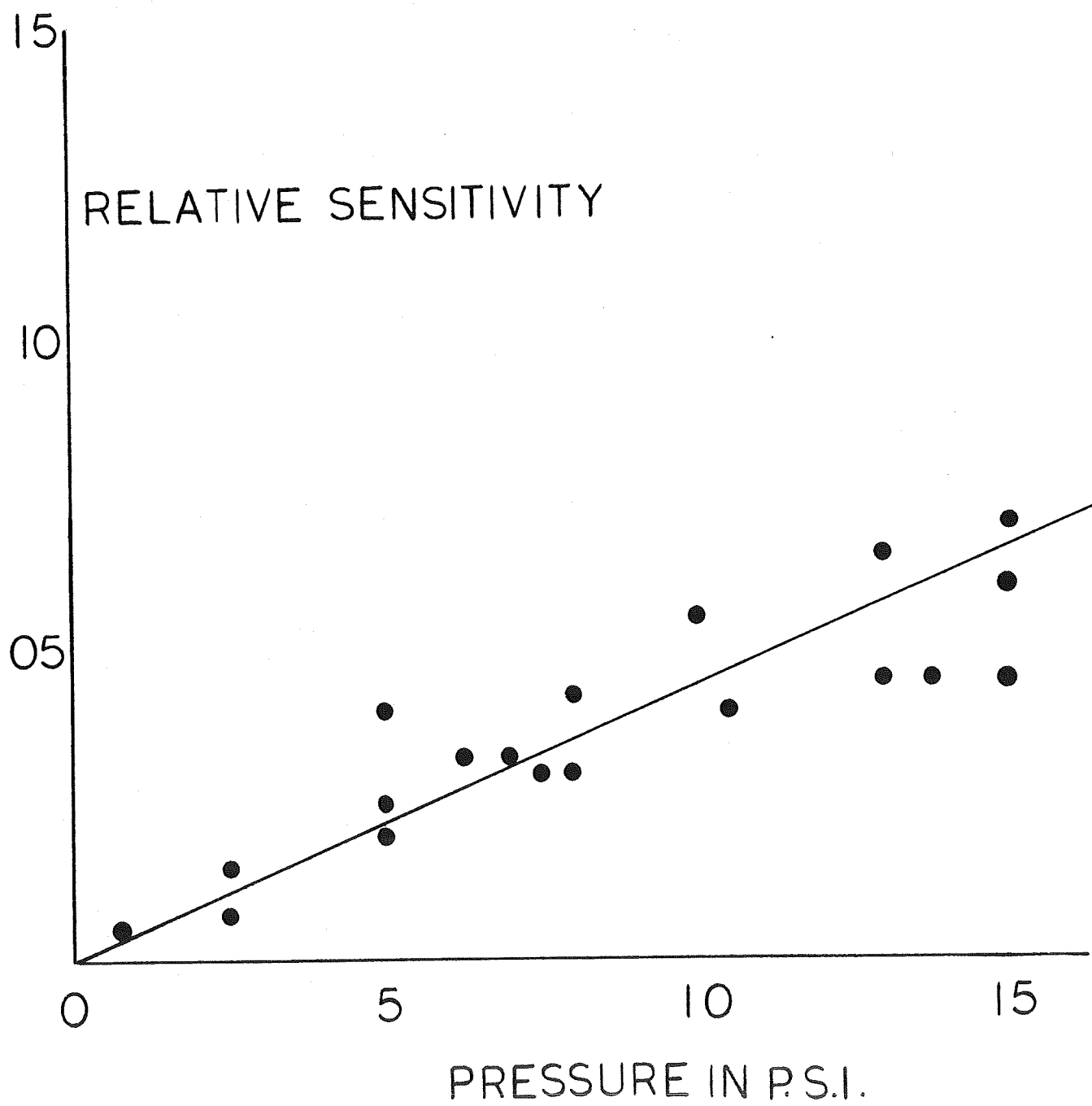
FIGURE 10.1-2

PLOT OF SENSITIVETY VS PRESSURE

10.1-5

to the collector electrode, jet and ignitor dif-
ficult and an undesirable source of leakage, gas
and electrical.

The detector was therefore designed with an outer
case and jet at ground potential and with the col-
lector and ignitor as a single continuous metal
construction insulated at a single point. (See
Figure 10.1-1.) Such a construction, which is
robust and reliable, is made possible by including
the ignitor and polarizing potential supplies in
the electrometer input lead. Both the ignitor and
polarizing supplies are fed to this lead through
PTFE insulated transformers with air cores operat-
ing at any convenient frequency between 1 and
10 MHz.

(7) Ignition and Ignition Indication: Ignition is by
means of a heated platinum wire which also serves
as a resistance thermometer indicating whether the
flame is or is not lit.

So far ignition under enclosed conditions has proved
to be the only intractable problem.

The pressure pulse, as the H_2O_2 mixture in the detec-
tor explodes, forces the oxygen and exhaust steam
back into the jet thereby displacing the hydrogen
flow. Instead of smooth ignition the detector goes
into a mode of relaxation explosions. These hard
starts remind one of the similar but grander pro-
blems of the "Centaur" motor.

The explosion mode is not invariable and is less
likely to occur at high oxygen flows. Further
study is required before the detector can be con-
sidered completely finished and ready for planetary
use.

(8) Performance: Figure 10.1-3 shows a chromatogram
made with the detector operating at 510 mm pressure
and with a flow rate of hydrogen of 225 ml/min.
NTP and oxygen 50 ml/min. NTP. Under the conditions
the noise level was 10^{-12} amperes* (0-1 Hz band pass)
and mostly attributable to small pressure fluctuations.
The background current was 4 x 10^{-10} amperes which
is rather high and may have been due to trace con-
tamination of the oxygen supply. The ionization
efficiency is in the expected range of 10^{-6} to 10^{-5}.

10.2 General Comments

There seem to be no insuperable problems preventing the
design of an efficient FID for planetary use. The ignition
problem has several possible routes to its solution, such as
optimization of Hydrogen and Oxygen ratios.

We would recommend for planetary use the consideration
of alternate detectors (eg. photoionization) so that the
most efficient and least costly device, in terms of weight and
power, is used.

---

* Much of the noise is believed to come from the laboratory
equipment used for the detector tests.
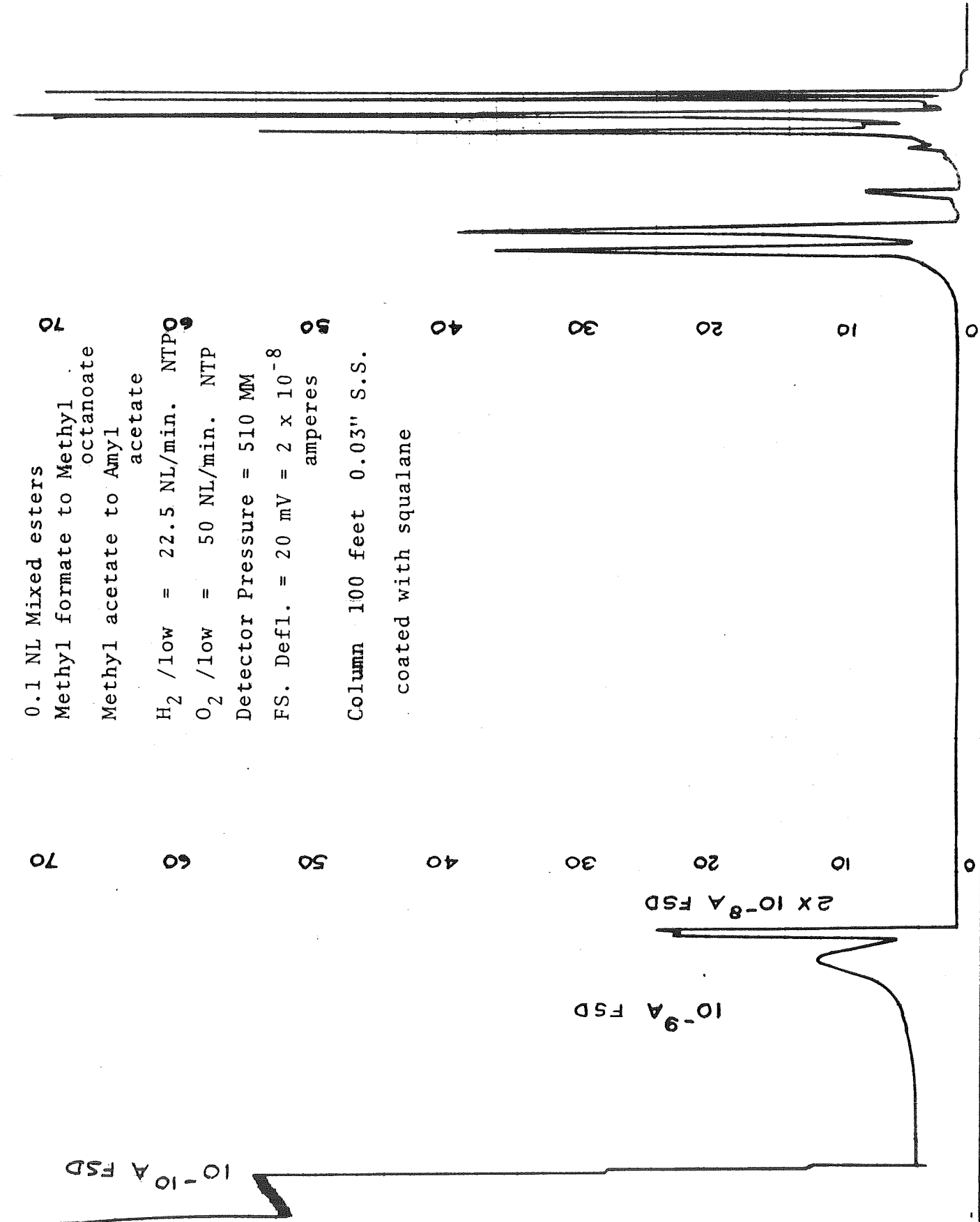
0.1 NL Mixed esters
Methyl formate to Methyl octanoate
Methyl acetate to Amyl acetate

H_2 /low = 22.5 NL/min. NTP
O_2 /low = 50 NL/min. NTP
Detector Pressure = 510 MM
FS. Defl. = 20 mV = 2×10^{-8} amperes

Column 100 feet 0.03" S.S. coated with squalane

2×10^{-8} A FSD

10^{-9} A FSD

10^{-10} A FSD

FIGURE 10.1-3 SAMPLE CHROMATOGRAM

11.0 RECOMMENDED SYSTEM

All techniques studied in this program are described in prior sections of this report, and in those sections dealing with systems felt to be clearly inadequate, explicit conclusions have been stated. After discarding several other techniques, or combinations of techniques, as being obviously inferior, a choice was made between two truly competitive systems, each having special advantages. The system which has been selected and described in subsections 11.1 and 11.2 contains the following two prominent and overriding features:

1) Automatic ranging is not required.

2) Analog-to-digital conversion is performed within the current-measuring feedback loop.

This system and its associated advantages are now described in detail.

11.1 Recommended Signal-Processing System

The analysis of electrometers and electrometer systems presented in the previous sections leads to a definite conclusion: If input leakage currents of the order of 10^{-12} A at room temperature are acceptable for systems operating on the Martian surface, where the daily temperature rarely reaches 20°C, then the digital integrating electrometer analyzed in Section 4.3 is the most desirable choice, because it possesses 7 or 8 decades of dynamic range without range switching. The digital output of the device may be counted by a straight binary counter (8 decades = 27 bits), a decimal counter, or may be digitally compressed, for example, by use of a logarithmic counter.

The same device, using commercial parts and without spaceworthy packaging, should be used as a laboratory electrometer, since there is no point in designing two different kinds of systems. Digital readout and control mechanization will of course be different for the laboratory instrument.

A block diagram of the complete electrometer section is shown in Figure 11.1-1. The system is the same as that shown in Figure 4.3-1, except that the postamplifier will probably not be required.

The baseline stabilization may be performed by analog methods as described, for example, in Reference 4.3.2-1. Alternatively, one may use the digital method shown in the figure, which has the advantage that there is no decay of the correction during the period of observation. Also, the output of the instrument is inherently digital, so that digital baseline stabilization and its special advantages can be achieved more simply than the digital stabilizing system discussed in Section 6.0.

In the technique illustrated in Figure 4.3-1, the baseline is stabilized by allowing the instrument to count for a short time. The accumulated count is proportional to the drift. A baseline current correction, with resolution comparable to the minimum feedback current, is applied by using a digital-to-analog converter to apply a stable voltage to the large-value resistor. It may be shown that the counting rate produced by the initial drift will decay exponentially to zero.

The ratemeter and recorder shown provide an output proportional to current for making chromatographs suitable for

11.1-1

RECOMMENDED SIGNAL-PROCESSING SYSTEM

FIGURE 11.1-1

conventional graphical presentation. The ratemeter may be linear with manual range switching, or logarithmic.

The system shown provides only one size of feedback charge and baseline correction, under the assumption that the detector baseline current will greatly exceed amplifier and switch leakages. If this assumption proves to be unjustified, both sizes of feedback may be used without a prohibitive increase in complexity.

Typical system parameters are listed in Table 11.1-1.

It should be emphasized that this almost entirely digital system is made practical by modern integrated-circuit technology. By the time the opportunity to land such an instrument on the surface of Mars presents itself, this technology will have advanced to the point where most of the system components will be packaged in only a few integrated units. Custom integrated circuit design will have advanced to the point where specialized devices can be made well within the budgetary confines of a single experiment. Finally, field-effect transistor technology, particularly that of low-noise insulated gate devices, while adequate for the proposed system, should have advanced to such a point that the dominant system errors will be produced entirely by the detector. A laboratory instrument, using presently available commercial components, may now be designed and built after which flight-type designs of similar configurations could be produced.

Maximum Input Charge	10^{-5} C
Minimum Input Charge	10^{-12} C
Maximum Signal Current	10^{-6} A
Minimum Signal Current	10^{-13} A
Observing Time	10^2 S
Integrator Saturation Voltage	10 V
Discriminator Threshold	0.1 V
Baseline Current	$< 10^{-11}$ A
Residual Baseline Current (after correction)	10^{-14} A
Threshold Charge	10^{-12} C
Feedback Charge (resolution)	2×10^{-12} C
Feedback Capacity (Q_t/V_t)	10 pF
Reference Voltage	0.1 V
Reference Voltage Stability (100°C)	~ 1 mV
Charge Pulser Capacitor	20 pF
Feedback Frequency	100 KHz
Accuracy	5%

Table 11.1-1

Typical System Parameters Recommended for Electrometer

11.2 Laboratory Programmer and Data Handling System

A laboratory instrument-programmer would retain many
of the functions included in the flight-instrument design.
Included are:

a) commands to the electronics,

b) timing adjustment,

c) clock data handling,

d) ignition trigger, and

e) heater driver.

The functions of these commands would be identical to those
of the flight instrument.

The inputs normally received by the flight instruments
from the capsule would be replaced by alternate mechanizations.
For example, the step-timing command could be a momentary-
contact switch suitably buffered from the timing adjustment
circuitry to preclude false triggering due to contact bounce.
This same mechanization could also be used for the enable-
analysis command. Bit-sync input could be eliminated since
the instrument clock is not required to operate in synchronism
with any other piece of equipment.

Shift-register 1 would be replaced by a set of lights to
indicate the particular timing sequence and the operating mode
of the instrument. In addition, a printer output could be
added to provide a permanent data record of the timing of a
given experiment.

The command sequence would be indicated by lights. Each
time a command was issued, a lamp would light, indicating that
a command had been sent and indicating progression of sequencing.

The data-handling mechanization would be identical to
that used in the flight instrument except that the data-ready
signal would activate a printer. The data would be sampled

and recorded by the printer upon receipt of this signal. The sequence used in printing the data would be

a) mode and timing adjustment,
b) calibrate 1,
c) calibrate 2,
d) scientific data, and
e) scale-factor information, if required.

This would ensure that all data logged are correlated. An additional option could be provided to indicate the date and time of experiment initiation, if desired.

Leaving the igniter and heater controls in the laboratory instrument would allow more precise control over timing of these functions than could be achieved using manual techniques. Since the timing of the experiment is dependent upon flame ignition and connection of the background or baseline current, it is essential that both ignition and heater-power application be closely controlled. The timing adjustment circuitry primarily controls the period following the connection of baseline current, the application of power to the pyrolysis oven and the termination of integration. The interval between each of these operations can be controlled individually to give the widest possible flexibility to experimental operation.

References

3.1-1   J. H. Marshall, <u>JPL Space Program Summary</u> 37-14, Vol. VI, pp 38-40.

3.1.1-1   H. Z. Reed, <u>Status Report on Physics Branch Low Current Detector Program</u>, Report No. X-623-65-391, Goddard Space Flight Center, Greenbelt, Maryland, 1965.

3.1.2-1   E. J. Kennedy, "Gate Leakage Current in MOS Field Effect Transistors," <u>Proceedings of IEEE</u>, p 109A, August, 1966.

3.1.2-2   R. A. Emerling, J. H. Mullins, J. Van Putten, J. O. Malloy, and H. G. Bartholomew, "Rocket Gamma Scattering of Nuclear Bursts," <u>IEEE Transactions on Nuclear Science</u>, Vol. NS-13, No. 1, p 569, February, 1966.

3.1.2-3   R. D. Middlebrook, <u>Differential Amplifiers</u>, John Wiley & Sons, New York, 1963.

3.2.1-1   C. S. Josias and J. L. Lawrence, Jr., "An Electrometer for Use in Scientific Space Instruments," <u>IEEE Transactions on Nuclear Science</u>, October, 1966.

3.2.2-1   ATC Staff, "Final Report on the Gemini Plasma Wake Instrument Development Program," prepared for Electro-Optical Systems, Inc., 1 January 1966,

3.2.2-2   J. E. Lovelock, "Electron Absorption Detectors and the Technique for Use in Quantitative and Qualitative Analysis by Gas Chromatography," Anal. Chem., Vol. 35, No. 4, p 474, April, 1963.

4.3.2-1   J. H. Marshall, "A Capacitor Storage Scheme for Gas Chromatograph Detector Quiescent Current Compensation," <u>JPL Space Program Summary</u> No. 37-24, Vol. IV, 213, Dec. 1963.

4.3.2-2   ATC Staff, "An Experimenter's Handbook for Space Instrument Design," Sections 3.1 and 3.7, 7/29/66.

4.3.2-3   T. M. Harrington, J. H. Marshall, "A Pulse-Height Analyzer for Charge-Particle Spectroscopy on the Lunar Surface." In Press.

4.3.4-1   S. Chandrasekhar, <u>Stockastic Problems in Physics and Astronomy</u>, Rev. Mod. Phys. 15, 1943.

4.3.4-2   S. O. Rice, "Bell Systems Technical Journal," $\underline{23}$, (1944); $\underline{25}$, 46 (1945).

4.3.4-3   M. Kac, American Journal of Mathematics, L X V, 609 (1943).

5.0-1   J. H. Marshall, "An Automatic Scale Factor Device for Use with Spacecraft Electrometers," JPL Space Program Summary 37-23, Vol. IV, 245, Oct. 1963.

Appendix I

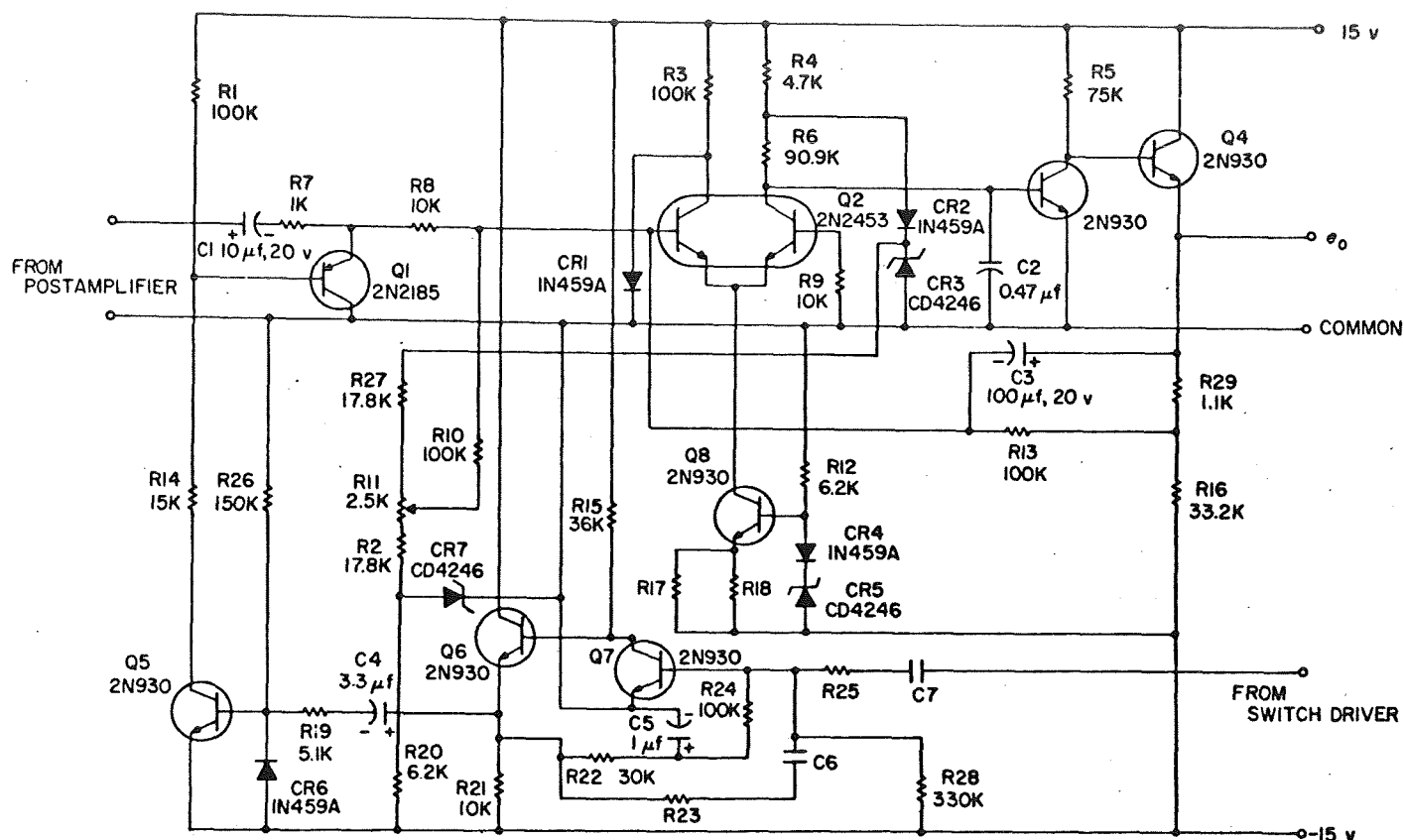Gas Chromatograph Instrumentation Development

Fig. 51. Microwave radiometer phase shift circuit, demodulator, and DC integrator amplifier

Because of the high over-all gains involved (approximately 10^7), gain tests for the entire post-RF electronics are not feasible due to pickup problems, but gain variations should be approximately the sum of the gain changes (measured in db) of the preamplifier and the remainder of the system. The over-all gain variations determined by this method are $+0.3$ db and -0.45 db. This is within the required ± 0.5 db. The worst-case phase shift as calculated by assuming all variations in the same direction produces a total phase variation of about ± 6 deg, well within the requirement of ± 10 deg.

Preliminary tests on the crystal show that besides impedance variations, the sensitivity varies about 20% as well. A large sensitivity change makes it difficult to determine if the post-RF electronics maintains the proper gain stability when the crystal is included in the system. Phase stability, noise and pickup interference, and output DC drift, however, can be determined independent of detector parameter variations.

The results obtained thus far show that the post-RF electronics will meet all the design requirements. It is

felt, as a result, that a basic improvement has been achieved for this system in stability of gain, phase, DC operating points and over-all circuit reliability.

N. Gas Chromatograph Instrumentation Development

This report describes those aspects of instrument technology developed recently that will be applicable in future flight-type gas chromatographs for analysis of planetary atmospheric composition and biological organics. The principal subjects discussed here are as follows: (1) laboratory chromatograph, (2) calibration of cross-section detector, (3) linear-logarithmic electrometer, (4) linear automatic scale changing electrometer, and (5) automatic baseline compensation.

1. Laboratory Chromatograph

The chromatograph (Fig. 52) consists of a valve that injects a sample into each of two parallel columns. A capillary restrictor in series with one column delays its output to the detector till the other column has completed its separations. The system uses a cross-section detector with helium as the carrier gas, and the output current is measured with a modified *Mariner 1962* Solar Plasma Analyzer electrometer (Fig. 53). The output of the electrometer is fed into wave-shaping circuits and from there into a one-shot multivibrator. The multivibrator triggers a printer that records the retention time and peak amplitude of the electrometer output. In a flight instrument application, however, more serious thought would be given to a measurement of the area under the chromatogram peak rather than its amplitude in anticipation of providing more reliable quantitative information.

The principal changes made to the *Mariner* electrometer were the addition of a 10^{10} ohm resistor in the primary feedback (Fig. 53) and reduction of secondary feedback for currents below 10^{-10} a. The resistor was added to permit the electrometer to be forced to zero by the self-zeroing system. The 10^{10} ohm value was determined by considerations described later in this section (3. *Baseline Compensation*). The secondary feedback modification improved the response of the electrometer to the low currents. The voltage-current characteristic for the combined logarithmic-resistive feedback electrometer is shown in Fig. 54.

2. Calibration of Cross-Section Detector

Good quantitative information as well as qualitative data on the separated gases requires that both the detector and electrometer amplifier be calibrated. The detector calibration (Fig. 55), as recommended by Dr. J. Lovelock (Ref. 32) of the Baylor Medical School, was accomplished as follows: With the carrier gas flow rate precisely known and controlled, the background current I_d was nulled to about 10^{-12} amp. The carrier gas was then disconnected, and the test gas (in this case N_2) was allowed to flow through the detector for about 2 min. This is necessary to ensure that the dilution vessel (Fig. 53) contains only the pure test substance. The test gas source is then replaced by the carrier gas source by means of a three-way valve. The carrier gas then begins to combine with the test gas in the dilution chamber. The two gases may be considered a homogeneous mixture since they are constantly being agitated by a magnetic stirrer. The percentage test gas in the resulting output from the dilution vessel will decay at an exponential rate. This decay, as measured by the electrometer amplifier, is plotted on a recorder (Fig. 56) which provides the detector calibration. The electrometer calibration is then accomplished by injecting precisely known currents into the summing point and recording the corresponding output voltage.

The calibration curve provided by the recorder may now be plotted, with the correction provided by the electrometer calibration, on semilog paper (Fig. 57). The non-linearity observable at the higher concentrations was due to the absorption of some of the lower energy particles by the test gas. The use of a higher energy source, which would be the case in a flight instrument application, would eliminate this problem.

The calibration procedure consists of correlating the concentration and current decay equations which are given by

$$C = C_o \epsilon^{-\frac{u}{v}t} \tag{1}$$

and

$$I = I_o \epsilon^{-mt} \tag{2}$$

where C_o is the initial concentration (100%), u the flow rate, v the dilution vessel volume, and I the output current of the detector. Where the detector characteristic is initially non-linear, the current I_o must be obtained by a straight-line extrapolation of the semilog plot to the intercept of the ordinate ($t = 0$). The proportionality between concentration and current on the linear portion of the detector characteristic may then be written

$$\frac{C}{C_o} = \frac{I}{I_o}.$$

The measured slope

$$m = 2.303 \frac{(\log i_1 - \log i_2)}{t_2 - t_1}$$

and the theoretical slope u/v can be compared to determine the accuracy of the measurement.

3. Baseline Compensation

a. Introduction. Most sensitive ionization detectors used with gas chromatographs possess a quiescent current large compared to the currents produced by eluted samples. Since this quiescent current is dependent on temperature, pressure, and ionization source intensity, the current cannot be assumed to remain fixed over long periods of time. Therefore, measurement of small concentrations of gas by a planetary-type instrument, after the long period of transit to the planet, requires automatic baseline compensation.
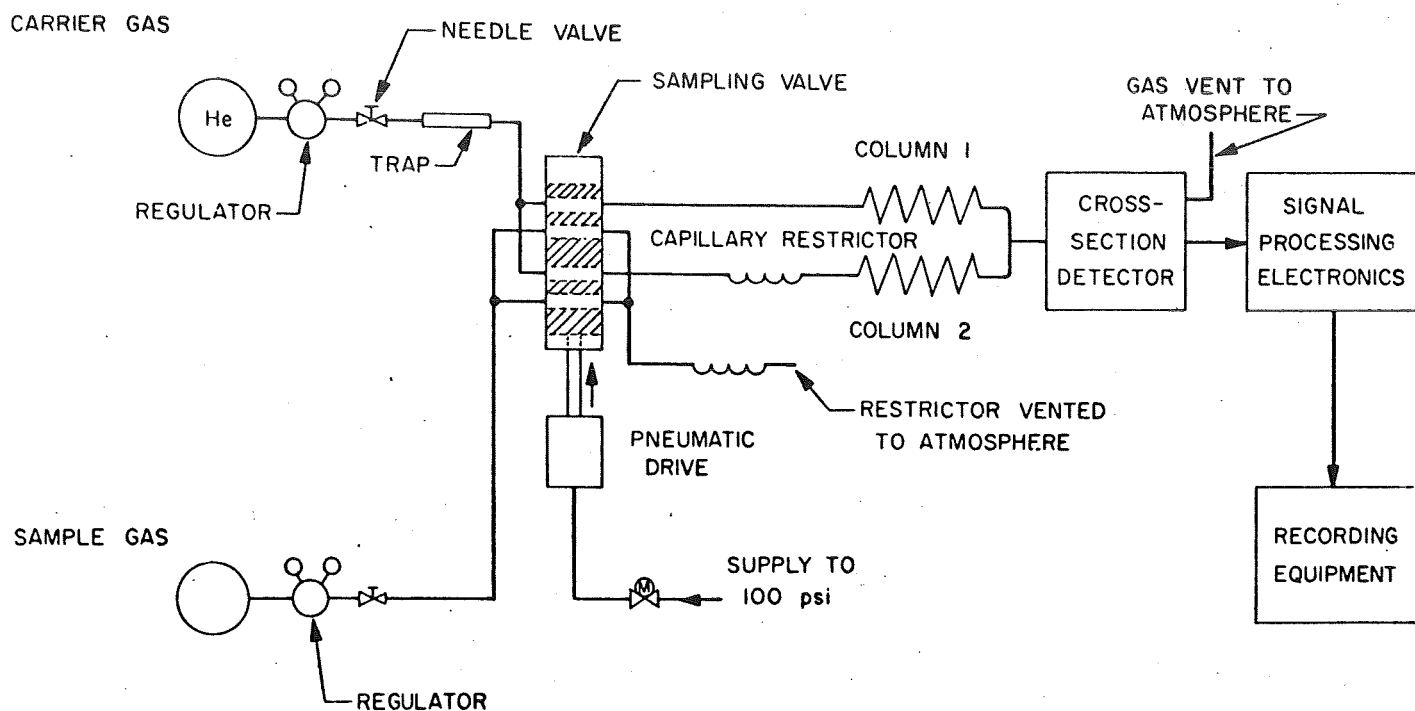
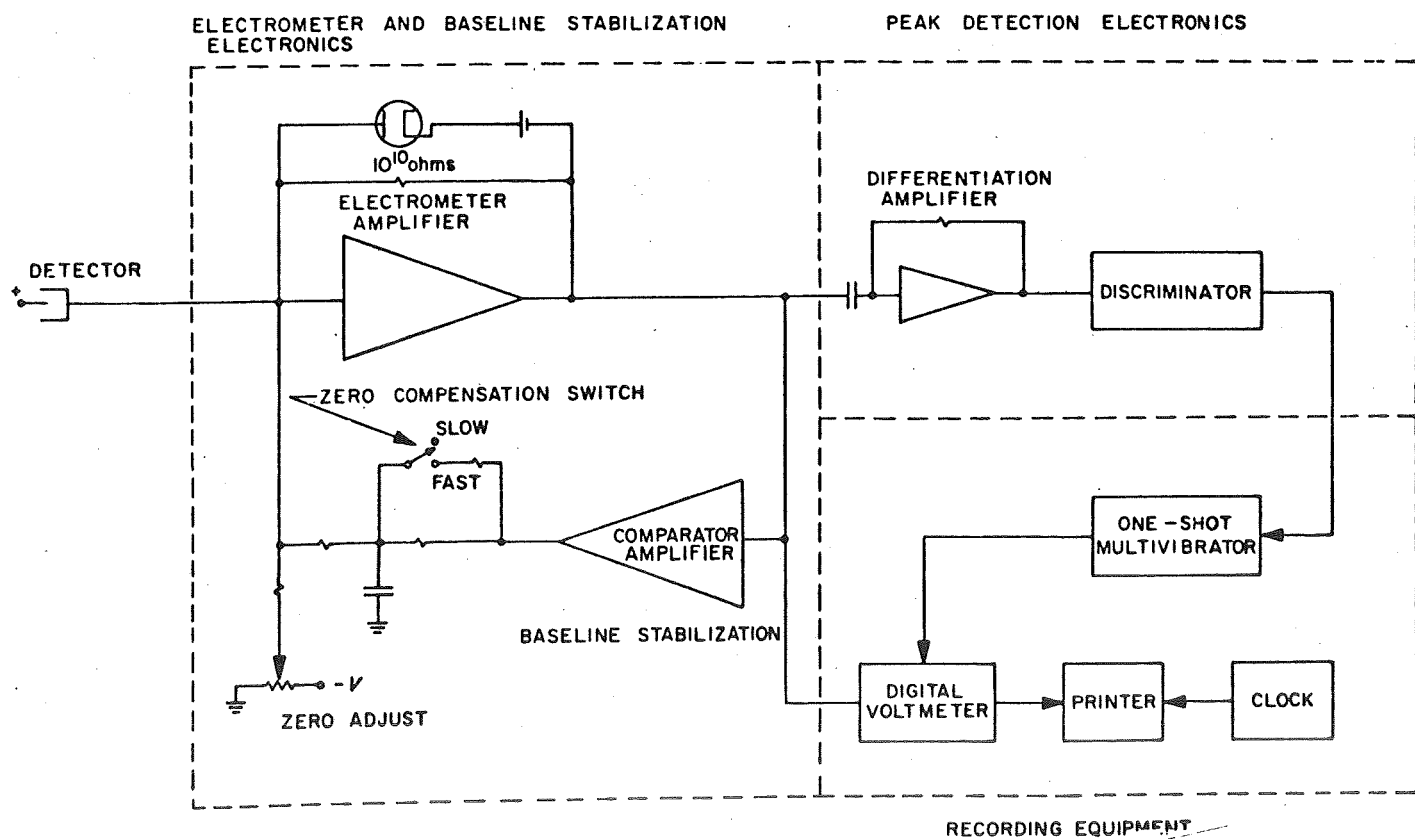Fig. 52. Planetary atmospheric gas chromatograph model

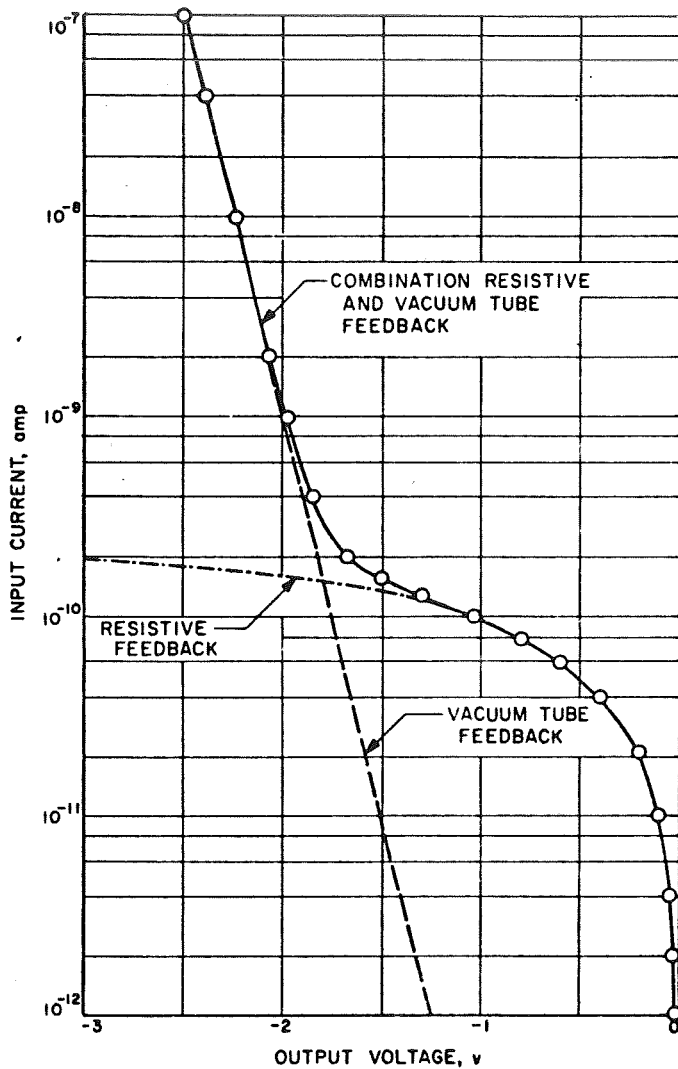Fig. 53. Gas chromatograph signal-processing electronics

Fig. 54. Volt-ampere characteristic of logarithmic-resistive feedback electrometer

The block diagram of a linear automatic system built and currently in operation at JPL is shown in Fig. 58. This approach is similar to one suggested in a study program for a Martian atmospheric gas chromatograph (Ref. 33). An electrometer amplifier (A_1) with a feedback resistor, R_{f1}, measures the current entering the summing point (P). If A_1 is sufficiently large that the summing point can be approximated as a virtual ground, then

$$V_{out} = - R_{f1}\left(i_d + i_c + \frac{V_b}{R_b}\right). \tag{1}$$

The zero compensating technique consists of adjusting i_c by means of feedback so that when only carrier gas flows

in the detector the electrometer output voltage approaches zero. Thus:

$$i_c = - \left\{ I_d + \frac{V_b}{R_b} \right\} \tag{2}$$

where I_d is the quiescent detector current.

In constructing such a system, several points must be considered. First, the maximum value of i_c which is required determines the dynamic range of the zero compensating system. Second, the accuracy to which the output must equal zero determines the gain, resolution, and stability of the zero compensating system. Third, the speed of response is partly determined by requiring that large peaks should not cause baseline shifts in excess of the allowed accuracy of the zero setting.

b. Analysis. Assuming that none of the amplifiers saturate, the response of the output to a detector current, i_d, is given by

$$V_{out} - V_o =$$

$$\frac{i_d\, R_{f1}\, (p\tau + 1)}{p\tau \left(\dfrac{R_{f1} + R_{f2}(1 - A_1)}{A_1\, R_{f2}}\right) + \dfrac{R_{f1}\,(1 - A_1 A_2)}{A_1\,(R_{f2} + R_{f3})} + \dfrac{(1 - A_1)}{A_1}} \tag{3}$$

where

$$\tau = \frac{C\, R_{f2}\, R_{f3}}{R_{f2} + R_{f3}}$$

and p is the Laplace transform variable. For values of A_1 large enough to make the summing point (P) a virtual ground, Eq. (3) may be rewritten

$$V_{out} - V_o = - \frac{i_d\, R_{f1}\, (p\tau + 1)}{p\tau + A_2' + 1} \tag{4}$$

where

$$A_2' = \frac{R_{f1}}{R_{f2} + R_{f3}}\, A_2.$$

Thus slow changes in i_c are reduced by a factor of $1 + A_2'$, and the ϵ^{-1} speed of response is given by

$$\tau_f = \frac{\tau}{1 + A_2'} = \frac{C\,(R_{f2} + R_{f3})}{R_{f2} + R_{f3} + R_{f1}\, A_2} \tag{5}$$

The response of such a system to a linearly rising current of the form $i_d = kt$, where k is in units of amp/sec,
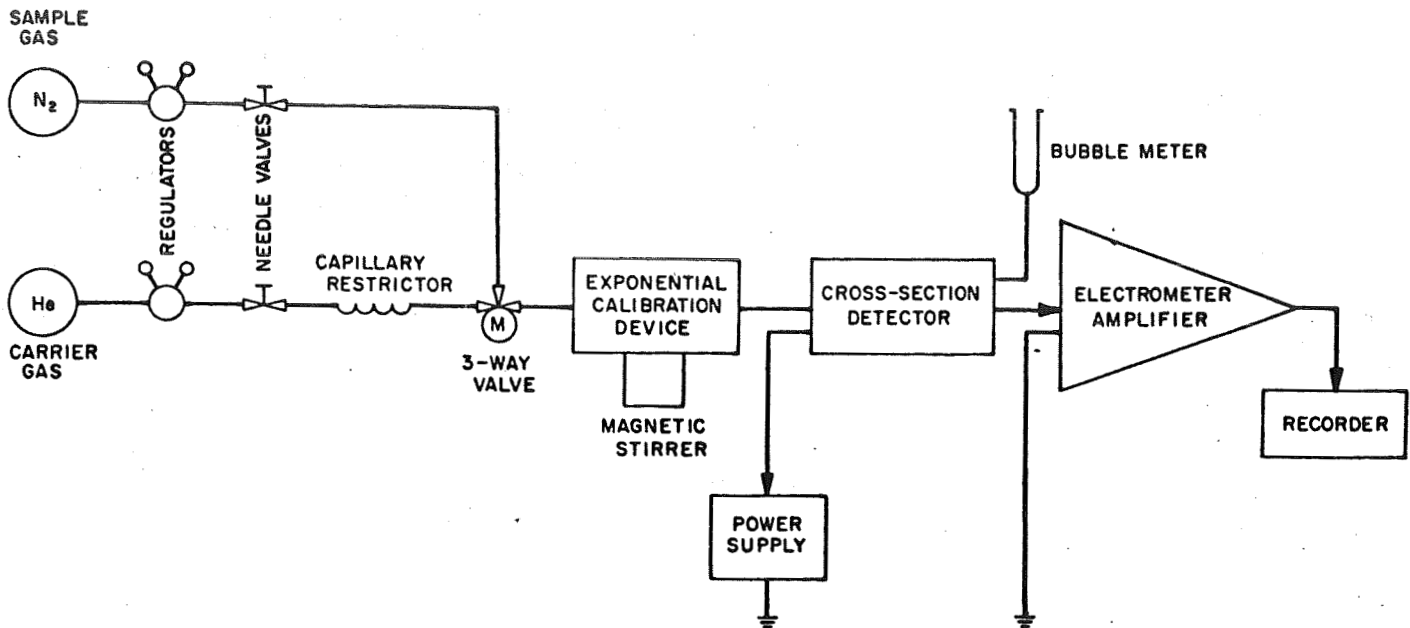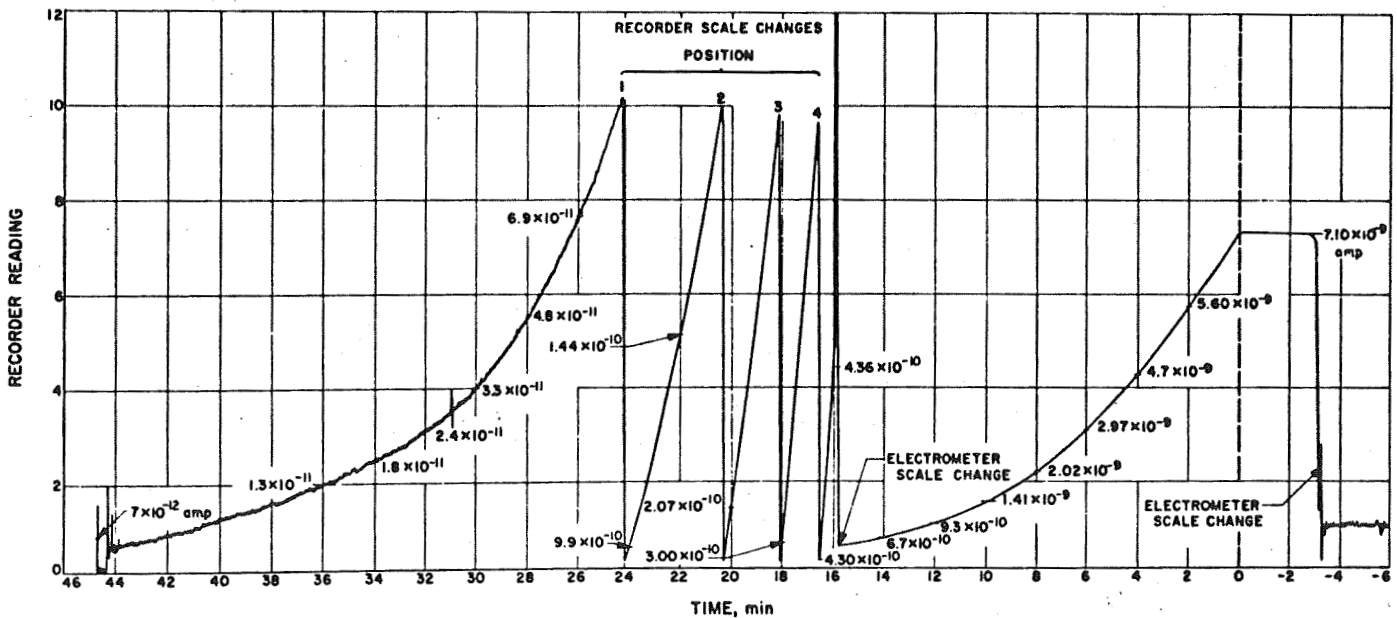
Fig. 55. Detector calibration system for permanent gases

Fig. 56. Cross-section detector calibration with automatic scale switching electrometer test gas, N_2

may be expressed respectively in complex and real-time terms as follows:

$$[V_{out} - V_o] = \frac{-R_f k \left(p + \dfrac{1}{\tau}\right)}{p^2 \left[p + \left(\dfrac{1 + A_2'}{\tau}\right)\right]}, \qquad (6)$$

$$[V_{out} - V_o] = -\frac{k R_{f1}}{(1 + A_2')}\left[\frac{\tau A_2'}{1 + A_2'}\left(1 - \epsilon^{-\frac{t}{\tau_f}}\right) + t\right], \qquad (7)$$

For times long compared to τ_f and for $A_2' >> 1$

$$V_{out} - V_o \simeq -\frac{k R_{f1}}{A_2}(t + \tau). \qquad (8)$$

EXPERIMENTAL SLOPE m = -0.19
THEORETICAL SLOPE $\frac{u}{v}$ = -0.21
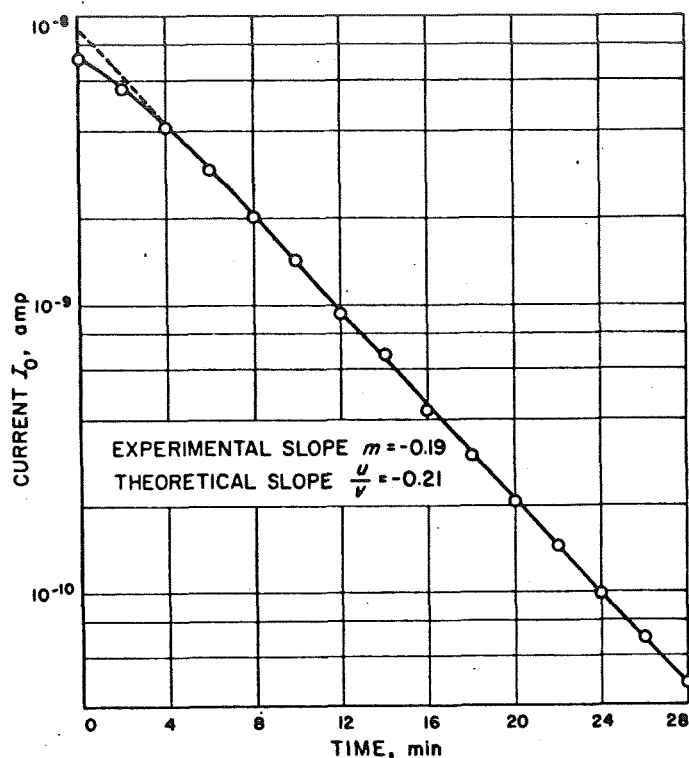
Fig. 57. Cross-section detector calibration with automatic scale switching electrometer

The above analysis holds for small, slow variations of the detector current. However, during peaks, whose widths are short compared to τ, the fast variations will usually cause the amplifier A_2 to saturate. If τ is long compared to the total time during which peaks are appearing, then the voltage across the capacitor (ΔV_c) is determined by the saturation voltage of A_2 (V_s) and the fraction (η) of the time that the peaks cause the amplifier to saturate.

Assuming in this design that the amplifier, A_2, is limited by current and voltage saturation at zero and $+V_s$ volts, respectively, the capacitor will then charge as follows after a time, T, of peaks:

$$\Delta V_c = \frac{I_c T \eta}{C} \qquad (9)$$

where I_c is the capacitive charging current.

In the general case, the charging currents may be written

$$I_c(+) = \frac{V_s}{R_{f3}} - V_{co}\left[\frac{R_{f3} + R_{f2}}{R_{f3} R_{f2}}\right] \qquad (10)$$

$$I_c(-) = \qquad - V_{co}\left[\frac{R_{f3} + R_{f2}}{R_{f3} R_{f2}}\right] \qquad (11)$$

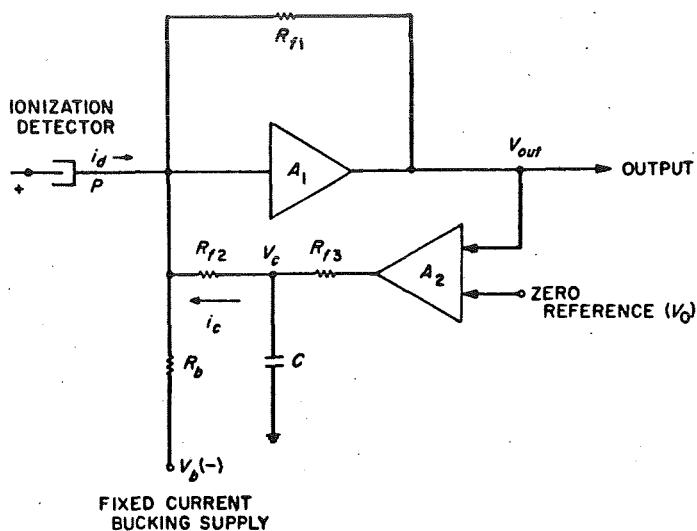**FIXED CURRENT BUCKING SUPPLY**

Fig. 58. Linear feedback with a low-pass filter

where V_{co} is the capacitor voltage at the start of the chromatogram. For the case of balanced operation where

$$|I_c(+)| = |I_c(-)| = I_{cb},$$

$$V_{co} = \frac{V_s}{2} \frac{R_{f2}}{R_{f3} + R_{f2}} \qquad (12)$$

and

$$I_{cb} = \frac{V_s}{2R_{f3}}. \qquad (13)$$

Under this condition, the capacitor voltage is given by

$$\Delta V_{cb} = \frac{V_s T_\eta}{2R_{f3} C}. \qquad (14)$$

If I_{min} represents the minimum peak current to be resolved, the current resulting from the capacitor charging should not exceed I_{min}. For a balanced condition this current is

$$\frac{\Delta V_{cb}}{R_{f2}} = I_{min} = \frac{V_s T_\eta}{2R_{f3} R_{f2} C}. \qquad (15)$$

The maximum correction current (I_{max}) that the zero compensation system can supply is

$$I_{max} = \frac{V_s}{2(R_{f2} + R_{f3})}. \qquad (16)$$

Therefore

$$\frac{I_{max}}{I_{min}} = \frac{R_{f3} R_{f2} C}{T_\eta (R_{f2} + R_{f3})} = \frac{\tau}{T_\eta}. \qquad (17)$$

c. Laboratory model. The block diagram of a laboratory system containing an automatic scale changing

electrometer and baseline stabilizer is shown in Fig. 59. In this system

$$R_{f1(max)} = 10^{10} \text{ ohms}$$

$$R_{f2} = R_{f3} = 5 \times 10^9 \text{ ohms}$$

$$C = 2\mu f$$

$$A_1 = 1000$$

$$A_2 = 1000$$

$$A_2' = 1000$$

$$\tau = 5000 \text{ sec}$$

$$V_s = 15 \text{ volts.}$$

The drift compensation available from the circuit when balanced is $\pm 0.75 \times 10^{-9}$ amp. Long-term drifts of this magnitude would then be reduced to $\pm 0.75 \times 10^{-12}$ amp. Columns requiring 2 minutes for a complete analysis, as an example, would produce an error current (I_{min}) of 1.8×10^{-11} amp if η were 100%. The cross-section detectors currently in use in our laboratory chromatograph are estimated to have a five-decade range of signal current superimposed on the baseline. The maximum and threshold levels are usually functions of detector saturation and noise, respectively. The total detector current is given by

$$I_{tot} = I_d + I_s \qquad (18)$$

where I_s is the current arising from the sample, and typically

$$10^{-3.5} < \frac{I_s}{I_d} < 10^{+1.5} \qquad (19)$$

If the baseline were assigned a representative value of 10^{-8} amps., the threshold would then be 3×10^{-12} amp. The automatic zeroing circuitry used in a 2-min column application would therefore preserve at least 4 decades of range in an automatic analysis in which only peak heights or peak areas were monitored.

Improvement of circuit thresholds requires variation of parameters that may alter the stability of the system. Referring to Fig. 60, the feedback factor (F) for the entire loop may be expressed approximately as follows:

$$F = \frac{A_2'}{1 - p\tau} \left[\frac{1}{1 + p\tau_1} \left(\frac{F_1}{1 - F_1} \right) \right] \qquad (20)$$

where $\tau_1 = R_{f1} C_1$, and F_1 is the electrometer feedback factor. In the circuit of Fig. 59, the electrometer is bandwidth limited so that the dominant time constant is provided by the term $F_1/(1 - F_1)$ and would be about 100
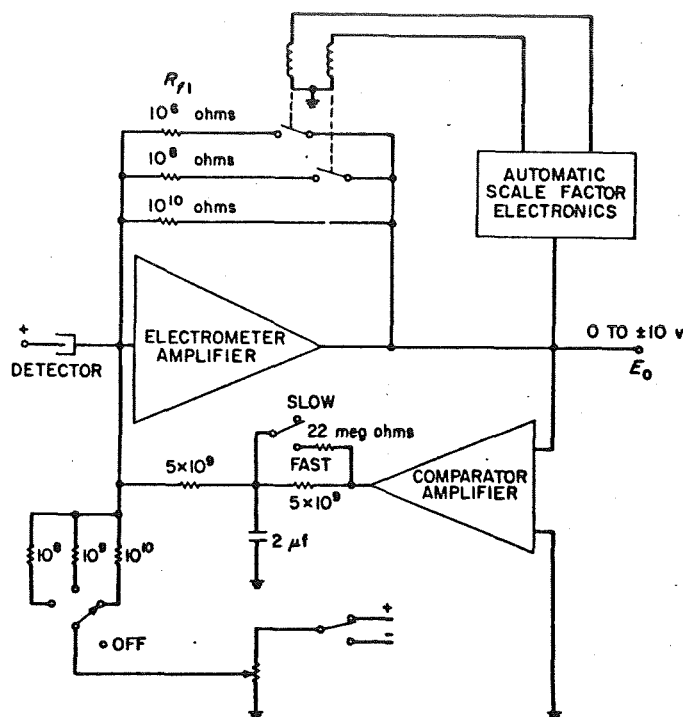

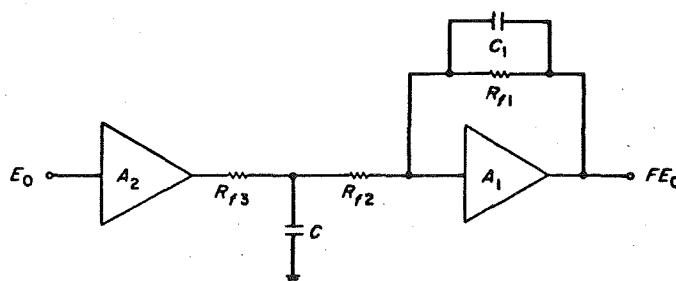Fig. 59. Block diagram of automatic scale switching electrometer with baseline stabilization

Fig. 60. Circuit for calculating loop transmission

msec. With $A_2' = 1000$ and $\tau = 5000$ sec, the loop gain margin is 34 db. Increasing R_{f1} by a factor of 10 raises A_2' also by a factor of 10 and decreases the electrometer bandwidth so that most of the gain margin is expended. Increasing R_{f2} and R_{f3} by a factor of 10 would restore the margin although the range of drifts that the zero system could accommodate would then be reduced by a factor of 10.

When a chromatogram has been completed, the baseline circuitry will require ηT seconds to restore the electrometer if the system were balanced at the outset. Provision for fast restoration at the end of a sample

analysis has been made by the inclusion of a lower-value switchable resistor in parallel with R_{f3}.

The scale changing electrometer is similar to a design generated for the experimental _Mariner_ Plasma Instrument by J. Lawrence. The design of the automatic scale factor device is discussed in _SPS 37-14_, Vol. VI, pp. 38–40. In its present configuration (see Fig. 61), the circuit contains 3 automatically switched feedback resistors enabling the electrometer to handle 7 decades of current between 10^{-12} and 10^{-5} amp. Speed of response on the low-current range ($R_{f1} = 10^{10}$ ohms) is about 100 msec, which makes the electrometer a useful device in monitoring outputs of fast capillary columns.

4. Summary

The electronic instrumentation described in this paper represents a reduction to practice of many significant chromatographic measurement requirements. The laboratory experimenter concerned with making rapid, effortless measurements now has at his disposal the following new tools: (1) automatic stabilization of electrometers against detector baseline drift, and (2) electrometers having a combination of stability, speed of response, and automatic dynamic range not commercially available. The laboratory chromatograph d scribed here is a convenient location for the insertion and examination of new elements such as columns and detectors. In time, laboratory elements such as valves, actuators, ovens, and other auxiliary d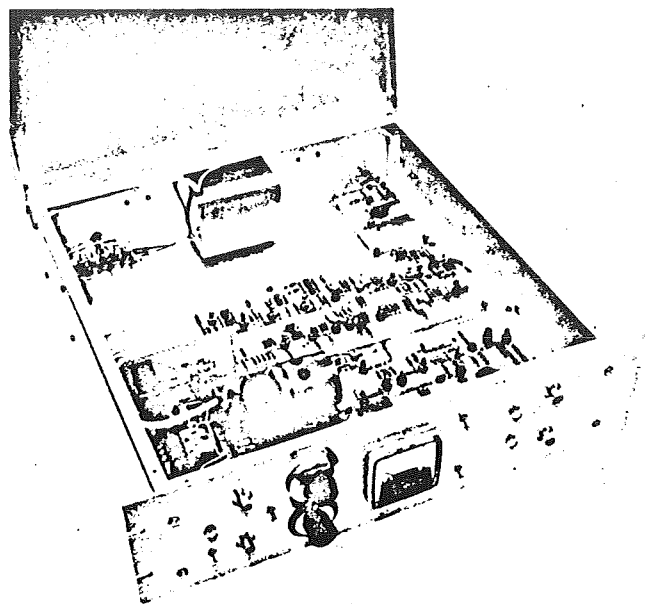evices will be replaced by miniature low-power electromechanical substitutes as the development program approaches the flight instrument phase.

Fig. 61. Photograph of experimental model of automatic scale switching electrometer with baseline stabilization

References

1. St. John, C. E. and Nicholson, S. B., "The Absence of Oxygen and Water Vapor in the Spectrum of Venus," _The Astrophysical Journal_, Vol. 56, p. 380, 1962.

2. Adams, W. S. and Dunham, T., "Absorption Bands in the Infrared Spectrum of Venus," _Publications of the Astronomical Society of the Pacific_, Vol. 44, p. 423, 1932.

3. Dunham, T., "Spectroscopic Observations of the Planets at Mount Wilson," _Atmospheres of the Earth and Planets_, G. P. Kuiper, Ed., Chapt. 11, University of Chicago Press, Chicago, Illinois, 1952.

4. Kellogg, W. W., and Sagan, C., "The Atmospheres of Mars and Venus," A Report of the Space Science Board, National Academy of Sciences — National Research Council (U.S.), 1961.

Appendix II

A Capacitor Storage Scheme
for
Gas Chromatograph Detector Quiescent Current Compensation

SPACE SCIENCES

XIX. Space Instruments Development

A. A Capacitor Storage Scheme for Gas Chromatograph Detector Quiescent Current Compensation

J. H. Marshall

1. Introduction

Because the quiescent current of an ionization detector used in a gas chromatograph does not remain constant for long periods of time, some form of automatic baseline stabilization[1] is required for spacecraft applications. This report describes a system in which current from a capacitor storage cancels the detector quiescent current at the electrometer input. This technique is applicable to chromatograms lasting as long as 30 min with peaks as small as 10^{-12} amp superimposed on baseline shifts of 10^{-9} amp.

2. General Description

A functional block diagram of a proposed electrometer system for a spacecraft gas chromatograph is shown in

---

[1] J. H. Marshall, "Gas Chromatograph Detector Quiescent Current Drift Compensation," JPL interoffice Technical Memorandum, December 5, 1962; *SPS 37-20*, Vol. IV, p. 169; *SPS 37-22*, Vol. IV, p. 213.

Fig. 1. The system consists of an ionization detector; a dynamic capacitor electrometer (Ref. 1) with automatic scale switching (*SPS 37-23*, Vol. IV, p. 245); fixed and variable quiescent current bucking supplies; and control logic.

For a spacecraft mission, the fixed-current bucking supply is adjusted on the Earth to null out the then present detector quiescent current. When the spacecraft reaches its destination, and while only carrier gas flows in the detector, the reed switches labelled "loop" are closed, and the electrometer is placed on its most sensitive scale (feedback resistor $= 10^{10}$ Ω). The comparator amplifier then adjusts the variable bucking current so that the electrometer output approaches zero according to
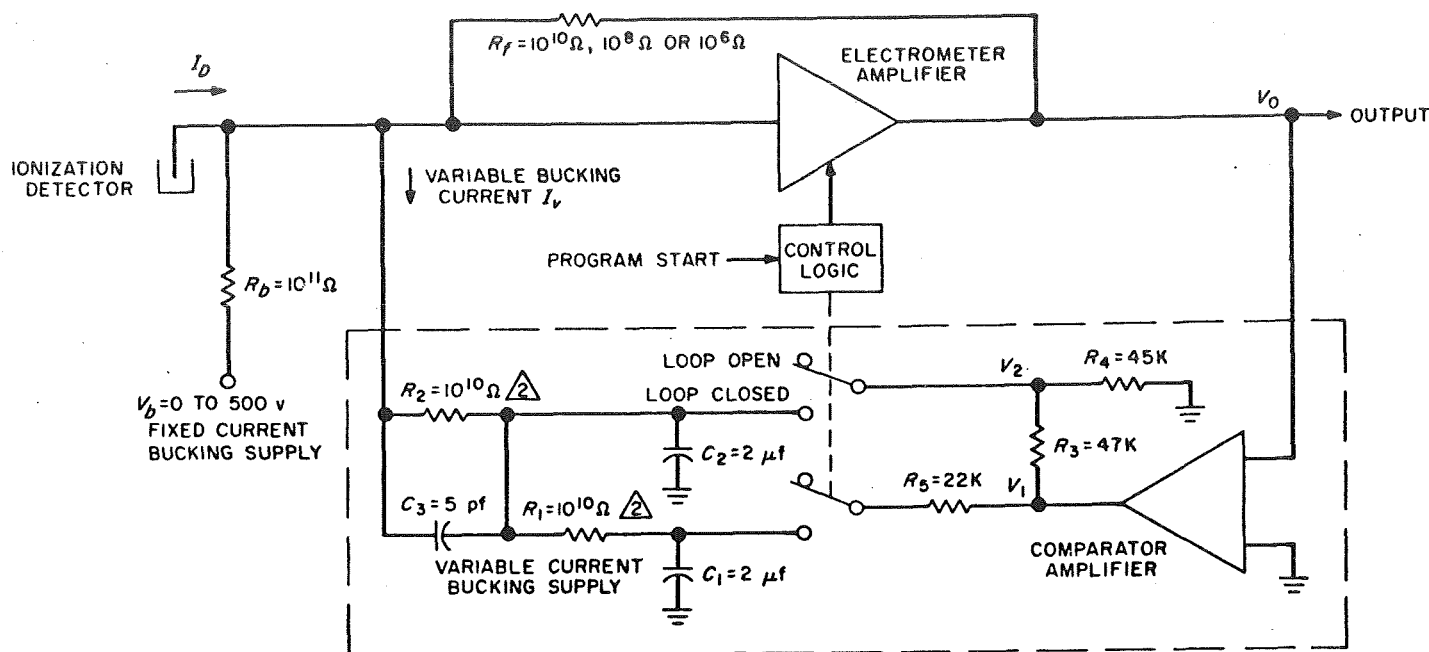
$$V_{oo} = -\frac{R_2 I_D}{M_0} + V_{os} \qquad (1)$$

where

$V_{oo} =$ electrometer output voltage with the loop switches closed

$I_D =$ detector current minus the fixed bucking current

$M_0 = \dfrac{R_4 M_2}{R_3 + R_4} = 1000$

Fig. 1. Electrometer with baseline stabilization

1. ALL CAPACITORS MUST HAVE LEAKAGE
   RESISTANCES IN EXCESS OF $10^{12} \Omega$
2. RESISTORS SELECTED SUCH THAT THE
   TEMPERATURE COEFFICIENT OF THE RATIO
   OF THEIR RESISTANCES IS LESS THAN 20 ppm/°C

M_2 = comparator amplifier gain = $\dfrac{V_1}{V_0 - V_{os}}$ = 2000

V_{os} = offset voltage of the comparator amplifier electrometer feedback factor $\gg 1$

$M_0 \gg 1$

As soon as the voltages on the storage capacitors (C_1 and C_2) have reached equilibrium, the loop is opened, and the sample to be analyzed is injected into the column. During the chromatographic analysis, the voltages on the storage capacitors decay toward zero, resulting in a decay of the variable bucking current and the following approximate change of the electrometer output voltage with time[2].

$$V_0 = -\frac{R_2 I_D}{M_0} + V_{os} - I_D R_f \left[t/\tau_L - \frac{1}{2}(t/\tau_Q)^2 \right] \quad (2)$$

where

V_0 = electrometer output voltage with the loop switches open

---

[2] For a derivation of the decay of the variable bucking current, see the double resistance-capacitor storage discussed in *SPS 37-22*, Vol. IV, p. 213.

t = time after the loop was last opened (small compared to τ_Q)

τ_L = 40,600 sec

τ_Q = 18,200 sec

R_f = electrometer feedback resistor

For $I_D \leq 10^{-9}$ amp, $R_f = 10^{10}\ \Omega$, and $V_{os} = 0$, and $V_0 = 0 \pm 20$ mv for 1970 sec after the loop was last opened.

The electrometer output can also be expressed in terms of the initial output voltage (V_{10}) of the comparator amplifier by

$$V_0 = -\frac{V_{10}}{M_2} - \frac{R_f}{R_2}\left[V_{10} + M_2 V_{os}\right]\left[\frac{t}{\tau_L} - \frac{1}{2}\left(\frac{t}{\tau_Q}\right)^2\right] \quad (3)$$

If the above quantities are sufficiently stable, and if I_D does not change during the chromatogram, then peaks of the same order as the decay of the variable bucking current can be measured by recording V_{10} and correcting for the initial value and decay of the baseline. As an additional check on the proper operation of the system,

the electrometer output voltage with the loop closed could also be recorded.

3. Circuit Details

A complete schematic of the baseline compensating circuits used in a laboratory gas chromatograph is shown in Fig. 2. The comparator amplifier and the resistance-capacitor storage are designed for spacecraft application. However, for the laboratory instrument the reed switches are controlled by toggle switches, and a meter indicates the comparator output voltage. Also, the electrometer can be used without baseline compensation by opening a reed switch between the capacitor storage and the electrometer input.

The comparator is a feedback dc amplifier with a gain of 2000 and a balanced, matched differential input stage. A pole of 100 sec and a zero of 100 msec are placed in the comparator feedback loop to stabilize the over-all system against oscillation. The calculated asymptotic frequency dependence of the comparator feedback factor (Fig. 3) shows that the comparator is safe from oscillation. A complimentary emitter-follower output stage allows the load to be driven rapidly positive or negative without large standing currents in the output

emitter-follower. The ammeter in the collector circuit of Q_2 is used to ensure that the comparator amplifier is operating within its linear range when the loop is closed.

The decay shape adjustment, which determines the initial voltages V_{10} and V_{20} on the storage capacitors C_1 and C_2, controls the time dependence of the variable bucking current after the loop is opened. The nominal value for the ratio of V_{20} to V_{10} is 0.486. An adjustment compensates for deviations of resistors and capacitors from their nominal values.

The loop toggle switch, which closes the reed switches connecting the output of the comparator amplifier to the storage capacitors, also holds cutoff transistors Q_{12} and Q_{13} in the automatic scale switching circuits (SPS 37-23, Vol. IV, p. 245). The electrometer feedback resistor then remains 10^{10} Ω regardless of the electrometer output voltage. The electrometer output will be zeroed to $\pm$ 10 mv in about 2 sec after the loop is closed.

The power supply voltages are identical with those used by the automatic scale switching circuits. The power to operate the circuits is 31.3 mw, with an additional 35 mw being required to close the loop reed switches (Table 1).
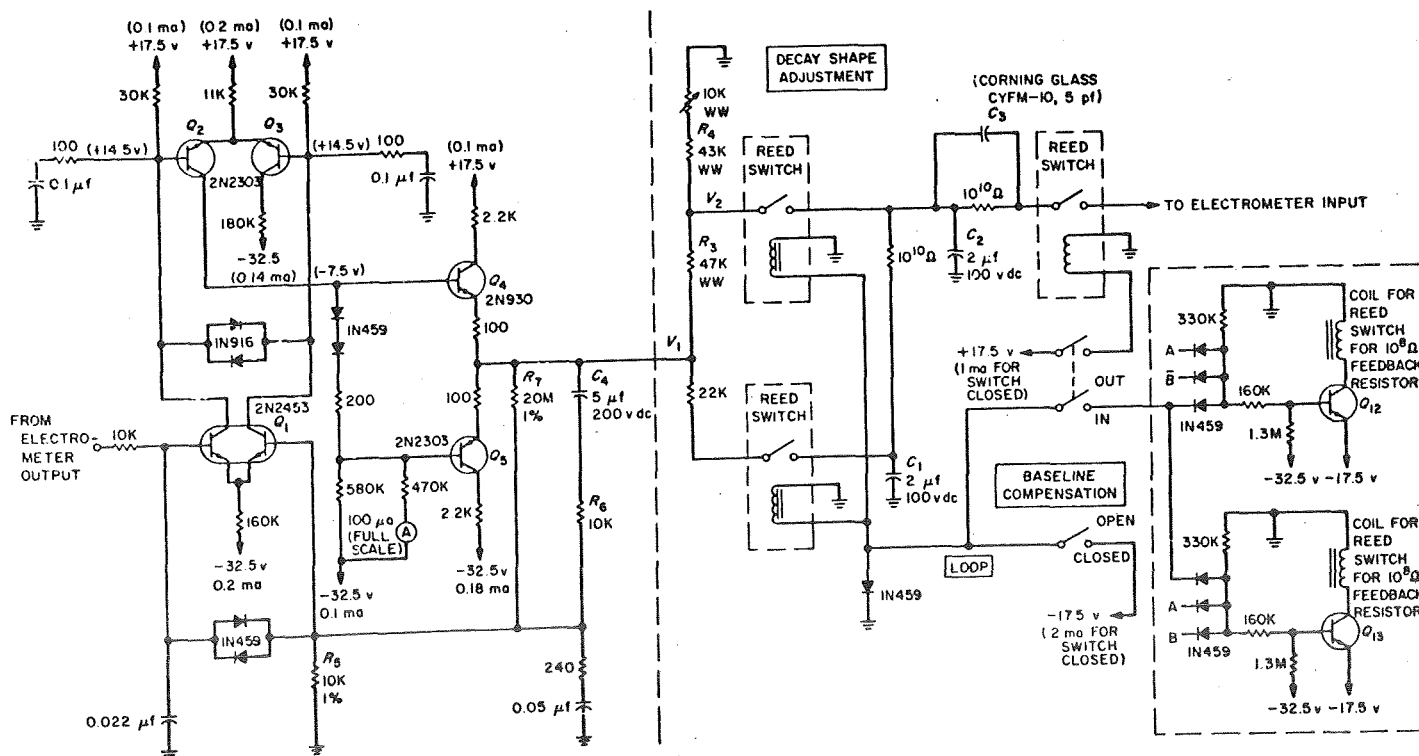

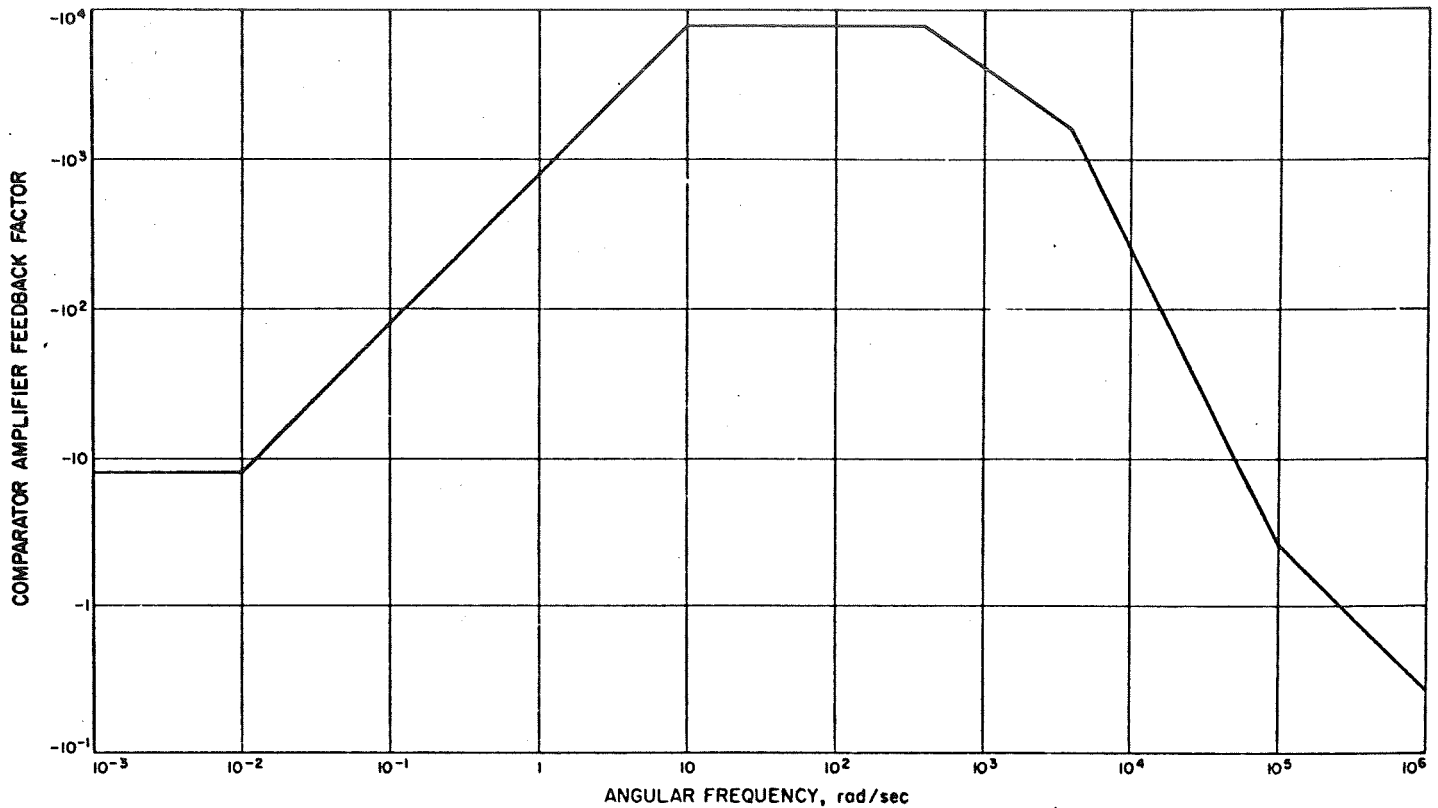Fig. 2. Baseline compensation circuits

Fig. 3. Asymptotic frequency response of the comparator amplifier feedback factor

Table 1. Power requirements

Voltage, v	Current, ma	Power, mw
+17.5[a]	0.54	9.5
−17.5[b]	0 or 2	0 or 35
−32.5	0.62	21.8
	Total power:	31.3 or 66.3 mw

[a] The current (1 ma) to operate the reed switch which connects the baseline compensation to the electrometer input was not included, because this switch probably would not be present in a spacecraft version.
[b] The −17.5 v current flows only when the loop switches are closed, during which time no −17.5 v current would be required for reed switches by the automatic scale switching circuits.

where

$$R_f = R_2$$

$$\frac{R_3 R_4 C_2}{R_3 + R_4} = R_2 C_3$$

$$R_7 \gg R_5 + R_6$$

$$C_2 \gg C_3$$

$$C_{in} = \text{electrometer input capacity}$$

$$C_{in} \gg C_3$$

$$C_{in} \gg C_f = \text{stray capacity across the electrometer feedback resistor}$$

$$A_1 = V_0/V_3$$

$$M_0 \gg 1$$

4. Feedback Factor

The feedback factor of the electrometer with the loop switches closed was calculated with the aid of Fig. 4 and is given approximately by

$$F = \frac{M_0 A_1}{2} \left\{ \frac{\left[1 + p\left(R_5 + R_6 + \frac{R_7}{M_0}\right)C_4\right]\left[1 + pR_f C_f\left(\frac{R_7}{R_7 + M_0(R_5 + R_6)}\right)\right]}{\left[1 + p\frac{R_f C_{in}}{2}\right]\left[1 + pR_7 C_4\right]} \right\} \tag{4}$$
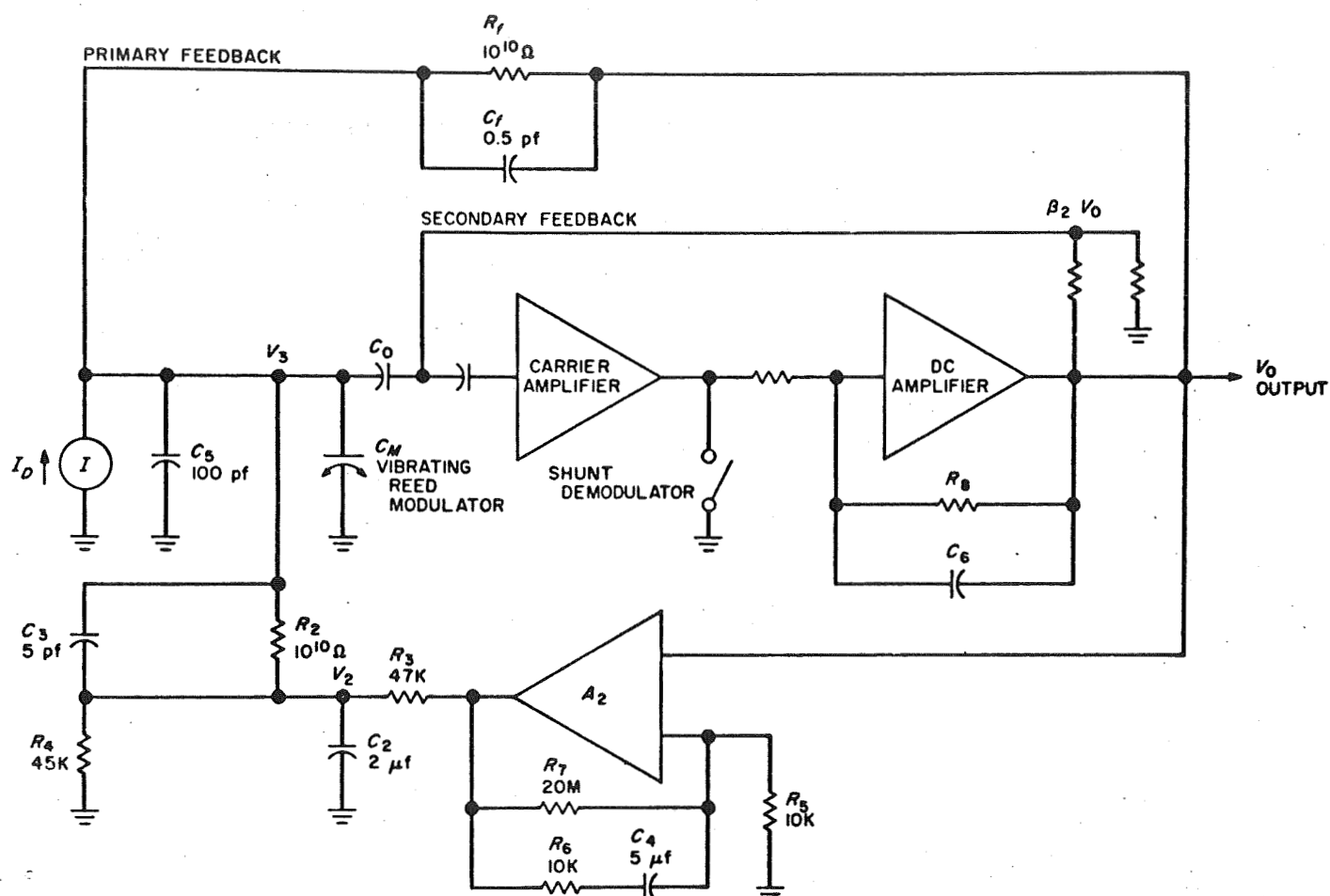
Fig. 4. Simplified schematic, closed loop configuration

Comparator amplifier feedback factor ≫ 1 for times longer than 1 msec

p = Laplace transform variable

The electrometer input capacity is almost entirely determined by the secondary feedback loop[3] and can be approximated by

$$C_{in} = \beta_2 A_0 C_0 + C_5 + C_M \qquad (5)$$

where

β_2 = secondary feedback attenuation

A_0 = dc open-loop gain of the electrometer amplifier

$\quad = |A_1|$

C_M = rest capacity of the vibrating reed modulator

Neglecting poles and zeroes smaller than about 3 msec, the electrometer amplifier gain (A_1) is given by

$$A_1 = \frac{-A_0}{1 + \dfrac{pR_6 C_6}{A_0 \beta_2}\left(\dfrac{C_0 + C_M + C_5}{C_0}\right)} \qquad (6)$$

The following values of A_1 and C_{in} were determined from the measured open-loop gain of the electrometer (without baseline compensation) versus frequency[4] (Fig. 5) and were found to agree reasonably well with Eqs. (5) and (6):

$$C_{in} = 2300 \text{ pf}$$

$$A_0 = -1000 \qquad (7)$$

$$A_1 = \frac{-1000}{1 + p25 \text{ msec}}$$

[3] J. H. Marshall, "Electrometer Open Loop Frequency Response," JPL interoffice Technical Memorandum, August 1962.

[4] J. L. Lawrence, "Electrometer Open Loop Response Versus Frequency for $10^{10}\Omega$ Feedback Resistor," private communication.
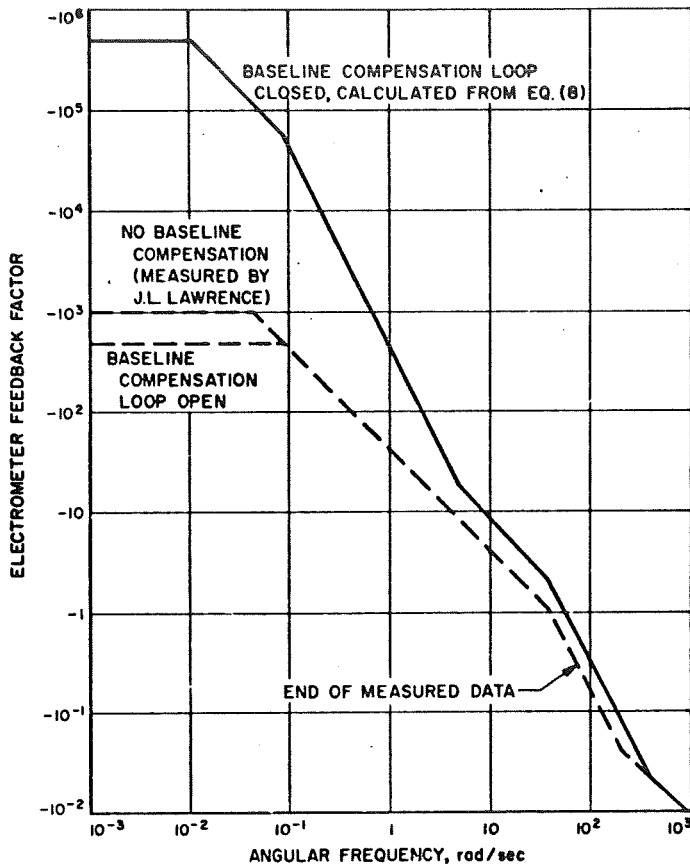
Fig. 5. Asymptotic frequency response of the electrometer feedback factor

The feedback factor is then given by

$$F = \frac{-5 \times 10^5 \,(1 + p200 \text{ msec}) \,(1 + p2.5 \text{ msec})}{(1 + p100 \text{ sec}) \,(1 + p11.5 \text{ sec}) \,(1 + p25 \text{ msec})}$$

(8)

The asymptotic frequency dependence of F is shown in Fig. 5 and compared with the frequency response for the electrometer without baseline compensation. Near gain crossover the feedback factor with the compensating loop is twice that without the compensating loop. Because the electrometer alone has more than 15 db gain margin, oscillation with the compensating loop appears safely prevented. If $R_2 C_3$ were made equal to $R_3 R_4 C_2 / 2(R_3 + R_4)$, then near gain crossover the two feedback factors would be identical.

The loading of the electrometer input with an additional $10^{10}\Omega$ resistor for the baseline compensation reduces the feedback factor with the baseline compensating loop open by 6 db. If the electrometer feedback factor is then too small, the gain of the carrier amplifier could be increased by 6 db. Because C_{IN} is proportional to the carrier amplifier gain, the feedback factor near gain crossover would not be changed, and the same gain margin should result.

5. Response to the Closing of the "Loop" Switches

The time required for V_2 to reach its equilibrium value after the loop switches are closed determines the minimum time that these switches must remain closed.

For C_1 and C_2 initially uncharged and for times long compared to the gain crossover time (30 msec) of the electrometer amplifier, the Laplace transform of V_2 is

$$V_2 = \frac{V_{10}\, pC_4\, R_5 - I_D\, R_f\, [1 + pC_4\,(R_5 + R_6)]}{\left[1 + \dfrac{pR_3\, R_4\, C_2}{R_3 + R_4}\right] [1 + p\,(3R_5 + R_6)\, C_4]\, p}$$

(9)

where

V_{10} = initial value of the comparator output voltage

$V_{os} = 0$

For $\quad I_D > \dfrac{V_s\, R_5}{R_f\, R_7} = 10^{-12} \text{ amp}$

(10)

where

V_s = saturation voltage of the comparator amplifier
= 20 v

then

$$V_{10} = -V_s$$

and

$$V_2 = -\frac{V_s\, p50 \text{ msec} + I_D \times 10^{10}\Omega\,(1 + p100 \text{ msec})}{(1 + p45 \text{ msec})\,(1 + p200 \text{ msec})\, p}$$

(11)

For $I_D = 10^{-9}$ amp, then

$$V_2 = \frac{-10 \text{ v}}{(1 + p45 \text{ msec})\, p}$$

(12)

and the time required for V_2 to reach 0.01% of its final value is 0.42 sec.

For $I_D = 10^{-12}$ amp, then

$$V_2 = \frac{-0.01 \text{ v}}{p} \left\{ \frac{(1 + p100 \text{ sec})}{(1 + p45 \text{ msec})\,(1 + p200 \text{ msec})} \right\}$$

(13)

and the time required for V_2 to fall to within 1 mv of its final value is 1.8 sec. Therefore, the loop switches should

be held closed for at least 1.8 sec to ensure that the electrometer is properly zeroed.

Because the 100-sec pole is placed in the comparator amplifier rather than later in the system, a large dynamic range is not required to prevent rate limiting. If, for example, C_2 were used to produce the 100-sec pole, and if the dynamic range of the comparator amplifier were not changed, over 100 sec could be needed to charge C_2 to its final value. When the 100-sec pole is early in the system, linear analysis is applicable, and 1.8 sec is sufficient to charge C_2.

Also, if the electrometer feedback resistor were less than 10^{10} Ω, the resulting decrease in the feedback factor would slow the charging of C_2. Therefore, when the loop switches are closed, the automatic scale switching circuits are bypassed, and the feedback resistor is fixed at 10^{10} Ω.

6. Performance

The comparator amplifier gain, offset voltage, and dynamic range were determined by measuring[5] the amplifier output voltage versus input voltage at several temperatures from -55 to $+125°C$. The 5-μF capacitor in the feedback loop was disconnected so that the amplifier output would quickly reach equilibrium. The data for -55, $+20$, and $+125°C$ are shown in Fig. 6. The gain, which was 1850 at room temperature, varied by $\pm3.3\%$ over the temperature range. The temperature coefficient of the offset voltage, which had a room temperature value of 1.6 mv, was $+10$ $\mu v/°C$, yielding a ±0.9 mv change over the temperature range. These temperature variations cause less than ±1.2 mv change in the closed loop electrometer output. The comparator amplifier dynamic range extending from $+14$ to -30 v provides variable bucking currents from -0.7×10^{-9} to $+1.5 \times 10^{-9}$ amp.

The small-signal comparator amplifier rise time, measured by applying a square-wave voltage to the amplifier input, agreed with the feedback factor calculations illustrated in Fig. 3. All rise-time effects in the comparator amplifier, except the 100-sec pole and 100-msec zero in the feedback loop, were negligible compared to the rise time of the electrometer alone.

In order to test the entire baseline compensating system, the detector was simulated by a stable power

supply connected to the electrometer input by a 10^{11} Ω resistor (Fig. 7). With the power supply voltage set to 91 v, the loop switches were closed, and the electrometer output settled to -7 mv, in good agreement with the -8 mv predicted by Eq. (1) and by the measured comparator amplifier gain and offset voltage. Then the loop switches were opened, and the electrometer output volt-
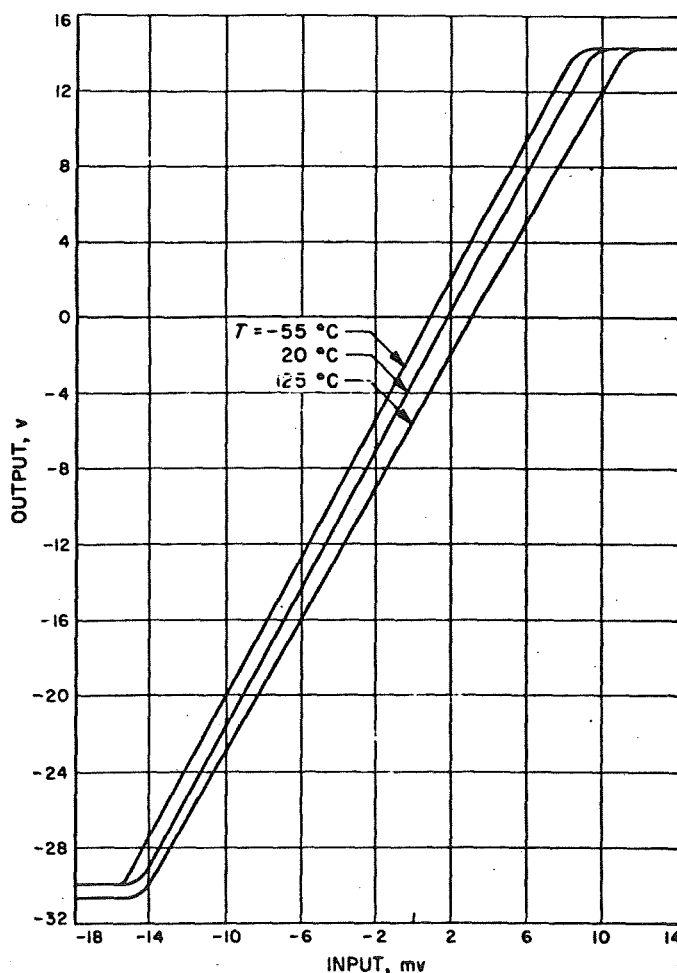

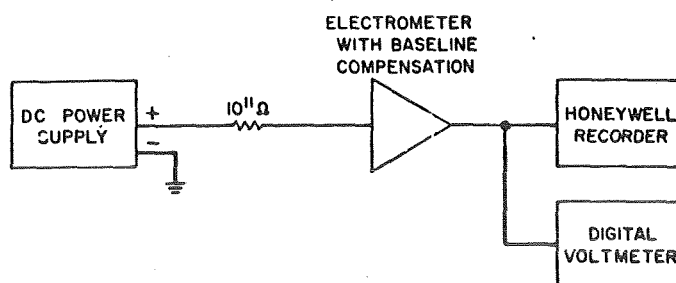Fig. 6. Comparator amplifier input-output characteristics

Fig. 7. Test setup

[5]H. Richeson, "Comparator Amplifier Test Results," JPL interoffice Technical Memorandum, October 1963.
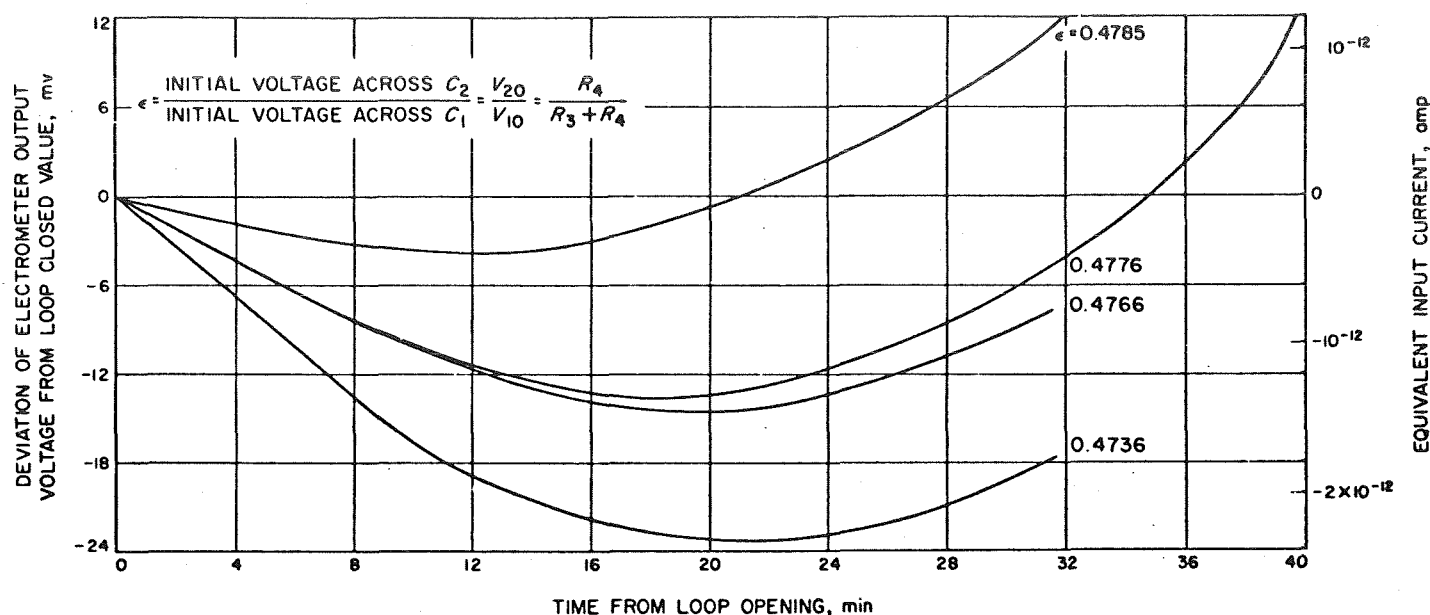
Fig. 8. Decay of the variable bucking current

age as a function of time was recorded (Fig. 8). The ratio of the initial voltages across the two storage capacitors was varied and is a parameter on the curves of Fig. 8. As predicted by Eq. (2), the electrometer output drifts no more than ±10 mv for 30 min, if the rather critical ratio of the initial capacitor voltages is correct. If the shape of the decay of the variable bucking current is to be predictable, then this ratio must be more stable than 0.05% and the ratio of R_1 to R_2 must stay constant to better than 0.2%.

In order to measure the rise time of the voltage across C_2 when the loop switch was closed, C_2 was initially discharged by the 10 MΩ oscilloscope probe impedance, and 9×10^{-10} and 2×10^{-12} amp currents were injected at the electrometer input. For times longer than 100 msec, the waveforms predicted by Eqs. (12) and (13) were confirmed.

Presently the electrometer with baseline compensation is being used for detector tests. The only difficulty anticipated in applying this technique to a spacecraft gas chromatograph is matching the temperature coefficients of R_1 and R_2.

B. Lightweight Sample Collector for Exobiology Experiments

S. B. Tuttle

An aerosol method of particulate sample collection has been developed, and it is currently considered feasible

for exobiology experiments. The equipment has not been optimized for material or weight, but there are no obvious problem areas.

This technique is capable of handling particles between 5 and 100 μ at a density of 2 or less. The rate of sample collection is roughly 0.02 g/min at a gas consumption 0.14 ft³/min, standard temperature and pressure. At these rates, a 0.5-g sample would require a storage volume for gas at 1800 psig equal to a sphere 4.5-in. D.

The aerosol system consists of an aspirator at ground level with suitable hoses connecting with the separator and instruments located on the spacecraft. The particulate matter is separated from entrainment and delivered to the experiments as a highly enriched aerosol mixture. Final separation at the experiments is by gravity.

A miniature aspirator has been developed for this specific application. It consists of a choked sonic jet in a constant area mixing chamber. This aspirator can be ejected from stowed position and will fall to ground due to gravity. It is discriminatory regarding size and density and will not pick up particles over approximately 100 μ. If several aspirators are ejected over a wide area, adequate sample volume is assured plus redundance against component failure. The general scheme of multiple aspirators is depicted in Fig. 9.

The particulate matter is separated from the sterile gas with a cyclone separator. This device utilizes centrifugal and vortex action to enrich the mixture. The efficiency with which a cyclone separator will retain small-diameter

Appendix III

An Automatic Scale Factor Device
for Use with
Spacecraft Electrometers

SPACE SCIENCES DIVISION

XVII. Space Instruments Development

A. An Automatic Scale Factor Device for Use with Spacecraft Electrometers

J. H. Marshall

1. Introduction

One particularly useful device for making measurements in interplanetary space and on other planets is an electrometer capable of a wide dynamic range; for example, the plasma probe on *Mariner 2* used an electrometer for measuring currents between 10^{-13} and 10^{-6} amp. Also, future experiments involving gas chromatography and mass spectrometry will probably require similar electrometers.

Since relatively uniform accuracy is desired over the entire dynamic range, some form of logarithmic scale compression must be used. On the *Mariner 2* plasma probe (Ref. 1), a vacuum diode operating in the retarded field region provided a logarithmic transfer impedance. This compression scheme had the disadvantages of slow response because of large ($\sim$5 pf) interelectrode capacity, relatively large instabilities resulting from dependence on tube characteristics, and the unreliability inherent in hot filament vacuum tubes. For these reasons, J. L. Lawrence developed an automatic scale-switching system which set the electrometer feedback resistor to one of three values so that the output voltage remained in a given range. This system possessed the reliability, stability, and fast response of resistive feedback, while still maintaining relatively constant accuracy over a seven-decade dynamic range.

However, the circuit developed by Lawrence possessed certain disadvantages for use in a general purpose electrometer. Because ac-coupled flip-flops were used, the logic could become blocked until a large change in the electrometer input forced a scale change. Furthermore, flight instrument schedules provided little time for optimizing the circuit. Finally, because the voltage for which the scale would change could not be predicted accurately, resistor values had to be selected after the unit was completed in order to set properly the scale shifting points.
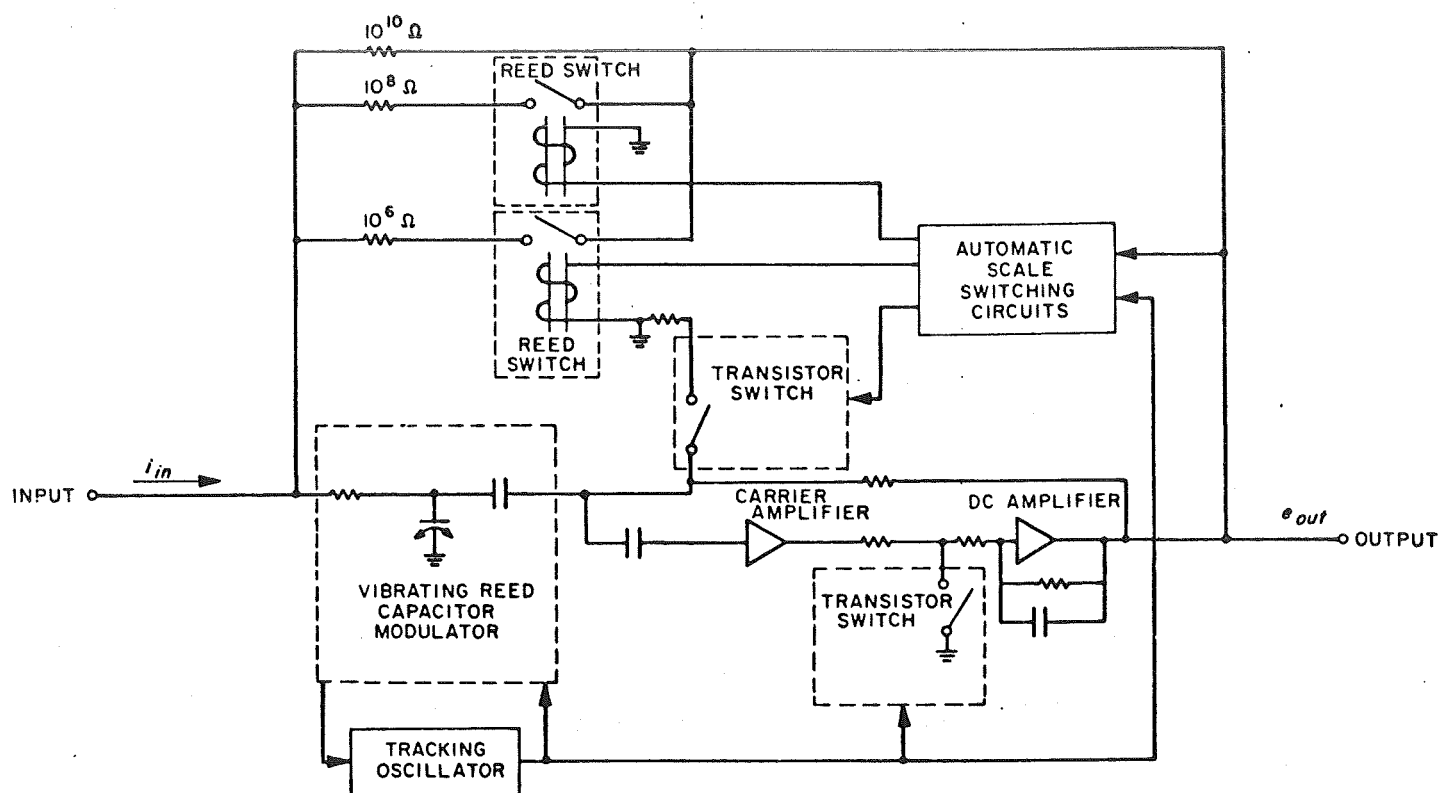
Fig. 1. Automatic scale switching electrometer block diagram

This report describes an improved version of the automatic scale factor device, which is primarily intended for an electrometer for use with a gas chromatograph. The above problems have been removed by using dc-coupled flip-flops and careful optimization of the circuit details. Furthermore, the scale changing levels can be accurately predicted and depend only on a single regulated voltage. Extensive tests on the circuit have been made and show stable operation from −50 to +125°C.

2. General Description of the Electrometer with Automatic Scale Switching

A block diagram of the automatic scale switching electrometer system is shown in Fig. 1. The electrometer itself consists of a vibrating reed capacitor modulator, a field-effect transistor carrier amplifier, a transistor shunt demodulator, and an integrating dc amplifier. The tracking oscillator drives the reed at its resonant frequency and supplies the synchronized drive signal to the demodulator. The automatic scale switching circuits (Fig. 2) consist of a transistor shunt chopper to convert the electrometer output voltage, which can have either polarity, to a sequence of rectangular pulses that are used to

trigger two discriminators, one of which is preceded by an ac amplifier with a gain of 150. The use of a chopper avoids the need for separate discriminators for positive and negative electrometer outputs and also makes possible the use of an ac amplifier, which simplifies the design of a discriminator to operate stably with a 50-mv threshold. The discriminator outputs control two flip-flops, which drive the reed switches that determine the value of the electrometer feedback resistor.

Since the feedback factor of the electrometer is about 1000, its output voltage e_{out} is related to its input current i_{in} approximately by

$$e_{out} = -i_{in} R_f \tag{1}$$

where R_f is the value of the feedback resistor. The automatic scale switching circuits select the proper feedback resistor to maintain the output voltage between 50 mv and 9.5 v, if the input current lies between 5×10^{-12} and 9.5×10^{-6} amp. A secondary feedback loop, which stabilizes the electrometer against oscillation, is also varied as the feedback resistor is changed so that the electrometer transient response remains optimum.
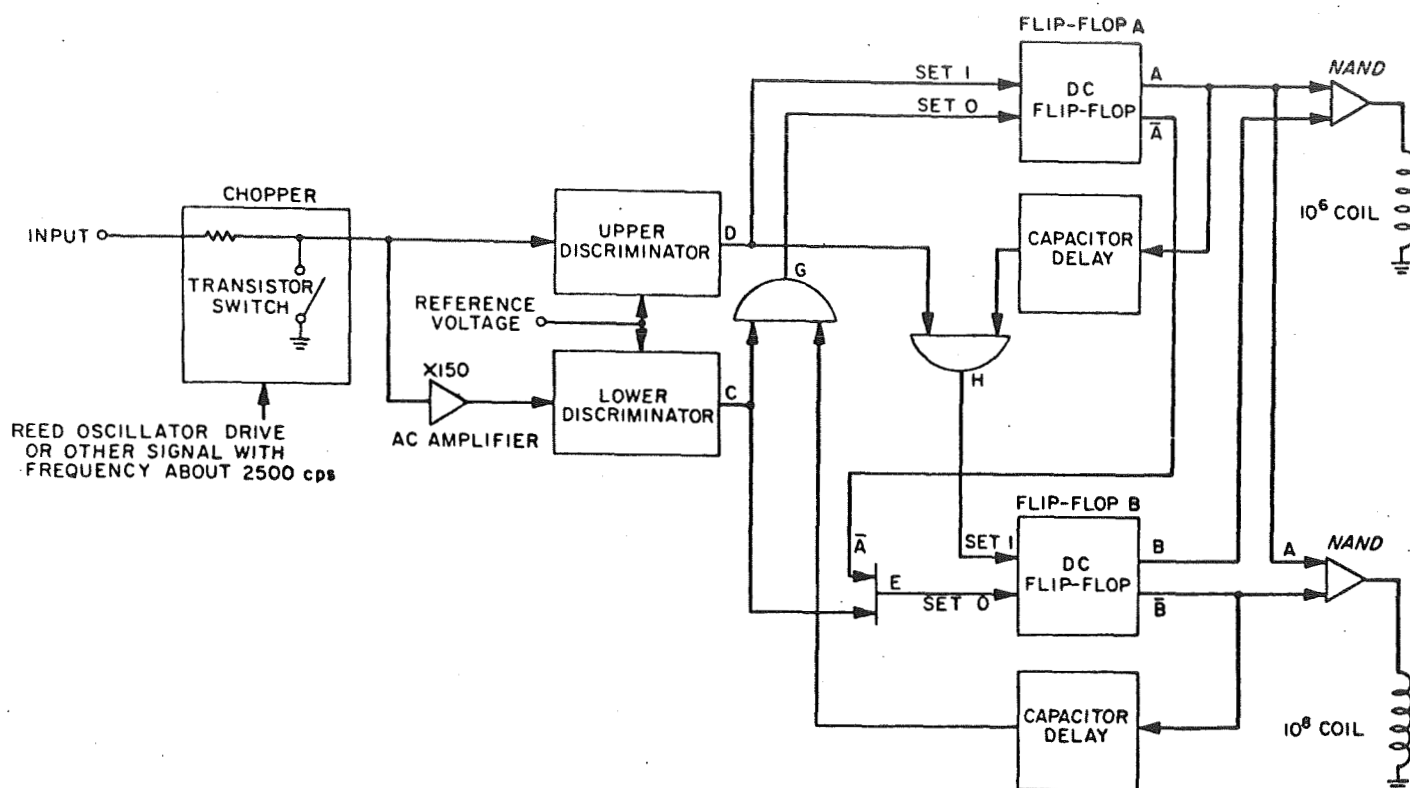
Fig. 2. Automatic scale switching circuits block diagram

3. Description of the Automatic Scale Switching Circuits

A schematic of the automatic scale switching circuits is shown in Fig. 3. The chopper (Q2 and Q3) is a shunt-pair operating at about 2.4 kc with an offset stable to better than 1 mv. The chopper base drive is coupled through a 1:1 transformer with small (~1 pf) capacity from the primary to the secondary to reduce "spiking."

During laboratory tests, the modulator drive signal was supplied by a difference amplifier (Fig. 4) that converted the 2.4-kc sine wave from the tracking oscillator to a symmetrical square wave. The positive and negative current pulses had equal durations to better than 1% and a zero dc level to prevent saturation of the transformer core. The circuit of Fig. 4 is not intended for spacecraft applications because of its rather low efficiency and because of the danger of interaction of the modulator drive signal with the electrometer carrier system. The final design of the modulator drive circuit depends on not yet determined spacecraft conditions, such as the availability of 2.4-kc square-wave power.

The chopper output drives two nearly identical discriminators (Q4 and Q7), the ratio of whose thresholds is

principally determined by the gain of the ac amplifier (Q5 and Q6) which precedes the lower discriminator. This amplifier has a gain of 150 with a feedback factor of about 15, provided by a single feedback loop which stabilizes both the ac gain and the dc operating points. Because each scale change is a factor of 100, the threshold of the lower discriminator must be safely less than $\frac{1}{100}$ of the upper discriminator threshold to prevent oscillation. In order to avoid non-linearity and an appreciable attenuation of the chopper output signal, the amplifier input impedance must remain high and relatively independent of input voltage up to signals of 10 v. Although a 10-v input obviously saturates the amplifier, the 2.2-μf by-pass capacitor charges until its average current is zero. Once equilibrium is achieved, the input transistor Q5 need only supply the currents in the 147K and 133K resistors, and the input impedance continues to be determined by the 100K resistor from the base of Q6 to ground. Even after the by-pass capacitor has become fully charged, the amplifier returns to its normal operating state within 40 ms after the input signal is removed.

The discriminator input signals are coupled to the base of a differential amplifier with regenerative feedback (Fig. 5) via a diode-restored capacitor and a filter. Series
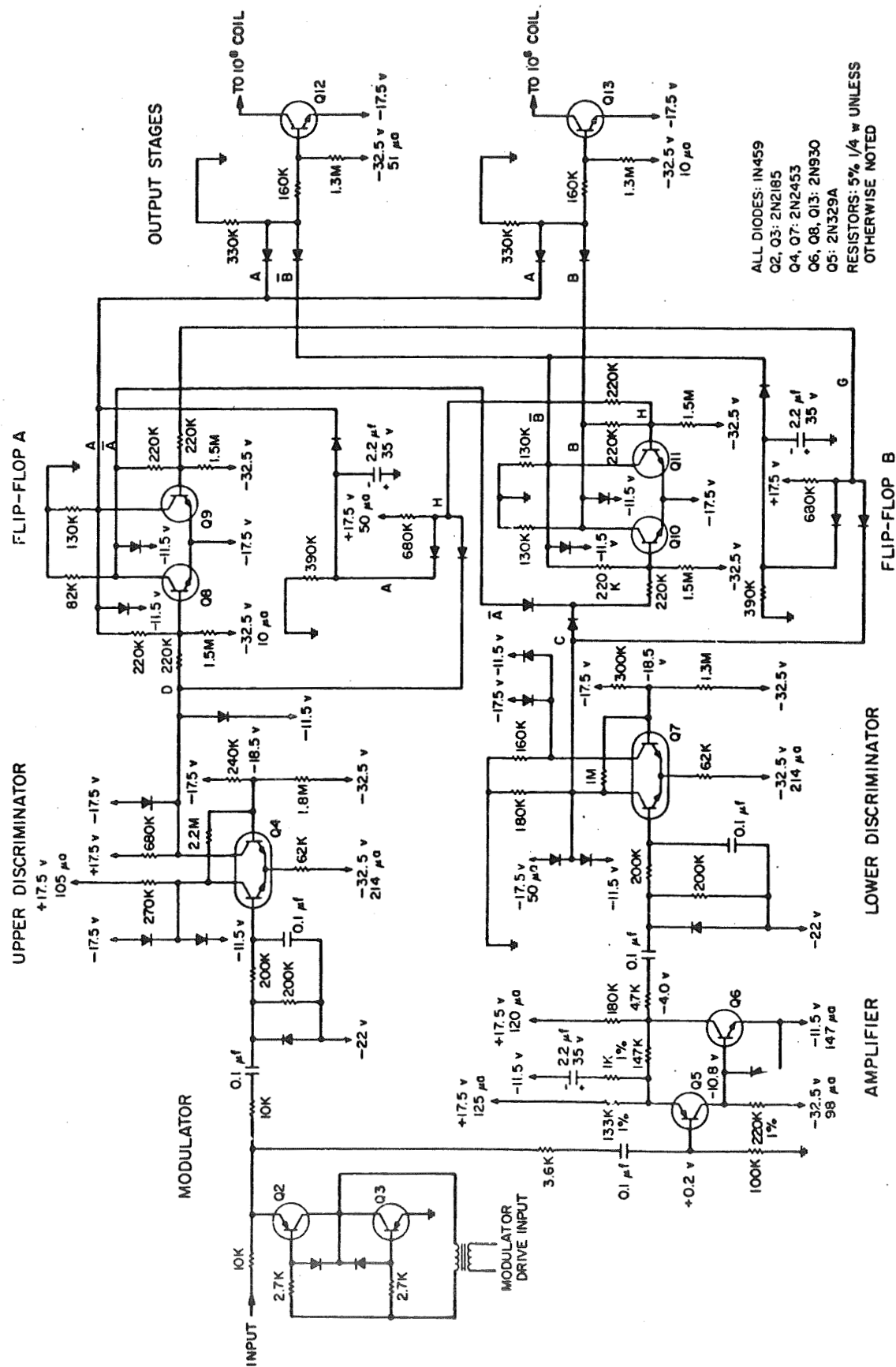
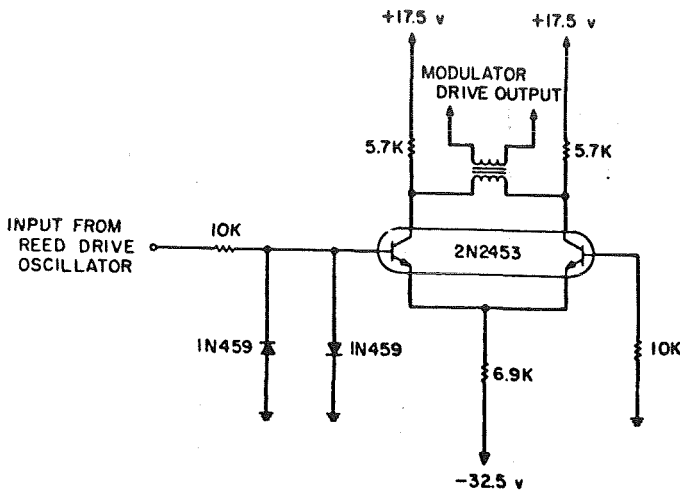Fig. 3. Automatic scale switching circuits schematic diagram

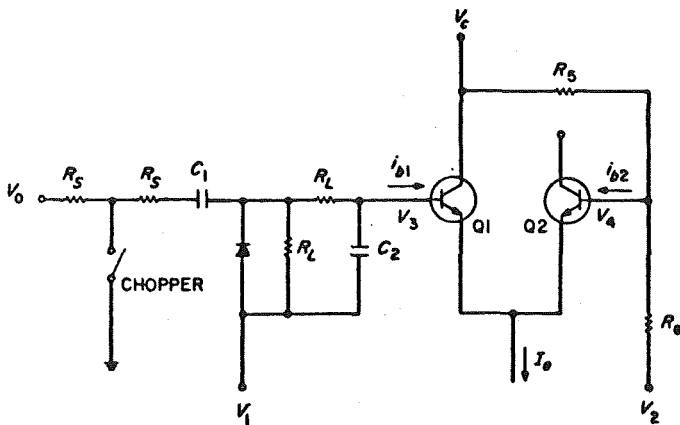**Fig. 4. Modulator drive circuit schematic diagram**

Fig. 5. Discriminator circuit simplified schematic diagram

resistors limit the initial charging currents to less than 1 ma. Assuming that the chopper switch is closed for one-half of each cycle, the dc voltage V_3 at the base of Q1 is related to the input voltage V_0 by

$$V_3 - V_1 = \left(\frac{R_L}{9R_S + 2R_L}\right) V_0 - \left(\frac{2R_L + 6R_S}{9R_S + 2R_L}\right) V_D$$

$$- R_L \left(\frac{2R_L + 12R_S}{2R_L + 9R_S}\right) i_{b1} \qquad (2)$$

where V_D = diode forward voltage drop and i_{b1} = base current of Q1. Because the collector of Q1 is clamped by a diode conducting a current of $I_e/2$, the discriminator changes state when the collector currents of Q1 and Q2 are equal. Since Q1 and Q2 are matched transistors, the collector currents will be equal for equal base voltages (to 5 mv) and currents (to $\pm 10\%$), that is when

$$V_3 = V_4 = \frac{R_6 V_C + R_5 V_2 - i_{b2} R_5 R_6}{R_5 + R_6}$$

$$i_{c1} = i_{c2} \qquad (3)$$

$$i_{b1} = i_{b2} = \frac{I_e}{2\beta}$$

where β = forward common emitter current gain.

Substituting Eq. (3) into Eq. (2), one obtains for the input triggering level

$$V_0 = \frac{(R_6 V_C + R_5 V_2)(9R_S + 2R_L)}{(R_5 + R_6) R_L} + \frac{I_e(9R_S + 2R_L)}{2\beta R_L}$$

$$\times \left[\left(\frac{2R_L + 12R_S}{2R_L + 9R_S}\right) R_L - \frac{R_5 R_6}{R_5 + R_6}\right] \qquad (4)$$

$$+ \left(\frac{9R_S + 2R_L}{R_L}\right)\left[\left(\frac{2R_L + 6R_S}{9R_S + 2R_L}\right) V_D - V_1\right]$$

In the case of the upper discriminator

$$R_S = 10K$$
$$R_L = 200K$$
$$R_5 = 2.2M$$
$$R_6 = (240K) 11 (1.8M) = 212K$$
$$V_C = -11 v \qquad (5)$$
$$V_1 = -22 v$$
$$V_2 = -19.3 v$$
$$I_e = 214 \mu a$$
$$\beta = 100$$
$$V_D = 0.5 v$$

then

$$V_0 = 2.24V_2 + 0.22V_C + I_e/\beta \, 22K + 2.45 (0.94V_D - V_1)$$
$$(6)$$

giving

$$V_0 = 9.40 v \qquad (7)$$

The dependence on the base current has been reduced an order of magnitude by making the impedance seen by the base of Q1 nearly equal to that seen by the base of Q2 and by using transistors with matched current gains (2N2453). Also, the 2.5 mv/°C temperature drift in V_D is compensated by generating V_1 (-22 v) with an emitter-follower (Fig. 6) that has the opposite temperature co-efficient. Similarly, drifts in V_C can be compensated.
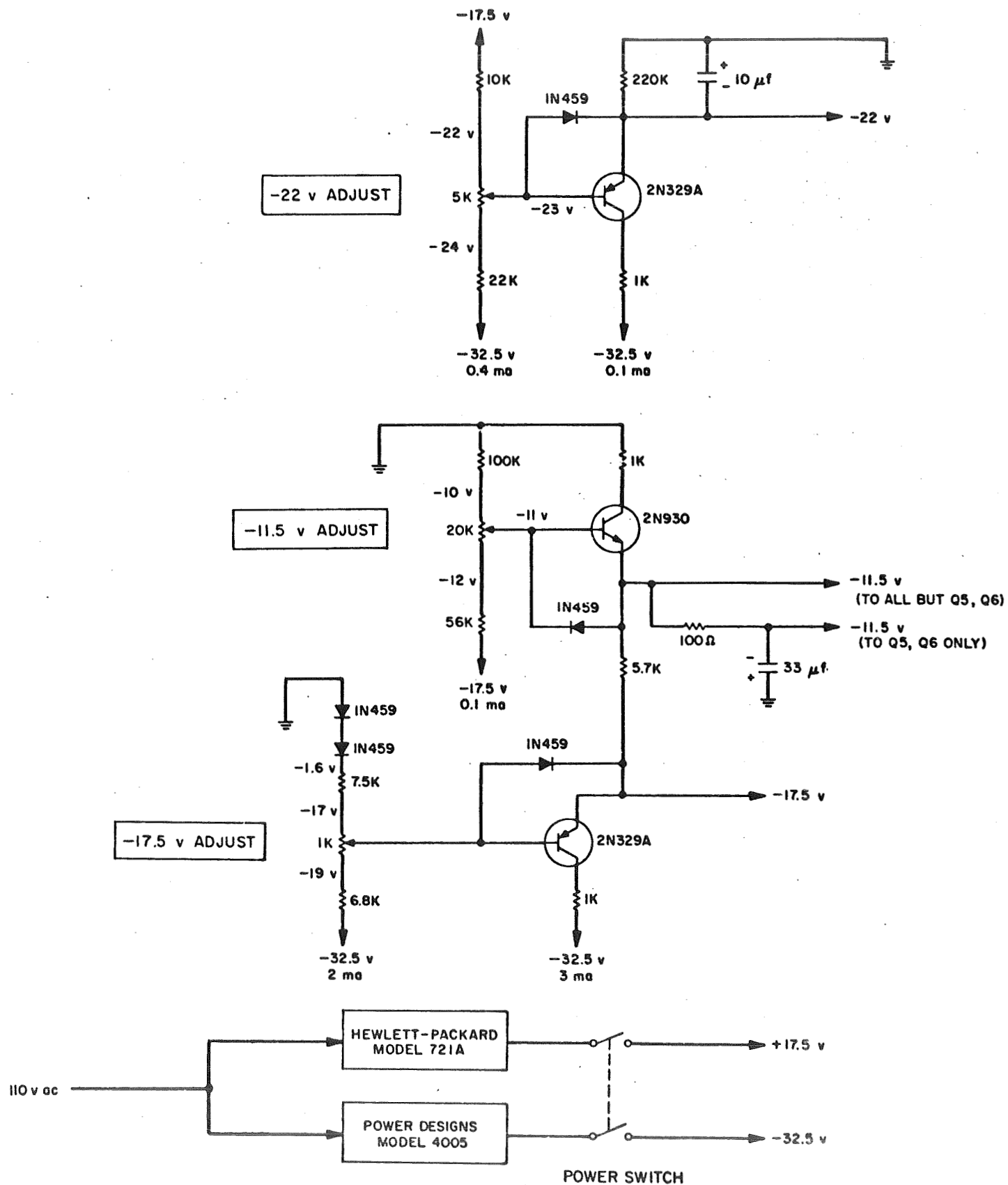
Fig. 6. Power supplies for the automatic scale switching circuits

Since the triggering level is approximately proportional to the difference between V_2 and V_1, both these voltages are referenced to nearly the same source (Figs. 5 and 6).

The upper discriminator output, which is taken from the collector of Q2, is in the zero state (-18 v) for input signals V_0 below 9.4 v in magnitude and is in the one state (-11 v) for inputs above 9.4 v.

The important transition of the lower discriminator occurs when the input signal falls below the triggering level. This level differs from the level for the upper discriminator by the gain of the amplifier and by the hysteresis caused principally by the change of V_C from -11 v in the zero state to -18 v in the one state. The triggering level for the return of the lower discriminator is then given by

$$V_0 \text{ (return)} = \frac{7.9 \text{ v}}{150} = 52 \text{ mv} \qquad (8)$$

In order to temperature-compensate this level, the bias current of the diode on the collector of Q1 has been chosen so that the collector currents are equal for the returning transition. The output signal, which in this case is taken from the collector of Q1, is in the zero state for inputs in excess of 52 mv in magnitude and in the one state for inputs less than 52 mv.

The discriminator outputs control flip-flops (F-F) A and B (Fig. 2), which, in turn, control the feedback resistor via two nand circuits as follows:

Feedback resistor	State of F-F A	State of F-F B
$10^{10}\ \Omega$	0	0
$10^8\ \Omega$	1	0
$10^6\ \Omega$	1	1
Forbidden combination	0	1

Because the reed switch coils, when open, must be grounded to prevent excessive leakage currents at the electrometer input, the logic circuits have all been referenced to -17.5 v instead of ground. Then the output stages Q12 and Q13 can each be a single transistor which is on only when its switch coil is energized. The zero level is formed by saturating a transistor against -17.5 v, and

the one level is determined by a diode clamp against -11.5 v. The clamping of the one level yields a low impedance and a well defined voltage level, which will be less subject to difficulties from transient pickup or component variations.

The scale changing logic sequences as follows: Assume that the feedback resistor is $10^{10}\ \Omega$ and that the electrometer output voltage is less than 9.4 v. Then, the signals (Fig. 2) have the following states:

Signal	State
A	0
B	0
C	0 or 1
D	0
E	1
G	0 or 1
H	0
Feedback resistor	$10^{10}\ \Omega$

No change occurs in the flip-flop states. If the input then exceeds 9.4 v, the upper discriminator will move to the one state causing F-F A to be set to a one and changing the feedback resistor to $10^8\ \Omega$. The electrometer output then falls by a factor of 100, and the upper discriminator returns to the zero state in about 30 ms. The capacitor delays signal A from reaching and gate H by 150 ms so that F-F B will not also be set to the one state unless the electrometer output still exceeds 9.4 v after the 150-ms delay. Now, the states are:

Signal	State
A	1
B	0
C	0
D	0
E	0
G	0
H	0
Feedback resistor	$10^8\ \Omega$

If the electrometer output once again exceeds 9.4 v, then D changes to the one state, and, because and gate H

is open, F-F B is set to a one. The 10^6 Ω feedback resistor is now in the circuit and the states are:

Signal	State
A	1
B	1
C	0
D	0 or 1
E	0
G	0 or 1
H	0 or 1
Feedback resistor	10^6 Ω

If the electrometer output now drops below 52 mv, the lower discriminator will change to the one state causing F-F B to be set to a zero and the feedback resistor changed to 10^8 Ω. The electrometer output then increases by a factor of 100, and signal C returns to the one state in about 10 ms. The capacitor delay prevents B from reaching *and* gate G before C returns to the zero state.

If the electrometer output again falls below 52 mv, then C moves to the one state and sets F-F A to the zero state via *and* gate G. Now the feedback resistor is 10^{10} Ω. Signal A, via *or* gate E, insures that F-F B is always zero when F-F A is zero.

The power supplies designed for laboratory use are shown in Fig. 6. Although these supplies were not designed to be highly efficient for spacecraft use, they incorporate the following characteristics that the spacecraft version should have. First, the −11.5- and −22-v supplies are referenced to the −17.5-v supply, because in most of the circuits the difference of the voltages from −17.5 v is more important than the absolute value. Because the discrimination level depends critically on the difference of the −22- and −17.5-v supplies, this differ-

ence should be regulated to at least 1%. Secondly, the temperature coefficients of the −11.5- and −22-v supplies are chosen to compensate diode drifts in the digital logic and the discriminators. Third, the emitter-followers are protected against excessive emitter currents by a collector resistor and against excessive back-biasing emitter-base voltages by diodes from the emitter to base. Fourth, the −11.5 v supplied to the amplifier is decoupled by an R-C circuit from the −11.5 v used by the remaining circuits.

The power requirements are shown in Table 1. The total power required is 63.7 mw, including the power to close one reed switch (17.5 mw), the power taken from the electrometer by the modulator for an electrometer output of 10 v, and the power for the modulator drive. Allowing for power supply inefficiency, it appears that the entire scale factor device should draw less than 100 mw of primary spacecraft power.

4. Operation

The automatic scale switching electrometer was tested (Fig. 7) by introducing at the input a linearly rising current from the sawtooth output of a Tektronix 535A oscilloscope. The sweep was set so that the voltage applied to a 10^9 Ω resistor rose from near 0 to +150 v in 10 sec. As can be seen in Fig. 8, which is a drawing of the observed electrometer output, the electrometer changes scale from 10^{10} to 10^8 Ω and thence to 10^6 Ω in response to the rising input signal, and returns to the 10^{10} Ω scale at the end of the sweep. Fig. 9 shows the electrometer output at the transition from 10^8 to 10^6 Ω on an expanded time scale (100 ms/cm).

At the times of the various scale changes produced by the sawtooth input, oscilloscope pictures were taken of all critical signals as the temperature was varied from

Table 1. Power requirements

	Requirement					Modulator drive	Electrometer output
	1	2	3	4	5		
Voltage, v	+17.5	−11.5	−17.5	−22	−32.5	3	10 (max)
Current, ma	0.39	0.42	1.26	0.002	0.58	2	0.5 (max)
Power, mw	6.8	4.8	22.0	0	18.9	6	5 (max)
Total Power = 63.7 mw							

Fig. 7. Test setup *

e_{in} = ELECTROMETER INPUT
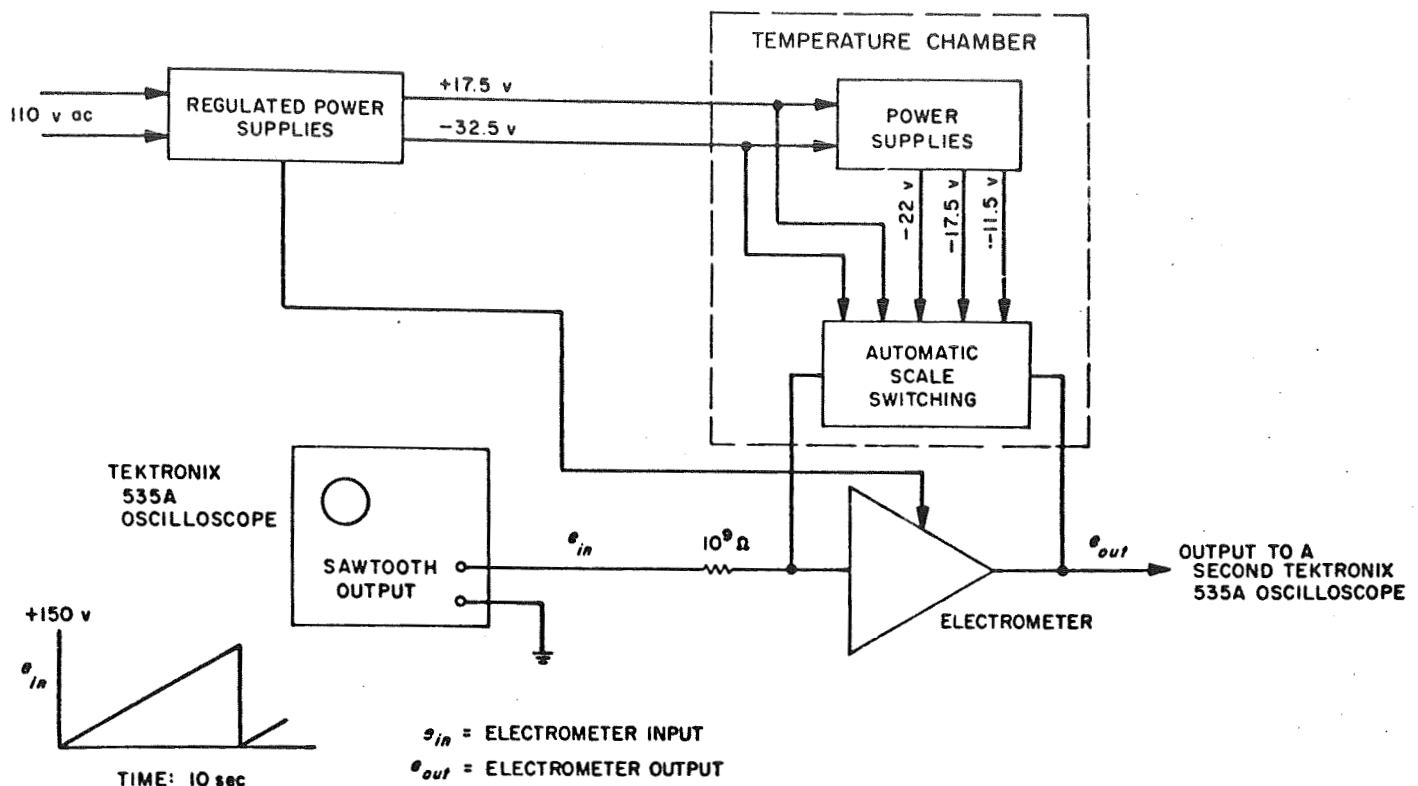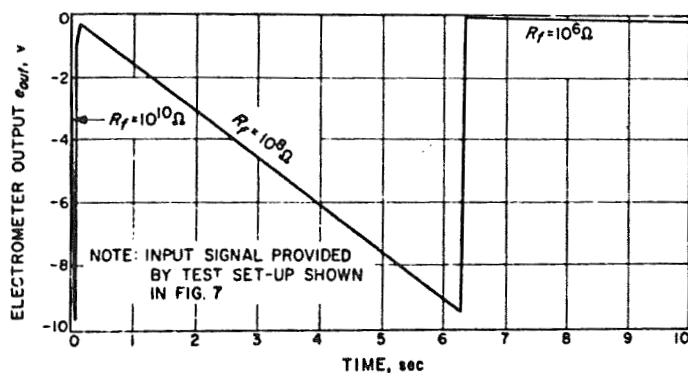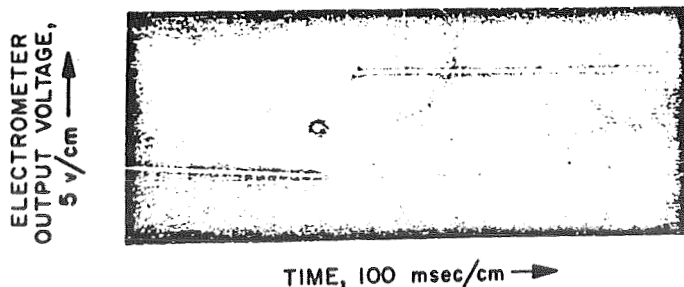
e_{out} = ELECTROMETER OUTPUT

Fig. 8. Electrometer response to ramp current input

Fig. 9. Transition from 10^8- to 10^6-Ω scale with ramp current input

−50 to +125°C. Since the drifts of the −22-, −17.5-, and −11.5-v power supplies were used to compensate drifts in the discriminators, these supplies were temperature-cycled with the scale switching circuits. No indications of possible marginal operation were observed over this temperature range.

The discriminators and amplifier were further checked by measuring the dependence of the discrimination levels on temperature. The upper level was found to be stable to ±1% from −50 to +125°C and the lower level to ±6% over the same range. The stability of the upper discriminator permits the upper level to be set safely at 95% of full scale. The lower discriminator stability is well within the 50% tolerance given by the condition that oscillation shall not occur.

The amplifier gain and output dc voltage were also checked from −50 to +125°C. The measured ±5% gain shift, which is consistent with a feedback factor of 15, is the principal cause of the drift of the lower discrimination level. The observed ±1-v shift of the output dc voltage produced no difficulty, because the discriminator needs only 8 v of the nominal 13 v dynamic range.

The margin in the capacitor delays was also checked. The circuits operated properly for capacitors as small as ¼ of the nominal value (2.2 μf), while the observed variation in the delay during temperature cycling was less than 10%.

For ±20% supply voltage variations and for ±50% variation of the −11.5-v supply with respect to the −17.5-v supply, the digital circuits operated normally at room temperature. As was expected, variations of the supply voltages cause shifts in the discrimination levels, but over the above range the discriminators otherwise performed satisfactorily.

Therefore, this method of logarithmic scale compression has been proved feasible for spacecraft application, and the most difficult circuit problems have been solved. Already this electrometer has found use as a laboratory instrument for checking ionization detectors and quiescent current compensating schemes for gas chromatographs.

B. Planetary Interferometer

H. T. Bull

A breadboard infrared interferometer has been constructed at Manchester University in England to do planetary interferometer spectroscopy on Mars and Venus, and to further the state of the art to support spacecraft interferometer design. The spectral range of the instrument is from 2 to 13 μ and it is desired to perform spectroscopy having a resolution better than 10 cm^{-1} through this region. The project is intended to yield new infrared spectra of the planets through the 8- to 12-μ atmospheric window and also to provide a comparison with spectrograms obtained with grating instruments in the near infrared atmospheric windows, particularly between 3–4 μ.

1. Theory of Operation

Chopped infrared radiation enters the interferometer by means of the collimating lens L_c and undergoes amplitude division at the beamsplitter BS. Two plane coherent wavefronts are then reflected back into the detector unit and interfere in the focal plane of the detector lens. The intensity at the detector at a given wavelength is the vector sum of the two components, hence, the total intensity is

$$I(\Delta) = \frac{1}{2} \int_0^\infty I(\nu)(1 + \cos 2\pi\Delta\nu)\, d\nu \qquad (1)$$

Only the phase-modulated term is of value in interference spectrometry and, taking the inverse transform, it follows that

$$I(\nu) = \int_{-\infty}^\infty I(\Delta) \cos 2\pi\Delta\nu\, d\Delta \qquad (2)$$

However, in practice, $I(\Delta)$ is measured only over a finite scan and Δ is not constant over the field of view. Also, $I(\Delta)$ is sampled discretely and is not measured as a continuous function of Δ. There is a finite number of grey levels which limit the amplitude resolution also. These practical limitations detract from the fundamental advantages of increased luminous flux throughout, for a given resolution, and, decreased noise bandwidth for a given scan time. Furthermore, the ideally constant term in Eq. (1) usually varies in space and time and may introduce serious spurious modulation. Two last experimental details are: (1) numerical apodization must be used to improve the basic sinc function profile of the instrument; and (2) there is usually a wavelength dependent phase shift which must be considered in the numerical analysis.

2. Optical Breadboard

The optical breadboard is shown schematically in Fig. 10 and is illustrated in the photograph of Fig. 11. The whole system is shown in Fig. 12 with the optical breadboard mounted on a dummy telescope. The Michelson configuration is the simplest possible, the overall principles being of prime interest.

Appendix IV

An Electrometer for Use In Space Instruments

AN ELECTROMETER FOR USE IN SCIENTIFIC SPACE INSTRUMENTS

C. Josias
J. Lawrence, Jr.

Analog Technology Corporation
Pasadena, California

AN ELECTROMETER FOR USE IN SCIENTIFIC SPACE INSTRUMENTS*

C. Josias[†]
J. Lawrence, Jr.[†]

Analog Technology Corporation
Pasadena, California

ABSTRACT

A wide-range vibrating-reed electrometer that obtained extensive detailed data on the "solar wind" during the Mariner II flight to Venus is described. This circuit used an inverting carrier-type dc amplifier with a logarithmic diode as its principal feedback element and represented the first successful application of a space-qualified dynamic capacitor electrometer. This system also represents one of the earliest all-semiconductor amplifiers to be used in a dynamic capacitor electrometer.

The wide dynamic range of the application $(10^{-13}$ to 10^{-6} A) required the stabilization of a closed loop having 7 decades of continuous variation in the dynamic resistance of the primary feedback element. Some details of design, analysis, and performance associated with the electrometer amplifier and its feedback system are presented.

I. INTRODUCTION

One of the instruments aboard the Mariner II spacecraft, which completed a successful flyby mission to Venus, was a solar-oriented, curved-plate electrostatic analyzer[1] capable of measuring the energy spectrum of the positive-ion component of a suspected "solar wind." During an operational flight of 129 days, this device returned extensive, detailed data to the Earth, verifying the presence of a constantly flowing solar wind.

This solar plasma analyzer used a vibrating-reed electrometer as its principal current-measuring device. The Venus mission proved that this type of electrometer, which had formerly been a useful but delicate laboratory instrument, could also be a rugged, long-lived, stable, and flightworthy instrument for detecting and reporting space phenomena.

The basic electrostatic analyzer system is illustrated in Fig. 1. Charged particles entering the instrument are deflected by an electric field approximately transverse to the particle velocity vector. Only those particles with a particular

charge sign and within a certain range of energy per unit charge and a certain range of angle of incidence are deflected through the curved tunnel onto the charge collector. The energy distributions of both positively and negatively charged particles entering the device can be determined by varying the polarity and magnitude of the deflection voltage. The charge collection rate is measured at each energy level by a wide-range electrometer.
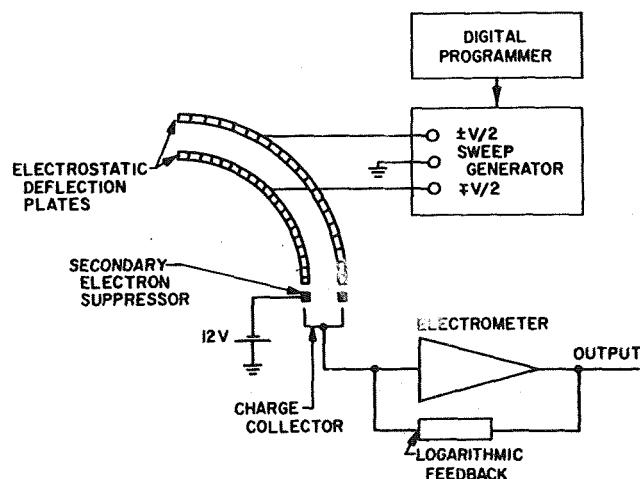

Fig. 1-Block diagram of basic solar plasma instrumentation

II. THE ELECTROMETER AMPLIFIER

A.   General

This electrometer employs the conventional operational amplifier configuration with a vibrating capacitor modulator and a nonlinear, thermionic feedback element. The operational amplifier configuration was chosen to minimize the leakage currents resulting from input (or summing-point) potentials and to reduce the dependence of the speed of response on input-to-ground capacitance.

The electrometer system used in the Mariner II solar plasma instrument is shown in block diagram form in Fig. 2. A vibrating capacitor modulates the dc summing-point potential into a sine wave with a frequency near 2400 Hz. After amplification by the carrier amplifier, this signal is half-wave demodulated with a transistor switch.

Direct-coupled amplification and filtering are performed by a Miller-type filter amplifier. The loop is then closed with a single logarithmic diode. An offset voltage reference used in the flight instrument is not shown in the block diagram of Fig. 2.
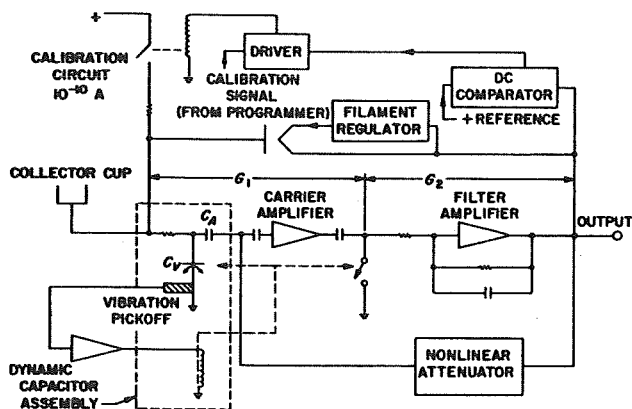

Fig. 2-Mariner II electrometer block diagram

A comparator that is referenced at a pre-saturation voltage for the electrometer output has been provided to preclude saturation of the amplifier, an event that could occur in the presence of small negative background currents. When this reference level has been exceeded, an input current source, which doubles as a calibration current, is activated, thereby bringing the electrometer to a midrange voltage.

A figure of 1000 was selected as the requirement for dc gain between the input and the output. If one neglects the effects of leakage current and resistance, the figure of 1000 becomes the dc feedback factor. This figure of amplifier tightness limits dynamic deviations to 0.1% of the output as obtained with infinite gain.

The carrier-amplifier approach was pursued because input-modulating comparators of the dynamic capacitor variety offered such attractive prospects as high resistance, stability, and long life expectancy. Furthermore, if the modulator parameters were properly chosen, the need for a vacuum-tube input to the carrier amplifier would be eliminated. In addition, if the modulator frequency were made sufficiently high, the electrometer speed of response would not be severely limited by amplifier bandwidth, which would also be commensurately higher.

B.   The Feedback Element

Since the 7-decade dynamic current range (10^{-13} to 10^{-6} A) required by the experiment exceeded the maximum signal-to-noise ratio of the dynamic-capacitor electrometer and also exceeded the range of available analog-to-digital

converters, a logarithmic transfer resistance was chosen. In this application a CK 5886 subminiature pentode connected as a diode provided the feedback from the output directly to the input. Operating in its retarded field region, [1,2] the diode produced a quite acceptable logarithmic compression of plate currents over a range in excess of the plasma experiment requirements. The equivalent small-signal resistance of this tube was approximately

$$r_D = \frac{1}{10\,I_p} \qquad (1)$$

where I_p = plate current in the tube; its parallel interelectrode capacitance was about 5 pF. Most of the 5886 diodes operating at regulated filament currents of 10 mA displayed characteristics having about 230 mV per current decade and thermal drifts of about 70 mV over an 80°C temperature range. While these drifts were both predictable and calibratable during the Mariner II flight, it is true that the thermionic log diode masked the inherent temporal and thermal stability of the electrometer amplifier, which would have been displayed had this system used resistive feedback.

Since the dynamic resistance of the feedback element varied as many orders of magnitude as the measurable input current, a secondary feedback loop was required to provide nonlinear damping, which resulted in an acceptable transient response over the entire dynamic range.

C.   The Modulator

The dynamic capacitor modulator, developed for the Jet Propulsion Laboratory (JPL) through a series of contracts with the Applied Physics Corporation of Monrovia, California, was mechanically resonant near 2400 Hz ($Q_m \cong 200$) and was electromagnetically driven at this resonance by a tuned class C amplifier. [3] The capacitor-drive oscillator loop was completed with a lead titanate transducer, which was affixed to the vibrating reed element. Typically, a 10% conversion efficiency, defined as the ratio of rms ac output voltage to dc input voltage, was achieved. The oscillator that drives the dynamic capacitor had a temperature-sensitive amplitude variation designed to maintain a more constant conversion efficiency than that obtained with a drive voltage that does not change with temperature.

The thermal stability of contact potential was better than 70 μV/°C and the 3-month pre-flight temporal stability was 5 mV, noncumulative. Further details on construction and performance of this unit appear in Ref. 1.

D.   The Carrier Amplifier

Following the modulator are a one-stage low-noise ac preamplifier and a 3-stage ac post-amplifier (see schematic of Fig. 3). The portion of the over-all gain incorporated into the carrier section was determined principally by considerations of noise and dc stability. The gain had to be made large enough to minimize adequately the
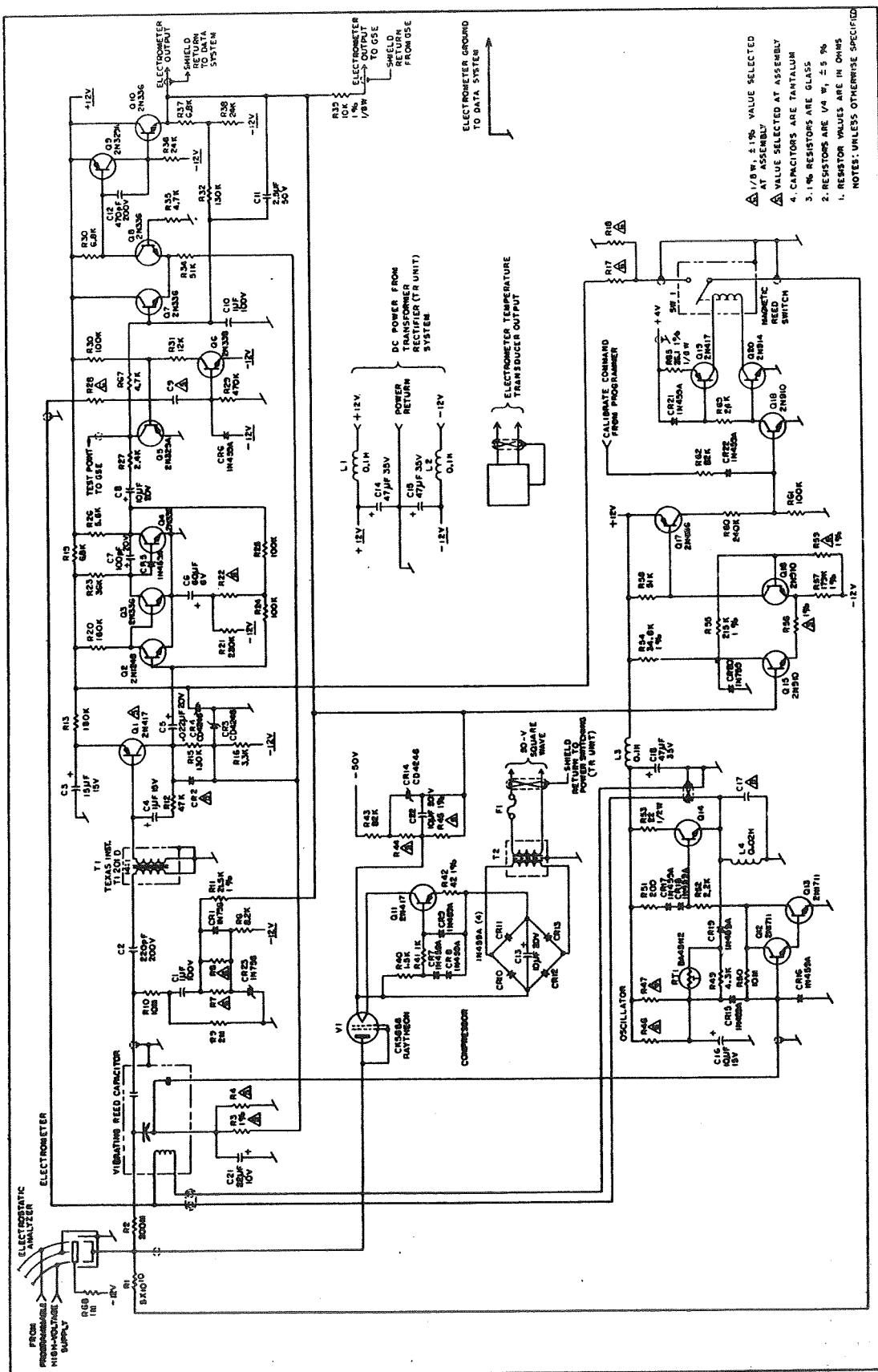
Fig. 3—Mariner II electrometer schematic diagram

effects of drifts in the demodulator baseline and the dc amplifier as seen at the electrometer input, but not so large as to permit input noise to drive the output stage of the ac amplifier into nonlinear operation. A representative gain of 35 for G_1 (see Fig. 2) reduced the thermally induced drifts from the dc section to the order of 1 mV as observed at the electrometer input. Noise at the output of the ac amplifier was about 100 mV rms within a linear dynamic capability of +2.5 and -6 V.

Since the transformer-rectifier power supply for the instrument was driven by a 50-V, 2400-Hz, square-wave source, it was certain that at least small amounts of 2400-Hz energy would be present in the carrier amplifier. The self-resonant dynamic capacitors used for Mariner were, therefore, ordered with mechanical resonances sufficiently displaced from 2400 Hz as to minimize internal beat-frequency signals.

The ac preamplifier presented one of the most likely areas for innovation. The question was whether the parameters of the customary vacuum-tube preamplifier could be replaced by those of a transistor. The number of stages needed for the carrier section turned out to be about the same both for a high input impedance bootstrapped amplifier and for conventional low input impedance common-emitter amplifiers. The low-impedance connection, as embodied in the circuit of Q1 in Fig. 3, was finally used. (This circuit predated the commercial availability of field-effect transistors.) The gain of the carrier amplifier was significantly increased by a current step-up transformer (n = 14:1) interposed between the preamplifier and the dynamic capacitor. The primary impedance, which was n^2 times the amplifier input impedance, was still relatively small compared with the capacitive source reactance of the dynamic capacitor. A phase-stable current gain of 14 could, therefore, be expected without increasing the noise component at the output of the carrier amplifier. Several germanium and silicon transistors were inspected in unloaded models of the preamplifier. The 2400-Hz gains of this highly degenerative circuit were experimentally confirmed to be equal and then the output noise content was inspected. The germanium 2N417 was selected for the application because of its superior noise performance as observed through this empirical procedure. The chief safeguard against high-temperature saturation of the transistor caused by collector leakage was the diode CR2, whose I_{co} characteristic was matched to that of the transistor to at least 70°C. The preamplifier bias configuration presented an optimum thermal stability (SI_c ≈ 1) along with reduced gain to 1/f noise.

The triplet postamplifier was a 3-stage, direct-coupled, feedback-biased cascade (Q2, Q3, Q4). At the carrier frequency, a substantial portion of the feedback used to bias the amplifier at dc was disconnected by the shunt capacitor C6.

Response of the entire carrier amplifier with respect to frequency is shown in Fig. 4. The low-frequency slope of 12 dB/octave was composed of two equal contributions: one 6-dB/octave rate from the capacitive source reactance to the transformer and another similar effect from the network coupling the preamplifier and the triplet. If the preamplifier output impedance were constant, one might expect a characteristic that would still be rising 6 dB/octave at the carrier frequency. This impedance, because it was affected by the preamplifier source impedance, was actually rising with frequency at 2350 Hz and was the principal cause of response flattening as seen in Fig. 4.
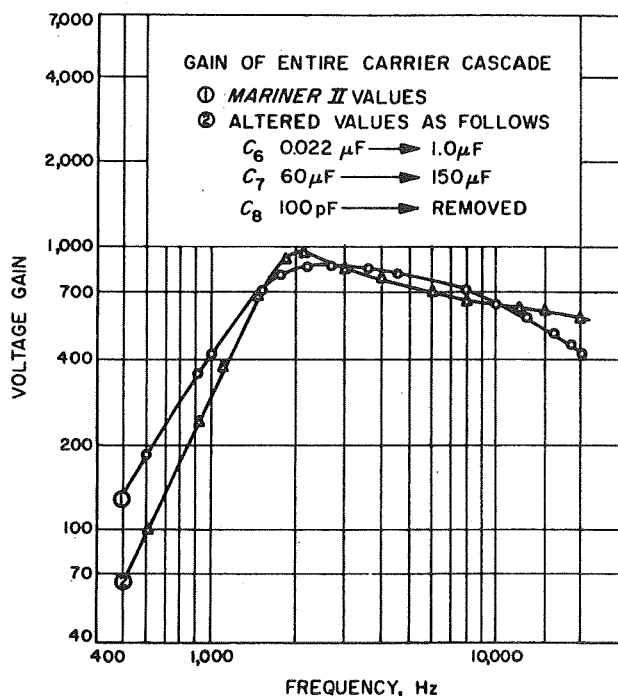

Fig. 4-Carrier amplifier performance curves

E.   The Demodulator

The ac signal from the carrier amplifier was reconverted to dc by means of synchronous detection. Synchronous shunt switching was performed by the transistor Q5, while R27 limited the maximum chopped currents in the shunt switch to prevent the triplet amplifier from cutting off on its positive swing.

In this type of system, maximum detection efficiency is produced at drive-to-signal phasings of 0 and 180 deg. At intermediate phasings, efficiencies are described by the cosine of the drive-signal phase angle.

The output developed across the synchronous switch was made up of two components, signal and pedestal. The pedestal was attributable to a dc voltage retained by the coupling capacitor as though it were the output filter of a rectifier system.

The dc voltage gain of the entire carrier section may be written

$$G_1 = \eta_C G_{AC} \eta_D \qquad (2)$$

where

η_C = dynamic capacitor conversion efficiency

G_{AC} = gain of the carrier amplifier at 2,400 Hz

η_D = demodulator efficiency

The laboratory model on which many of these tests were run, like the flight electrometers, had its carier gain adjusted with R_{22} to a nominal value of 35. Using the measured value of G_{AC} (910) and the calculated value of η_D (32.4%) for the sake of illustration, the dynamic capacitor conversion efficiency producing the requisite gain of 35 was calculated to be 12%. The static transfer characteristic of the carrier section is shown in Fig. 5.
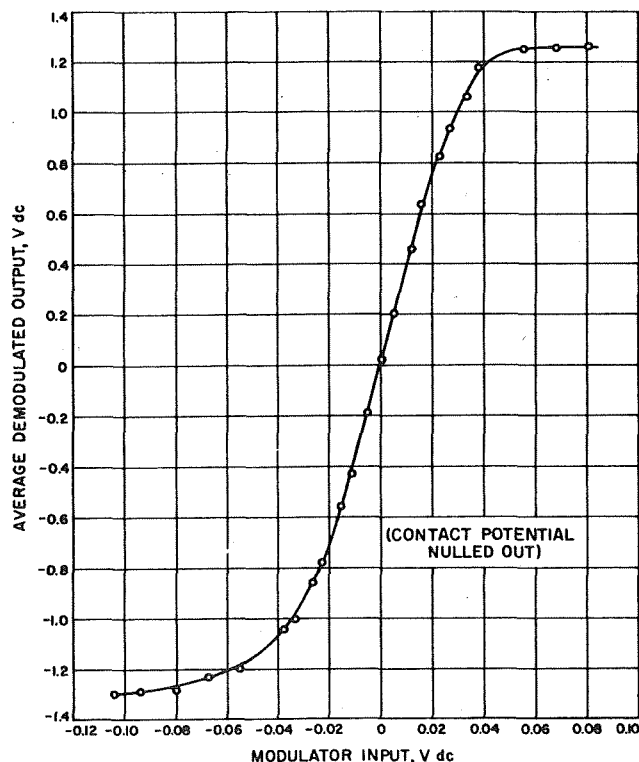

Fig. 5-Static transfer characteristic of carrier section

It is interesting to note that when a signal suddenly appears at the output of the triplet amplifier, only the signal component is transmitted at first. The pedestal component, however, builds up in accordance with the charging of the capacitor. The effect on the carrier envelope or on the average demodulated signal, in a low-pass sense,

is that of a network producing a phase-lag doublet with corner frequencies between 2 and 4 Hz.

F. The DC Amplifier

The dc amplifier, which was the final element in the electrometer and comprised transistors Q7, Q8, Q9, and Q10, provided the following functions:

     a.   Supplementary gain for required loop tightness,
     b.   Suitably wide output dynamic range,
     c.   Demodulation ripple filtering, and
     d.   Low output impedance.

Consider the gain requirement. The dc gain between modulator and demodulator was designated to be 35. The section following the demodulator must also provide a dc gain of 35 if the arbitrary standard of tightness, the zero-frequency feedback factor, is to be about 1000. The filter capacitor, located across the amplifier in this design, must reduce the ripple component at the output of the electrometer to within tolerable limits for external measuring equipment but should not be made so large as to produce a serious voltage rate-limiting problem. Such a problem is often caused by a combination of (1) limited dynamic range in the carrier amplifier and (2) too large a filter capacitor. Since this capacitance is an important term in one of the corner frequencies for the low-pass loop transmission characteristic, it must also be scrutinized from the viewpoint of loop stability.

A resistive T feedback network performs, as its principal function, the zero-signal level adjustment of the output, which must be above zero to accommodate the log diode characteristic. This amplifier possesses a dc gain of 37.5 and an integrating time constant of 0.435 sec with a feedback factor of about 30.

The rate limit of the electrometer is the slope of the integrated output of the filter-amplifier produced by the maximum signal available from the carrier amplifier. Maximum values for positive and negative demodulated voltages will be somewhat different because of asymmetrical current-handling capabilities in the output stage of the triplet amplifier on negative and positive swings. In the actual transfer characteristic as shown in Fig. 5, the maximum average positive demodulator voltage of 1.2 V establishes an amplifier charging rate limit of

$$\frac{dE_o}{dt} = \frac{E_D}{R_{67}C_{11}} = -100 \text{ V/sec.}$$

This permits the amplifier to negotiate a negative 5-V step in 50 msec if no other factors are involved.

In most applications where the output of a sensitive device such as this electrometer must be protected against electrostatic coupling of external power and signal transients, it is imperative

to furnish the amplifier with a suitably low output impedance. Over-all electrometer feedback does not necessarily ensure wide-band protection, because at low input-current levels the dynamic feedback resistance is high, and unity-gain cross-over for the loop feedback factor occurs at low frequencies. The result is a total absence of impedance degeneration above a few cycles per second. For this reason, local feedback in the filter-amplifier is required to provide low-output impedance independent of the over-all loop. The emitter-follower, Q10 for instance, may have an output impedance of 300 ohms, further degenerated by the local feedback to about 10 ohms. The dc impedance of 10 ohms is further reduced at frequencies where C_{11} produces increased local feedback. The static output impedance, as previously suggested, is also enhanced by the dc feedback factor of the entire loop, which reduces the filter-amplifier impedance by 1000 to a small fraction of an ohm.

III.   PERFORMANCE

A.   Offset Stability

There are three main contributions to drift at the electrometer input. These are

1. Variation in dynamic capacitor contact potential,
2. Variation in balance of the dc amplifier comparator, and
3. Variation of the demodulator offset.

Contact potential drift in the modulator appears directly at the electrometer input. Changes in modulator reference potentials are similarly reflected directly at the input. As a precaution against inverse-polarity leakage currents, the modulator is referenced so that a nominal negative potential appears at the summing point. Leakage produced by input resistance will therefore cause a small error current, of the same polarity as positive-ion current, to flow in the feedback element.

The comparator stage of the dc filter-amplifier is a relatively coarse device. The drift in the differential stage composed of Q7 and Q8 is characteristically about -50 mV between -20 and +70°C, yielding an average temperature coefficient of -0.6 mV/°C. If the gain of the carrier section between the modulator and demodulator were assumed constant at 35 over this temperature range, the drift at the summing point attributable to the dc amplifier instability would be 1.4 mV.

The demodulator transistor (Q5) is likewise coarse in performance. A 2N329A PNP alloy transistor is used in the normal configuration for its superior current gain, thereby forsaking the stability of the inverted connection. It is estimated that drifts in its saturation voltage attributable to temperature and alpha changes will not exceed 10 mV. The full-cycle average drift, 5 mV, would correspondingly produce a 0.14-mV shift at the electrometer input. The combined

demodulator-dc amplifier drift reflected to the electrometer input would therefore be small compared with the modulator contact potential drifts, which fall in the 5- to 10-mV range.

B.   Feedback Stability

The electrometer transfer characteristic may be written

$$E_o = I_{in} Z_f \left(\frac{A\beta}{1 - A\beta} \right) \qquad (3)$$

where

A = forward dc amplifier gain

β = portion of output returned to summing point

Z_f = feedback impedance.

The amplifier, as is implied in Eq. (3), is dependent upon the feedback factor $A\beta$ for such important characteristics as static accuracy, speed of response, and loop stability. Trying to satisfy conditions for loop stability presents an unusual problem, in that R_f, one of the principal parameters in the calculation of $A\beta$, varies in excess of seven decades.

Since the feedback resistance varies as an inverse function of the feedback current, the secondary feedback, or damping, must also be non-linear. No single condition of feedback will satisfy requirements for both loop stability and speed of response at all currents within the measurable range of the instrument. A nonlinear attenuator composed of R7, R8, R11, and zener diode CR1 provides a two-point compensation characterized by zero damping at low currents, fixed damping at high currents, and a transition corresponding to about one current decade. The use of C_A in the dual role of damping element and carrier-frequency coupling capacitor was suggested by an earlier commercial application.

To correlate actual performance with predicted behavior and to verify adequacy of phase margins, a set of tests was performed on a laboratory electrometer using the experimental arrangement of Fig. 6. The signal generator was placed in the feedback loop so that the feedback would still stabilize the dc operating point and that output levels would be determined by the equivalent series generator voltage, i.e.,

$$E_o = V_g \left(\frac{F}{1 - F} \right) \qquad (4)$$

where

$$V_g = E_T - F E_T$$

F = feedback factor = $A\beta$.

The open-loop amplitude and phase responses were obtained by taking oscilloscope pictures of the waveforms on both sides of the floating signal generator, which also supplied scope trigger
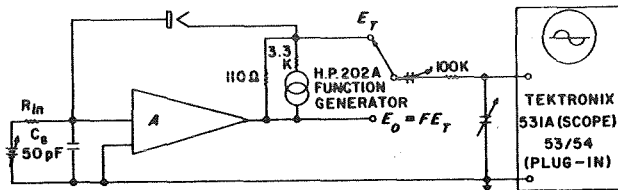
Fig. 6-Test setup for loop transmission measurements

pulses. The dc bias current in the tube was determined by resistors connected between a 1-V battery and the electrometer input. This resulted in a 10% reduction in A_0 and in a small modification to the responses of F vs the frequency that would have been obtained with perfect current sources. A 50-pF capacitor with a leakage resistance greater than 10^{15} ohms simulated the capacitance between the collector and its electrostatic shield. An R-C filter at the scope input reduced the 60-Hz signals generated in the loop by the large floating generator; as a result, measurements above 20 Hz were somewhat unreliable. For bias currents greater than or equal to 10^{-10} A, the secondary feedback was removed by disconnecting R10. Figures 7 through 12 show gain and phase shift of the amplifier measured at frequencies from 0.01 to 100 Hz for bias currents between 10^{-6} and 10^{-13} A.
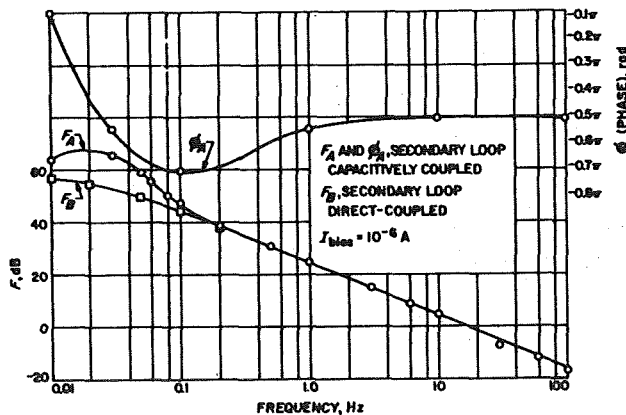

Fig. 7-Gain and phase curves with secondary feedback in (I_{bias} = 10^{-6} A)

The laboratory electrometer used for these tests contained several components whose values were different from the nominal flight-unit values or had changed since those components were installed. Since there was some variance between measured responses and nominal curves, comparison was then made between measured component values and values providing the best fit to the experimental curves (see Table I).

The best-fit component values agree reasonably well with the measured values except for C_s, where the dispersion is not fully understood at this time. Most notable departures from expected
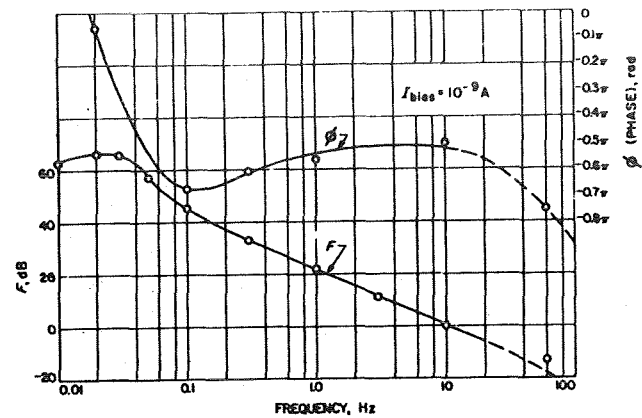

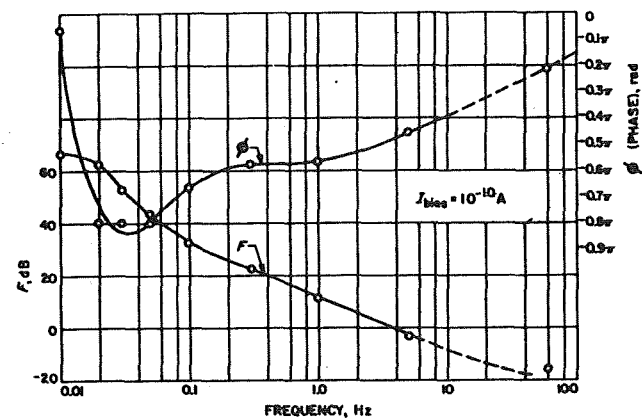Fig. 8-Gain and phase curves with secondary feedback in (I_{bias} = 10^{-9} A)

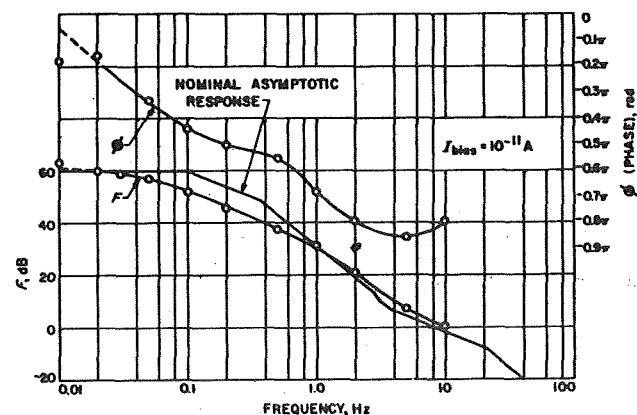Fig. 9-Gain and phase curves with secondary feedback in (I_{bias} = 10^{-10} A)

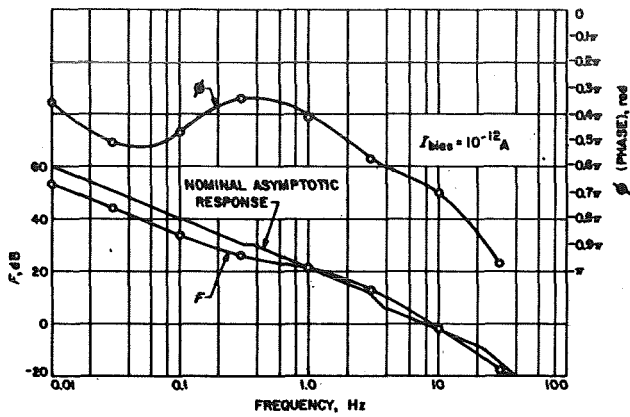Fig. 10-Gain and phase curves with secondary feedback in (I_{bias} = 10^{-11} A)

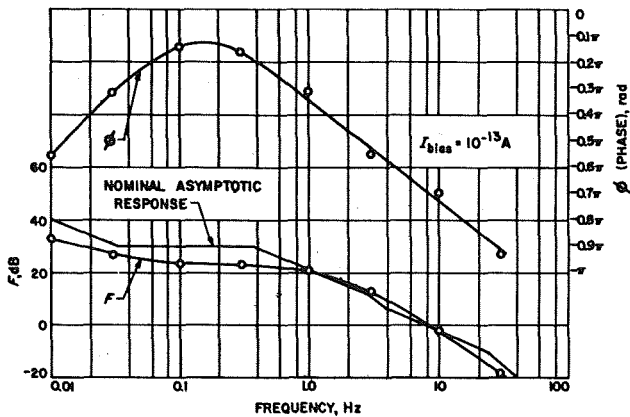Fig. 11-Gain and phase curves with secondary feedback out ($I_{bias} = 10^{-12}$ A)

Fig. 12-Gain and phase curves with secondary feedback out ($I_{bias} = 10^{-13}$ A)

Table I. Component values

Component	Value		
	Nominal	Measured	Best fit
			Assumed
C_0, pF	50	150	150
C_2, pF	220	–	220
C_1, μF	1	–	1
R_{32}, K	130	150	150
R_{37}, K	6.8	9.1	9.1
R_{38}, K	24	24	24
R_{11}, K	21.5	21.5	21.5
R_c, K	60 (max)	60 (max)	60 (max)
R_9, Meg	2	2	2
R_f, Ω	$\frac{1}{10} I_{bias}$	$\frac{1}{10} I_{bias}$	$\frac{1}{10} I_{bias}$
			Calculated
C_s, pF	50	63	154
C_A, pF	70	60	59
C_{11}, μF	2.5	0.96	0.93
C_f, pF	5	5	5.3
R_2, Meg	200	160	208
A_0	-1000	–	-1000

values were in the cases of the filter capacitor C11 and the dynamic capacitor rest capacitance, C_0. The filter capacitor, a bipolar tantalum unit, may have deteriorated with age. The dynamic capacitor, a non-flightworthy developmental model, had apparently acquired a reduced reed-to-anvil spacing.

Of the six bias conditions for which curves have been drawn, minimum margin occurs with a bias current of 10^{-11} A (Fig. 10). In this curve, the rolloff rate at gain crossover (10 Hz) is about 8 dB/octave with a -144-deg phase shift, although the phase shift in this case does reach a pre-crossover maximum of -153 deg at 6 Hz. Deviations in the capacitances C_0 and C_8 reduced the corner frequency produced by one of the dominant poles from a nominal 22 Hz to less than half its standard value. This placed that corner frequency near gain crossover, thereby reducing margins in the laboratory instrument, though not to intolerably small levels. The flight instruments were generally adjusted for transition between secondary feedback states at about 5 x 10^{-12} A.

C. Closed-Loop Performance

When the electrometer is driven by a current source, its transfer impedance may be expressed in the following modified form of Eq. (3):

$$Z_T = \frac{-E_o}{I_{in}} = Z_f \left[\frac{1}{1 - (1/F)} \right]. \tag{5}$$

If the loop transmission characteristic is approximated at gain crossover (f_{gc}) by a 6 dB/octave rolloff rate, the transfer impedance is then given by

$$Z_T = \frac{R_f}{(1 + p\tau_4)(1 + p\tau_{gc})} \tag{6}$$

where

$$\tau_{gc} = \frac{1}{2\pi f_{gc}}$$

Table II.   Dominant time constants and corner frequencies for nominal closed-loop response

Bias current A	Time constant, sec			Corner frequency, Hz		
	τ_4	τ_{gc}	τ'_{gc}	f_4	f_{gc}	f'_{gc}
10^{-6}	5×10^{-7}	-[a]	0.0094	3.7×10^5	-	17
10^{-9}	5×10^{-4}	-[a]	0.014	370	-	11
10^{-10}	0.005	-[a]	0.053	37	-	3.0
10^{-11}	0.05	0.018	0.45[b]	3.7	9	0.35
10^{-12}	0.5	0.018	4.5[b]	0.37	9	0.035
10^{-13}	5	0.018	45[b]	0.037	9	0.0035

[a]Secondary feedback connected at these currents; for applicable time constant, see τ'_{gc} column.

[b]Secondary feedback customarily disconnected at these currents; values listed denote theoretical values that would be obtained if secondary feedback were connected.

Table II lists the time constants of Eq. (6) and their associated frequencies as a function of bias current. The gain-crossover frequency with secondary feedback (f'_{gc}) is also listed.

Families of closed-loop frequency responses are shown in Figs. 13 and 14 for secondary feedback in and out, respectively. Electrometer biasing was similar to that used in Fig. 10, and a signal current was inserted into the summing point by a function generator connected in series with a suitably large resistor. The only parameter significantly different from the ones used in the loop transmission tests was the modulator rest capacitance (C_0), which was 59 pF for the dynamic capacitor used in this case.
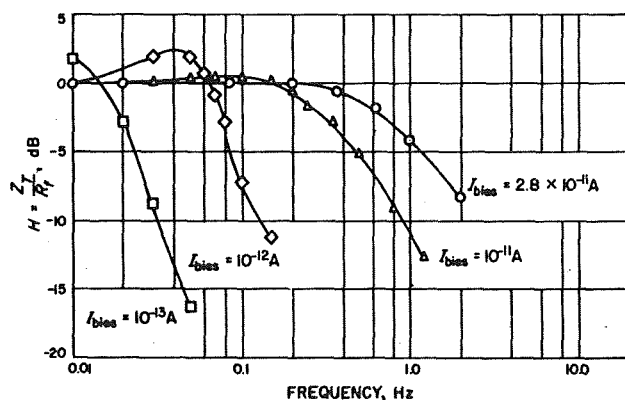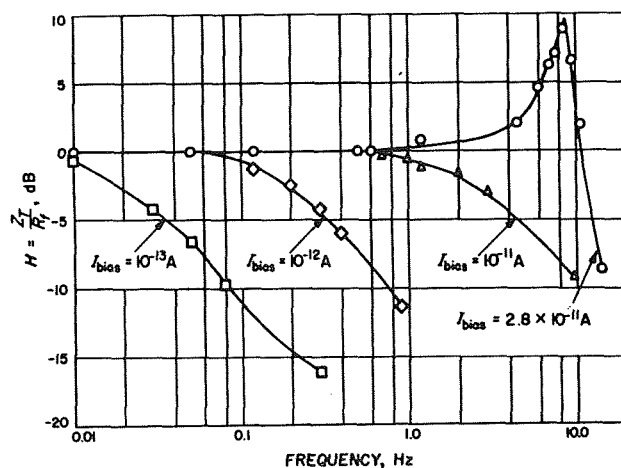

Fig. 14-Closed-loop frequency response without secondary feedback

Peaking that occurs at lower currents in Fig. 13 is directly attributable to phase shifts associated with peaks in loop transmission characteristics that are not sufficiently removed from gain crossover. The overshoots associated with transient response to these characteristics were not observed in flight instruments, since secondary feedback transition occurred at about 5×10^{-12} A. The peaks are removable, however, by direct coupling of the secondary feedback. This is considered a generally advisable procedure for this configuration providing that capacitor C_A has a sufficiently large leakage resistance.

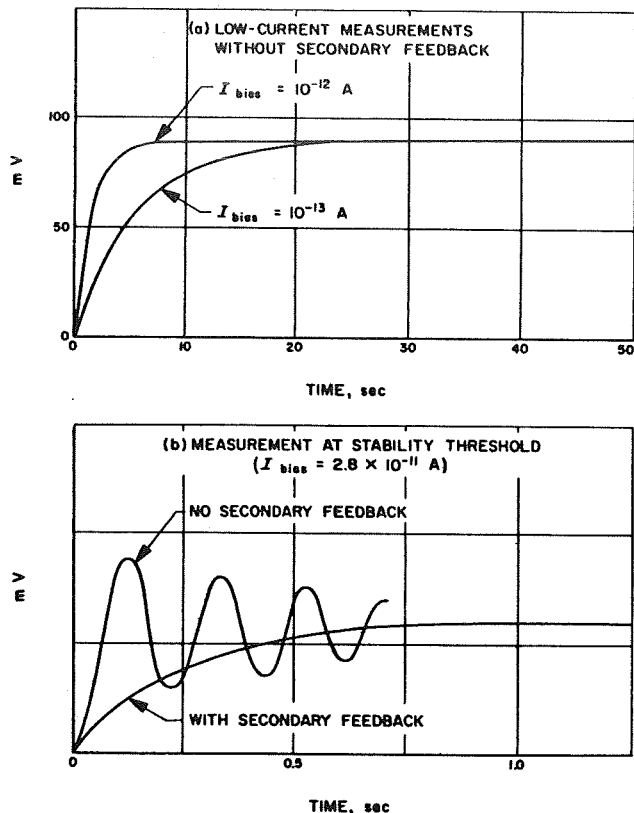Fig. 13-Closed-loop frequency response with secondary feedback

TIME, sec

Fig. 15-Closed-loop transient response

Closed-loop transient responses (Fig. 15) were recorded by changing the sine-wave signal used in the previous closed-loop tests to a square wave. Care was taken to keep the signal amplitude down to swings of not more than a quarter of a decade from quiescent levels, lest nonlinearities in the feedback tube mask the true small-signal performance.

IV. THE MARINER II FLIGHT ELECTROMETER

A. Preflight Calibrations

The curves and tables presented here describe the preflight performance of the Mariner II solar plasma instrument electrometer. Part of the logging operation, which started after completed construction of each unit, consisted of monitoring important instrument performance parameters and power supply levels in addition to the customary calibrations. Table III presents results of characteristic measurements taken in the 4-month period prior to launching. The mechanical resonance of the dynamic capacitor is measured by the frequency of its feedback-driven oscillator. The importance of this measurement is that large increases in frequency with time are indicative of leaks in the modulator vacuum seal, which suggests damping effects such as reduction in conversion efficiency and alteration in mechanical Q. Acceptance standards for frequency stability were based upon statistical data obtained from Ranger instrument modulators. During this period

of time, loop gain variations were within +1.6 and -3.7 dB of the nominal 60 dB. Input error signal potentials were, therefore, about +2 mV for the tabulated values at input currents of 10^{-6} A. As a result, if -2 mV corrections are made to tabulated values of V_{in}, one has a thermal and temporal history of modulator contact potential.

The curves of Fig. 16 provide the basic temperature calibration for the electrometer system, but for final adjustment they must be normalized to the last preflight temperature calibration. The effective translational drift of calibrations between May 8 and August 5, 1962, was about 8 mV.
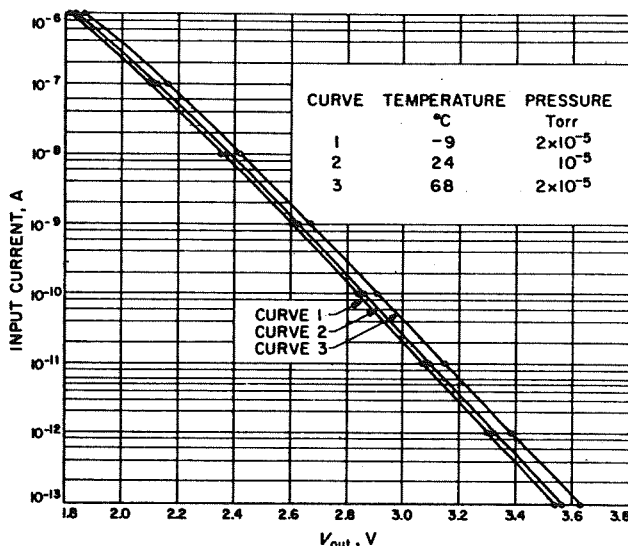

Fig. 16-Vacuum-temperature electrometer calibrations, May 8, 1962

B. Flight Performance

The Mariner II flight to Venus lasted approximately 109 days, during which time an over-all flight distance of about 180 million miles was traversed. At Venus encounter, the spacecraft communicated its scientific data to Earth over an interplanetary distance of 36 million miles.

Radio signals from the Mariner spacecraft were heard for the last time by the JPL Deep Space Instrumentation Facility station in Johannesburg, South Africa, at the conclusion of its acquisition period at 2:00 a.m. EST on January 3, 1963. At that time the spacecraft was 53.9 million miles from the Earth and 5.6 million miles beyond Venus, and had traveled 223.7 million miles since launch on August 27, 1962. During the 129 days between launching and the final loss of radio contact with the spacecraft, the interplanetary or cruise science instruments, of which the solar plasma instrument was one, operated for a total of 118.2 days, and data produced by these instruments were actually recorded by the tracking stations for approximately 104.1 days.

Table III.　Preflight electrometer performance

Date	Modulator frequency f_0, Hz	Loop gain F_0	V_{in} at $I_{in} = 10^{-6}$ A mV	Temperature[a] °C	Pressure torr
5/8/62	2,259.7	1,150	-26.5	+24	1 atm
(JPL)	2,259.4	1,150	-26.1	+26	10^{-4}
	2,259.3	650	-25.4	-9	2×10^{-5}
	2,261.1	1,110	-25.8	+68	2×10^{-5}
	2,258.8	1,130	-28.4	+24	10^{-5}
	2,259.1	1,110	-29.7	+23	1 atm
6/28/62	2,260.5	1,080	-25.3	Amb + 25[b]	1 atm
(AMR)	2,260.9	730	-21.6	Amb - 20	
	2,262.0	910	-25.5	Amb + 70	
	2,260.0	1,051	-23.8	Amb + 25	
8/5/62	2,260.8	1,110	-28.0	+28	1 atm
(Final at AMR)	2,260.2	1,200	-23.7	+40	1.3×10^{-4}

[a]Unless otherwise noted, all temperatures are those at the instrument chassis.

[b]"Amb" denotes ambient temperature.

Information on cruise science experiments was recorded without interruption for one period of 38.3 days and for three other periods of more than 9 days.

The Mariner II solar plasma instrument operated successfully throughout the entire flight, in both the cruise and planet encounter modes. The plasma experiment required 3.7 minutes to acquire a complete energy spectrum of the plasma and during the flight of Mariner II, approximately 40,000 such spectra were obtained. Perhaps the most interesting new information to arise from the very large volume of data on interplanetary fields and particles is the demonstration that solar plasma flowing radially out from the Sun was detectable in every one of the 40,000 spectra obtained in the 4-month mission and is therefore presumably always present.

A detailed analysis of engineering flight data pertinent to the solar plasma instrument and its electrometer is presented in Ref. 1. Scientific results may be found in Refs. 5, 6, and 7.

V.　DISCUSSION AND CONCLUSIONS

The Mariner II Venus mission, with its successful utilization of a vibrating-reed electrometer to analyze solar plasma data, not only verified the existence of the solar wind, but also proved that such an electrometer could withstand a launch environment and the rigors of deep-space flight and could serve as a stable and reliable device for detecting and reporting space phenomena.

Although improved versions of this type of electrometer are now available with stable resistive feedback, with smaller and more stable modulators, and with higher gain, lower-noise transistors, the applicable fundamentals of design, analysis, and performance of carrier electrometers will not necessarily be new, for, as the authors have attempted to demonstrate, the art is an established one.

VI.　ACKNOWLEDGMENTS

It is with pleasure that we acknowledge H. R. Mertz and L. D. Bowman for their engineering contributions to the development of the Mariner II plasma instrument. We wish to thank J. H. Marshall and J. R. Locke for their assistance in the preparation of evaluation and performance data on the Mariner II electrometer. Valuable suggestions by R. Heacock and R. Heyser, perhaps remembered only vaguely by them as conversational ideas, were subsequently incorporated into the designs presented in this paper. We also note the efficient dynamic capacitor drive oscillator designed by D. W. Slaughter.

The dynamic capacitor was one of the most important elements in this instrumentation, and for its timely development we wish to express our appreciation to the Applied Physics Corporation of Monrovia, California. We especially want to thank W. Williams of that company for his personal cooperation and diligence in delivering stable and reliable modulators to JPL.

REFERENCES

1. C. Josias and J. Lawrence, Jr., An Instrument for the Measurement of Interplanetary Solar Plasma, Technical Report No. 32-492, Jet Propulsion Laboratory, Pasadena, California, May 1, 1964.

2. B. Chance, V. Hughes, D. Sayre, and F. C. Williams, Waveforms, Massachusetts Institute of Technology Radiation Laboratory Series, Vol. 19, McGraw-Hill Book Co., Inc., New York, 1949, pp. 58-67.

3. D. W. Slaughter, "Reed Drive Oscillator for a Vibrating-Reed Electrometer," Research Summary No. 36-12, Vol. 1, Jet Propulsion Laboratory, Pasadena, California, January 2, 1962, pp. 11-13.

4. J. J. Ebers and J. L. Moll, "Large-Signal Behavior of Junction Transistors," Proceedings of the IRE, Vol. 42, Part 2, December 1954, pp. 1761-1772.

5. C. Snyder, M. Neugebauer, U. R. Rao, "The Solar-Wind Velocity and Its Correlation With Cosmic-Ray Variations and With Solar and Geomagnetic Activity," Journal of Geophysical Research, Vol. 68, No. 24, December 15, 1963, pp. 6361-6370.

6. C. Snyder and M. Neugebauer, "Interplanetary Solar Wind Measurements by Mariner II," Space Research IV, North-Holland Publishing Co., Amsterdam, 1964.

7. C. Snyder and M. Neugebauer, "The Mission of Mariner 2: Preliminary Observation-- Solar Plasma Experiment," Science, December 7, 1962, pp. 1095-1096.